



**Université Lille 1 Sciences et Technologies**  
**Laboratoire Génie Civil et géo-Environnement**  
**Ecole doctorale Sciences Pour l'Ingénieur**

## **THÈSE**

Pour l'obtention du grade de  
Docteur de L'Université des Sciences et Technologies de Lille  
Discipline: Génie Civil  
Sous le titre de:

---

# **Composite Element Method for Modelling Transient Groundwater Flow in Fractured Media and its Application to Slope Stability Problem**

---

par

**Xiaoping HOU**

Présentée et soutenue publiquement le **29 Juin 2017**

Devant le jury constitué de:

<b>SHAHROUR Isam</b>	<b>Professeur, Université Lille 1</b>	<b>Directeur de thèse</b>
<b>CHEN Shenghong</b>	<b>Professeur, Wuhan University</b>	<b>Directeur de thèse</b>
<b>AL HEIB Marwan</b>	<b>Professeur, Ecole des Mines Nancy</b>	<b>Rapporteur</b>
<b>WU Aiqing</b>	<b>Professeur, Yangtze River Scientific Research Institute</b>	<b>Rapporteur</b>
<b>ABBAS Oras</b>	<b>Docteur, A+Métérologie -groupe Apave</b>	<b>Examineur</b>
<b>FU Shaojun</b>	<b>Professeur, Wuhan University</b>	<b>Examineur</b>



## Résumé

Ce travail de thèse propose un modèle numérique complet pour l'écoulement transitoire des eaux souterraines dans les milieux poreux et fracturés et son application sur l'analyse de la stabilité des pentes sous l'effet d'une diminution du niveau de l'eau dans un réservoir. L'écoulement de l'eau dans les milieux fracturés est complexe, en raison de la présence d'un grand nombre de fractures et de fortes variations dans les propriétés géométriques et hydrauliques de ces milieux.

La thèse est organisée en six chapitres.

Le premier chapitre présente les problèmes abordés et les objectifs de la thèse. Le 2<sup>nd</sup> chapitre présente une synthèse des analyses numériques de l'écoulement dans les milieux fracturés et de ses effets sur la stabilité des pentes.

Le 3<sup>ème</sup> chapitre présente le développement d'un modèle numérique d'écoulement transitoire saturé dans des milieux fracturés avec une surface libre en utilisant la méthode des éléments composites (CEM). Le 4<sup>ème</sup> chapitre présente un modèle numérique d'écoulement transitoire à saturation variable, dans les milieux fracturés à l'aide du CEM.

Le 5<sup>ème</sup> chapitre présente une étude de la stabilité des pentes sous l'effet de variation des paramètres hydrauliques et de résistance des sols, et de la géométrie des pentes.

Le 6<sup>ème</sup> chapitre présente une étude paramétrique de l'influence des caractéristiques de fracture sur l'écoulement transitoire et la stabilité d'une pente soumise à des conditions de diminution.

**Mots-clés:** écoulement des eaux souterraines; milieux fracturés; écoulement à saturation variable; surface libre; méthode élément composite; stabilité de la pente; méthode d'équilibre limite; vidange rapide

## Abstract

This thesis presents a comprehensive numerical method for analyzing transient groundwater flow in porous and fractured media and its application to the analysis of the stability of soil and rock slopes subjected to transient groundwater flow induced by reservoir drawdown conditions. Compared to that of porous media, the analysis of flow in fractured media is relatively complex, due to the presence of a large number of fractures and strong variations in geometric and hydraulic properties.

The thesis is organized in six chapters.

Chapter 1 presents the issues to be addressed and the thesis objectives. Chapter 2 discusses basic theories related to the numerical analysis of groundwater flow in fractured media and its effects on slope stability.

Chapter 3 develops the numerical model of transient, saturated flow in fractured media with a free surface using the composite element method (CEM). Chapter 4 presents the numerical model of transient, variably-saturated flow in fractured media using the CEM.

Chapter 5 includes an investigation of the stability of homogeneous soil slopes under drawdown conditions, depending on the drawdown rate, hydraulic and strength parameters of soils, and slope geometry.

The last chapter presents a parametric study on the influence of fracture characteristics on transient flow and stability of layered rock slope subjected to drawdown conditions.

**Keywords:** groundwater flow; fractured media; variably-saturated flow; free surface; composite element method; slope stability; limit equilibrium method; rapid drawdown

## Summary

The study of groundwater flow in fractured media can be distinct from that of flow in porous media due to the complex geologic configurations of fractured media. In modelling study of flow in fractured media, the discrete fracture approach is a preferable approach because it has the potentiality to describe the fractures in more detail. However, the difficulty of using this approach is the explicit representation of the geometry of fractured media, which, in numerical modelling, refers to the discretization of the fractured media into computational meshes. The composite element method (CEM) has a prominent advantage on the discretization, so it is quite suited for developing the numerical model of groundwater flow in fractured media, which is the first task of this work. The analysis of groundwater flow often plays an important role in the solution of slope stability problems. The drawdown condition is a common scenario in slope stability. However, the current investigations for the drawdown condition are not deep enough. One of the main reasons is that the pore-water pressures within the slopes during drawdown are not accurately estimated. The second task of this work is to use the developed numerical model to obtain accurate pore-water pressures and then to make reasonable evaluation for the stability of slopes subjected to drawdown conditions. The above contents are presented **in Chapter 1**.

**In Chapter 2**, some basic problems involved in the numerical analyses of groundwater flow in fractured media and its effects on slope stability are considered. In the aspect of the groundwater flow in fractured media, the basic law of single fracture flow, the modelling approaches for flow in fractured media, the composite element method for analyzing discretely-fractured media, and the flow characteristics of variably-saturated system, are respectively discussed. The problems existing in the previous modelling studies of flow in fractured media are pointed out, as well as the capability of the CEM in solving these problems. Then, the research progress of the CEM in analyzing the fractured media is given a certain introduction. In the aspect of the effects of groundwater flow on slope stability, three actions of groundwater on slope stability are described, and the limit equilibrium and the numerical methods for stability analysis are summarized. Particular mention is made of the importance of the reservoir's rapid drawdown to slope stability analysis. The discussion of these problems provides theoretical bases for subsequent studies.

**In Chapter 3**, a three-dimensional numerical model for simulating transient, saturated

flow in fractured media with a free surface is constructed using the CEM. The model does not require generation of specific elements for representing fractures, but, instead, inserts the fractures into the elements so as to form the composite elements. The governing equation for the composite element containing both fractures and matrix is derived by using the variational principle. It provides accurate descriptions of fracture flow, matrix flow and exchange of water between fractures and matrix. The relevant solution algorithms are presented, including those of CEM pre-processing, numerical integral calculation, treatment of boundary conditions and solving large, sparse, symmetric system of equations. In particular, an iterative scheme for locating the shifting free surface is introduced. The validity and reliability of the model are verified by a synthetic example. The capability of the model is demonstrated by simulations of the flow problems in complicated fractured aquifers.

**In Chapter 4**, the CEM is used to further develop the numerical model for simulating transient, variably-saturated flow in fractured media. Since the constitutive relations (saturation–pressure head and relative permeability–saturation relations) for fractures may be highly linear and different than those for matrix, a fast and stable iterative scheme using under-relaxation technique is implemented to solve the variably-saturated flow equations. The techniques of mass matrix lumping and adaptive time stepping are used to further enhance accuracy and efficiency. The effectiveness of the developed model is verified by simulations of one-dimensional infiltration into dry soils and the synthetic example which was discussed in Chapter 3 and simulated by assuming water flowing only in the saturated zone with a shifting free surface. The simulation results are compared with the semi-analytical solution and those obtained from a commercial software COMSOL. Several illustrative problems that demonstrate the complexity of variably-saturated flow in fractured aquifers are presented in the end of this chapter.

**In Chapter 5**, the stability of homogeneous soil slopes under reservoir drawdown conditions is studied. The composite element modelling of transient, saturated flow with a free surface (assuming non-deforming slope media) is used to calculate the transient free surfaces and pore-water pressure distributions in the slopes during reservoir drawdown. Using the calculated pore-water pressure distributions, the limit equilibrium analyses are then conducted to derive the variations of the safety factor of homogeneous soil slopes during drawdown. It has been found from the theoretical analyses of transient flow and slope stability that the variation of safety factor of the slopes during drawdown depends on the

hydraulic index  $k/(S_y v)$  and the strength index  $c'/(\gamma H \tan \phi')$ . Therefore, these two indexes are employed in systematically investigating the influence of various drawdown rates and material parameters on transient flow and stability of homogeneous soil slopes. These investigation results serve for the formulation of criteria for judging rapid drawdown conditions. In this criteria, the rapid drawdown is defined as the one which results in more than 4% reduction in the safety factor of homogeneous soil slopes during reservoir drawdown. Hopefully, this criteria can be adopted in engineering practice.

**In Chapter 6**, the stability of layered rock slopes under reservoir drawdown conditions is studied. These slopes are assumed to contain one group of evenly spaced, parallel and persistent fractures (inter-layers). Due to the presence of the fractures, the transient flow processes in the slopes under drawdown conditions are different from those in the homogenous soil slopes studied in Chapter 5. This chapter conducts a parametric study using the CEM, to specially investigate the influence of various geometric characteristics of the fracture group on transient flow in the layered rock slopes during drawdown. These characteristics include fracture aperture, spacing, and dip angle. Then, the pore-water pressures obtained by transient flow simulations are used as groundwater conditions for slope stability analyses to obtain the variation of the safety factor of the layered rock slopes during drawdown. The investigation results provide quantitative verification of the impact of the reservoir drawdown on the stability of rock slopes with certain geological structure features. Since there are a large number of factors that may control groundwater flow in rock slopes, it is only possible in this work to study one of the simplest rock slope types (i.e., layered rock slope with persistent fractures), and to give a small amount of quantitative verification. However, the methodologies, including the CEM and the combined CEM-LEM analysis approach, are available for further investigations of the stability of complex rock slopes that suffer from the reservoir drawdown conditions.

# Table of Contents

Résumé.....	I
Abstract.....	II
Summary.....	III
Table of Contents .....	VI
List of Tables.....	X
List of Figures .....	XI
Chapter 1 Introduction .....	1
1.1 Introduction and motivation.....	1
1.2 Objectives and scope.....	4
1.3 Outline of thesis .....	5
References.....	7
Chapter 2 Basic Considerations .....	10
2.1 Introduction.....	10
2.2 Flow through single fractures.....	10
2.2.1 Classical cubic law .....	10
2.2.2 Correction of the cubic law .....	11
2.3 Flow in fractured media .....	13
2.3.1 From single fractures to fractured media .....	13
2.3.2 Modelling approaches for flow in fractured media .....	13
2.3.3 The use and weakness of discrete fracture network model .....	14
2.4 Composite element method.....	16
2.4.1 Basic principle of the CEM.....	16
2.4.2 Research progress of the CEM.....	18
2.5 Flow in variably-saturated systems .....	18
2.6 Effects of groundwater on slope stability.....	20
2.6.1 Mechanical action of groundwater .....	20
2.6.2 Softening and erosion actions of groundwater .....	20
2.6.3 Rapid reservoir drawdown .....	20
2.7 Stability analysis methods.....	21



2.7.1 Limit equilibrium methods.....	21
2.7.2 Numerical methods .....	22
2.8 Conclusions.....	23
References.....	25
Chapter 3 Composite Element Method for Modelling Transient, Saturated Flow in Fractured Media with a Free Surface .....	30
3.1 Introduction.....	30
3.2 Mathematical descriptions of transient, saturated flow problem.....	32
3.3 Composite element model construction .....	34
3.3.1 Hydraulic head within composite element.....	34
3.3.2 Composite element formulation .....	35
3.4 Relevant solution algorithms.....	38
3.4.1 CEM pre-processing.....	38
3.4.2 Numerical integral calculation .....	39
3.4.3 Treatment of boundary conditions.....	41
3.4.4 Solving large sparse symmetric equations .....	42
3.5 Verification example .....	42
3.5.1 Flow in a synthetic fractured rock mass.....	42
3.6 Simulations of flow problems in complicated, saturated fractured aquifers .....	48
3.6.1 Flow in a 2D fractured network .....	48
3.6.2 Transient groundwater flow in a rock slope following reservoir rapid impounding .....	50
3.7 Conclusions.....	52
References.....	56
Chapter 4 Composite Element Method for Modelling Transient, Variably-Saturated Flow in Fractured Media .....	58
4.1 Introduction.....	58
4.2 Mathematical descriptions of transient, variably-saturated flow problem .....	59
4.3 Composite element model development .....	60
4.3.1 Constitutive relations for matrix and fractures.....	60
4.3.2 Fracture-matrix interaction area factor.....	62

4.3.3 Composite element formulation .....	62
4.4 Key techniques for improving numerical accuracy and efficiency .....	64
4.4.1 Under-relaxation iteration .....	64
4.4.2 Mass matrix lumping.....	65
4.4.3 Adaptive time stepping.....	65
4.5 Verification examples.....	66
4.5.1 1D infiltration into dry soil.....	66
4.5.2 Flow in a synthetic fractured rock mass .....	67
4.5.3 Vertical drainage of a fractured tuff column.....	67
4.6 Simulation of flow problem in complicated, variably-saturated fractured aquifer .....	72
4.6.1 Transient flow in an aquitard-aquifer system under recharge and pumping .....	72
4.7 Conclusions.....	77
References.....	80
Chapter 5 Investigation of Stability of Homogeneous Soil Slopes Under Drawdown Conditions .....	83
5.1 Introduction.....	83
5.2 Theories and approaches used for this investigation.....	85
5.2.1 Analysis of transient flow in a 2D slope.....	85
5.2.2 Analysis of slope stability with respect to circular sliding .....	86
5.2.3 Design specifications for allowable $SF$ and acceptable reduction in $SF$ .....	88
5.3 Investigation of drawdown in homogeneous soil slopes.....	89
5.3.1 The decline of the free surface within slopes during drawdown.....	90
5.3.2 The variation in $SF$ of slopes during drawdown .....	92
5.3.3 Comparisons between old and new criteria for judging rapid drawdown.....	93
5.4 Charts for quick judgment of rapid drawdown in homogeneous soil slopes.....	95
5.5 Conclusions.....	99
References.....	101
Chapter 6 Investigation of Stability of Layered Rock Slopes Under Drawdown Conditions .....	102
6.1 Introduction.....	102
6.2 Analysis of slope stability with respect to planar sliding .....	103
6.3 Investigation of drawdown in layered rock slopes.....	104
6.3.1 Parameters influencing transient flow in layered rock slopes .....	105

6.3.2 Parameter setting and analysis protocols.....	106
6.3.3 Sensitivity analyses of fracture characteristics.....	107
6.4 Conclusions.....	112
References.....	114
Chapter 7 Conclusions and Recommendations.....	115
7.1 Conclusions.....	115
7.2 Recommendations for future research.....	116

## List of Tables

Table 2.1 Some expressions of $C$ and $b_c$ .....	12
Table 2.2 Advantages and disadvantages of each modelling approach for flow in fractured media (refer to [National Research Council,1996] and [Cook, 2003]) .....	15
Table 2.3 Equilibrium conditions required for each limit equilibrium method [Chen, 2015] .....	22
Table 2.4 Inter-slice force characteristics and relationships for each limit equilibrium method [Chen, 2015] .....	22
Table 3.1 Parameters of four groups of fractures and their probability models .....	51
Table 4.1 Parameters of three groups of fractures and their probability models .....	74
Table 4.2 Tabular data describing the saturation–pressure head and relative permeability–saturation relations .....	75
Table 5.1 Allowable safety factors for slopes at reservoir area [National Development and Reform Commission of P.R. China, 2006] .....	89
Table 5.2 Input parameters for drawdown analyses of homogeneous soil slopes shown in Figures 5.3 and 5.5 .....	90
Table 5.3 Values of $k/(S_y v)$ and $c' / (\gamma H \tan \phi')$ for quick judgment of rapid and slow drawdown in homogeneous soil slopes with different geometrical features .....	97
Table 6.1 Classification of layered rock mass and associated failure mode (referring to [Chen, 2015], and slightly modified) .....	103
Table 6.2 Input parameters for parametric analyses of fracture characteristics shown in Figure 6.3- 6.7 .....	107

## List of Figures

Figure 2.1 Conceptual models of a single fracture: (a) a pair of smooth, parallel plates; and (b) a pair of rough-walled surfaces [Brush, 2001] .....	11
Figure 2.2 Two types of composite elements and their internal sub-elements.....	17
Figure 3.1 Cross section of an unconfined fractured aquifer with four types of boundaries: the prescribed head boundary $\Gamma_1$ , the prescribed flux boundary $\Gamma_2$ , free surface F and seepage face S .....	33
Figure 3.2 A composite element containing four matrix sub-elements and four fracture fragments .....	34
Figure 3.3 Workflow of the pre-processor to insert the fracture surfaces into the generated mesh	39
Figure 3.4 Synthetic fractured rock mass.....	43
Figure 3.5 Two computational meshes respectively used in (a) composite element model, and (b) COMSOL.....	43
Figure 3.6 Evolution of the hydraulic head on the profile $y=5$ m using composite element model in case 1.....	45
Figure 3.7 Comparisons of the hydraulic head distributions along the centerline at different times obtained with (a) composite element model, and (b) COMSOL in case 1.....	46
Figure 3.8 Evolution of the hydraulic head on the profile $y=5$ m using composite element model in case 2.....	47
Figure 3.9 Comparisons of inflow, outflow and drainage fluxes in the domain obtained with (a) composite element model, and (b) COMSOL in case 2.....	48
Figure 3.10 Hydraulic head distribution in the domain after three-year pumping obtained with the composite element model.....	50
Figure 3.11 Fractured rock slope: (a) geometry, and (b) computational mesh.....	51
Figure 3.12 Evolution of the hydraulic head in the fractured rock slope using the composite element model.....	53
Figure 3.13 Groundwater velocity vectors in the fractured rock slope obtained with the composite element model .....	54
Figure 4.1 Distributions of the pressure head along depth at $t=6$ h.....	68
Figure 4.2 Number of iterations in each time step required to achieve convergence.....	68

Figure 4.3 Evolution of the hydraulic head on the profile $y=5$ m using composite element model in case 2 (recalculated by simulating transient, variably-saturated flow) .....	69
Figure 4.4 Comparisons of inflow, outflow and drainage fluxes in the domain obtained with the two composite element models respectively developed in Chapter 3 and in Chapter 4 and COMSOL .....	70
Figure 4.5 A fractured tuff column.....	70
Figure 4.6 Relations between (a) saturation, (b) relative permeability, and (c) effective area factor and pressure head.....	71
Figure 4.7 Variations of the pressure head with time at four given points in (a) case 1, and (b) case 2.....	73
Figure 4.8 A aquitard-aquifer system.....	74
Figure 4.9 Contours of the hydraulic head at $y=45$ m (a) initially, and (b) after 500 d pumping....	77
Figure 4.10 Location of the free surface after 500 d pumping.....	78
Figure 5.1 Forces acting on a slice through the sliding mass enclosed by a circular slip surface...87	
Figure 5.2 A drawdown problem in a homogenous soil slope .....	89
Figure 5.3 The calculated free surfaces at different drawdown levels $H_D/H$ under conditions of $k/(S_y v)=0.1, 1, 10, 100$ and $1000$ .....	91
Figure 5.4 Relation between $k/(S_y v)$ and $(H_D-\Delta H_D)/H_D$ at end of drawdown.....	91
Figure 5.5 Variations of the computed $SF/\tan\phi'$ with $H_D/H$ , under conditions of $k/(S_y v)=0.1, 1, 10, 100$ and $1000$ , when $c'/(\gamma H \tan\phi')=0.137$ .....	93
Figure 5.6 Relation between $k/(S_y v)$ and relative reduction in minimum $SF$ caused by drawdown	94
Figure 5.7 Conditions for rapid and slow drawdown in homogeneous soil slopes with $L/H=1.2$ and $m=2$ .....	94
Figure 5.8 Charts for quick judgment of rapid and slow drawdown in homogeneous soil slopes with different geometrical features.....	97
Figure 6.1 Forces acting on a sliding mass enclosed by a planar slip surface .....	104
Figure 6.2 A drawdown problem in a layered rock slope containing one group of fractures dipping away the slope.....	105
Figure 6.3 Free surfaces and contours of the hydraulic head at end of drawdown in the layered rock slopes with different fracture apertures: (a) $b=12.1 \mu\text{m}$ ; (b) $b=26.1 \mu\text{m}$ ; (c) $b=56.1 \mu\text{m}$ ; and (d) $b=121.0 \mu\text{m}$ .....	108

Figure 6.4 Variations of the computed  $SF/\tan\phi'$  with  $H_D/H$  for the layered rock slopes with different fracture apertures: (a)  $b=12.1 \mu\text{m}$ ; (b)  $b=26.1 \mu\text{m}$ ; (c)  $b=56.1 \mu\text{m}$ ; and (d)  $b=121.0 \mu\text{m}$ ..... 109

Figure 6.5 Free surfaces and contours of the hydraulic head at end of drawdown in the layered rock slopes with different fracture spacings: (a)  $d=1.0 \text{ m}$ ; (b)  $d=2.5 \text{ m}$ ; (c)  $d=5.0 \text{ m}$ ; and (d)  $d=10.0 \text{ m}$  ..... 110

Figure 6.6 Variations of the computed  $SF/\tan\phi'$  with  $H_D/H$  for the layered rock slopes with different fracture spacings: (a)  $d=1.0 \text{ m}$ ; (b)  $d=2.5 \text{ m}$ ; (c)  $d=5.0 \text{ m}$ ; and (d)  $d=10.0 \text{ m}$  ..... 111

Figure 6.7 Free surfaces and contours of the hydraulic head at end of drawdown in the layered rock slopes with different fracture dip angles: (a)  $\psi=30^\circ$ ; (b)  $\psi=40^\circ$ ; (c)  $\psi=50^\circ$ ; and (d)  $\psi=60^\circ$  . 111

# Chapter 1 Introduction

## 1.1 Introduction and motivation

Groundwater flow is a ubiquitous phenomenon in the Earth's crust, and the analysis of this phenomenon plays an important role in solution of many geotechnical problems, especially those concerning the stability analyses of slopes. Compared to that in porous media, flow of groundwater in rocky media (which are usually fractured) is relatively complex. The complexity is mainly resulted from the presence of a large number of fractures and the strong variations in geometric and hydraulic properties, such as fracture aperture, shape, orientation, position, and hydraulic conductivity. Thus, different—though in many cases complementary—theories and methods must be considered. This thesis is aimed at developing a comprehensive numerical method for analyzing groundwater flow in porous media and fractured media. Then, the method is applied to the problem of the stability analyses of soil and rock slopes subjected to groundwater flow, which is the second aim of this thesis.

The modelling is a significant component for understanding the hydraulic behavior of the media. The finite element method (FEM) [Zienkiewicz et al., 1966] is the most commonly used method for flow analysis. According to different ways of fracture simulation, the existing numerical models for solution of flow in fractured media can be grouped into two categories: one is the implicit (continuum) model which takes the impact of fractures into the hydraulic properties of equivalent porous media but ignores their exact positions (e.g. [Barenblatt et al., 1960; Warren and Root, 1963; Snow, 1969; Duiguid and Lee, 1977; Long et al., 1982; Peters and Klavetter, 1988; Narasimhan and Pruess, 1988; Carrera et al., 1990]); the other is the explicit (discrete fracture) model which uses special elements to exactly simulate the geometric and hydraulic properties of fractures (e.g. [Louis, 1972; Schwartz et al., 1983; Andersson et al., 1984; Andersson and Dverstorp, 1987; Cacas et al., 1990; Hyman et al., 2015]). The former can be applied into large-scale engineering problems with a large number of fractures, whereas the latter has the potentiality to describe the fractures in more detail and hence gives more accurate solution.

From the practitioner's point of view, the main difficulty in the explicit simulation of fractures is to generate finite element meshes representing the heterogeneous media, which are used to solve various engineering problems based on the FEM. This arises from two aspects:



- On the one hand, there are a large number of fractures with different sizes and that are interlaced mutually.
- On the other hand, the specific elements representing fractures have definite nodes in their location, and some of these nodes should be the common ones of the surrounding rock elements.

The difficulty, along with complex configuration of geotechnical structures such as dam foundation, rock slope and underground cavern, leads to time-consuming and tedious pre-processing work.

The composite element method (CEM) [Chen et al., 2002] has been proposed to solve the difficulty discussed above, and has been implemented for rock fractures, rock bolts, drainage holes and cooling pipes [Chen and Qiang, 2004; Chen et al., 2004a, 2004b, 2011; Chen and Feng, 2006; Hou et al., 2015]. A prominent feature of the CEM is to place the fractures, or bolts, or drainage holes, or cooling pipes inside the elements. In this way less restraint is imposed on the mesh generation for complicated geotechnical structures with considerable amount of fractures, bolts, drainage holes and cooling pipes. **The first task of this work** is to use the CEM to develop numerical model of groundwater flow in complex fractured media. This model can be placed into a category of the explicit model, because the fractures are explicitly simulated within the composite elements. If there are no fractures, the CEM can be automatically degenerated into the FEM, which is another prominent feature of the CEM, and then, the model can be used to solve flow problems in porous media.

It has been widely recognized that groundwater flow—or specifically speaking, its resulting actions—have a significant effect on the stability of slopes [Hodge and Freeze, 1977]. The pore-water pressure undermines the stability by diminishing the shear strength on the potential slip surface. The pore-water pressure in tension cracks or nearly vertical fissures also reduces the stability by additional slip driving forces. In general, the vast majority of natural slopes have stabilized after long-term geological effects (including long-term steady flow of groundwater). However, when slopes are subjected to surrounding environmental changes, such as rainfall infiltration or reservoir level fluctuation, the pore-water pressures in the slopes will change, thus changing the original balance situation. For a slope originally approaching or being in a limit stability state, this change may cause the instability of the slope. Estimation of pore-water pressures plays an important role in the slope stability analysis.

Landslide induced by rapid drawdown of reservoir is one of the common geological hazards. When the reservoir level is high, the hydrostatic pressures help to stabilize the slope

adjacent to the reservoir. A reduction of the reservoir level has two effects: a decrease in the external stabilizing hydrostatic pressures and a modification of the internal pore-water pressures. If the reservoir level is lowered rapidly, the pore water within the slope cannot drain in time so that the pore-water pressures in the slope still remain high values. This may lead to the temporarily increased hydraulic gradients and cause that the stability of the slope cannot be sustained. Eventually a failure occurs.

Stability analysis of the slope subjected to reservoir's rapid drawdown condition has become one of the most important considerations in the design of embankment dam and the stabilization of reservoir bank slope [National Development and Reform Commission of P.R. China, 2006; U.S. Army Corps of Engineers, 2003]. However, the current stability computations for rapid drawdown condition are mostly based on certain assumptions, thus resulting in insufficient understanding of the impact of reservoir drawdown on the slope stability. The main assumptions and the resulting insufficiency are as follows:

- Firstly, the concept of “sudden drawdown” (or “fully rapid drawdown”) is widely used for slopes with various hydrogeological, and soil and rock conditions [Wright and Duncan, 1987]. The so-called “sudden drawdown” refers to the change in reservoir level happening without allowing the time needed for drainage of slope soils or rocks, and thus the groundwater level or the free surface in the slope maintains the original position. However, the rate of drainage is actually related to the slope material type and the drawdown rate. If the material is a clayed soil with weak permeability or the drawdown rate is relatively fast, the “sudden drawdown” condition will be easy to reach because of poor drainage condition. On the contrary, if the medium is a sandy soil or highly fractured rock with strong permeability or the drawdown rate is relatively slow, the water can readily drain and thus the “sudden drawdown” will not occur. In either cases, the assumption of “sudden drawdown” can lead to conservative evaluation of the stability of slope, which will result in project waste.
- Secondly, even considering the change of the groundwater level in slope during reservoir drawdown, most prior studies simply substitute a hydrostatic distribution of pore-water pressures derived by the groundwater level for a hydrodynamic distribution of pore-water pressures [Rinaldi et al., 2004]. The empirical method [U.S. Army Corps of Engineers, 1970] approximates the height of the free surface by the values of the material hydraulic conductivity, porosity and the drawdown rate. The approximated free surface is then used for constructing the “static” flow

nets and estimating the pore-water pressures. These pore-water pressures may be inaccurate, given that they are changing with the time factor. Moreover, if the hydraulic conductivity of slope material exhibits anisotropy or heterogeneity, this approximation for the free surface as well as the construction for the flow nets would produce bigger error.

- Thirdly, in examining rock slopes containing fractures, the rock masses are frequently assumed as continua similar to the soils, and the flow and stability analysis methods used for soil slopes are applied to the rock slopes. This renders that the influence of the fractures within rock slopes on groundwater flow and the slope stability cannot be reasonably estimated, thus affecting the final evaluation results for the stability.

Based on these considerations, **the second task of this work** is to use the developed numerical model of groundwater flow to accurately estimate the pore-water pressures in soil and rock slopes during reservoir drawdown and thus to make more reasonable evaluation of the stability of the slopes.

## 1.2 Objectives and scope

On impel of the above two motivations, the overall objectives of this work are twofold: (i) to develop the numerical model of groundwater flow in fractured media using the CEM; and (ii) to investigate the stability of soil and rock slopes under reservoir drawdown conditions. In the investigation, groundwater flow in the slopes is simulated by using the numerical model, and then stability analyses are conducted by applying the limit equilibrium method and using pore-water pressure distributions obtained by the flow simulations.

It is worthwhile noting that groundwater flow within the slope subjected to reservoir drawdown condition is actually a transient process. In developing the numerical model of flow in fractured media, special consideration is given to transient groundwater flow problem. Moreover, two kinds of descriptions of transient flow problems are considered: one is of transient, saturated flow with a free surface and the other is of transient, variably-saturated flow. The difference between them is briefly stated as follow:

- In modelling *transient, saturated flow with a free surface*, only the saturated zone is treated and the effect of the unsaturated zone on flow in the saturated zone is approximated by using the concept of delayed yield.

- In modelling *transient, variably-saturated flow*, the saturated and unsaturated zones are simultaneously treated by using the variably-saturated flow equation (i.e. Richards' equation).

Obviously, the latter has a stronger describing ability than the former. However, a common difficulty in treating both zones simultaneously is that a great deal more data, such as capillary pressure characteristics, relative permeability and initial state of saturation, are required for the unsaturated zone than are required for the saturated one. Since such data is often difficult to obtain and most of the engineering problem is primarily concerned with flow in the saturated zone, the analysis of transient, saturated flow with a free surface has obtained more application [Neuman and Witherspoon, 1971]. In investigating the stability of slopes under drawdown conditions, the numerical model developed for transient, saturated flow with a free surface will be employed to estimate the free surface and pore-water pressure distributions within the slopes. In addition, given that increasing attentions are focused on the unsaturated fractured rock recently from the urgent need to safely dispose of radioactive waste, several example problems involving complex fractured aquifers will also be discussed.

### **1.3 Outline of thesis**

This work is subsequently organized as follows:

Following this chapter, chapter 2 considers some basic problems involved in the numerical analyses of groundwater flow in fractured media and its effects on the slope stability. The discussion of these problems provides theoretical basis for subsequent studies.

Chapter 3 develops the numerical model for simulating transient, saturated flow in fractured media with a free surface. The composite element formulation and the solution algorithms are presented. In particular, an iterative scheme is introduced to locate the transient free surface. The effectiveness of this model is verified by a synthetic example and simulations of flow in complicated, saturated fractured aquifers.

Chapter 4 develops the numerical model for simulating transient, variably-saturated flow in fractured media. The constitutive relations for fractures and matrix are first discussed, as well as the fracture-matrix interaction mechanisms in the variably-saturated flow. Then, the composite element formulation are established. To solve the variably-saturated flow equations an iterative scheme is introduced. Finally, verification examples are presented, along with illustrative problems that demonstrate the complexity of variably-

saturated flow in fractured aquifers.

Chapter 5 studies the stability of homogeneous soil slopes under reservoir drawdown conditions. The numerical model for transient, saturated flow with a free surface is used to calculate the transient free surface and pore-water pressure distributions in the slopes during drawdown. Using the pore-water pressure distributions as input groundwater conditions, the stability analyses are performed to derive the variations of the safety factor of slopes. The influences of various factors, including the drawdown rate, hydraulic and strength parameters of the soils and slope geometry on transient flow and the stability of homogeneous soil slopes, are investigated in detail. As a result, quantitative relationships between the drawdown condition and its resulting slope behaviors are established.

Chapter 6 studies the stability of layered rock slopes under reservoir drawdown conditions. Due to the presence of the fractures, the transient flow in the rock slopes is different from that in homogeneous soil slopes. A parametric study is conducted using the CEM in order to specially investigation the influence of fracture characteristics on transient flow processes as well as pore-water pressure distributions within the layered rock slope subjected to drawdown conditions. The stability analyses of the slopes are subsequently performed to determine the variations of the safety factor during drawdown.

Finally, conclusions from the conducted studies and recommendations for future research are presented in Chapter 7.

## References

1. Andersson J, Dverstorp B. Conditional simulations of fluid flow in three-dimensional networks of discrete fractures. *Water Resources Research* 1987; **23**(10): 1876–1886.
2. Andersson J, Shapiro AM, Bear J. A stochastic model of a fractured rock conditioned by measured information. *Water Resources Research* 1984; **20**(1): 79–88.
3. Barenblatt GI, Zheltov IP, Kochina IN. Basic concepts in the theory of seepage of homogenous liquids in fissured rocks. *Journal of Applied Mathematics and Mechanics* 1960; **24**(5):1286–1303.
4. Cacas MC, Ledoux E, Marsily GD, Tillie B, Barbreau A, Durand E, Feuga B, Peaudecerf P. Modeling fracture flow with a stochastic discrete fracture network: calibration and validation, 1. The flow model. *Water Resources Research* 1990; **26**(3): 479–489.
5. Carrera J, Heredia J, Vomvoris S, Hufschmied P. Modeling of flow on a small fractured monzonitic gneiss block. *Hydrogeology of Low Permeability Environments* 1990; **2**: 115–167.
6. Chen SH, Egger P, Migliazza R, Giani GP. Three dimensional composite element modeling of hollow bolt in rock masses. In *Proceedings of the ISRM international symposium on rock engineering for mountainous regions - Eurock 2002*, Gama CD, Sousa LR (eds). International Society for Rock Mechanics, 2002; 25–28.
7. Chen SH, Feng XM. Composite element model for rock mass seepage flow. *Journal of Hydrodynamics* 2006; **18**(2): 219–224.
8. Chen SH, Qiang S. Composite element model for discontinuous rock masses. *International Journal of Rock Mechanics and Mining Sciences* 2004; **41**(5): 865–870.
9. Chen SH, Qiang S, Chen SF, Egger P. Composite element model for the fully grouted rock bolt. *Rock mechanics and rock engineering* 2004a; **37**(3): 193–212.
10. Chen SH, Su PF, Shahrour I. Composite element algorithm for the thermal analysis of mass concrete: simulation of cooling pipes. *International Journal of Numerical Methods for Heat and Fluid Flow* 2011; **21**(4): 434–447.
11. Chen SH, Xu Q, Hu J. Composite element method for seepage analysis of geotechnical structures with drainage hole array. *Journal of Hydrodynamics* 2004b; **16**(3): 260–266.
12. Duguid JO, Lee PCY. Flow in fractured porous media. *Water Resources Research* 1977; **13**(3): 558–566.
13. Hodge RA, Freeze RA. Groundwater flow systems and slope stability. *Canadian*

- Geotechnical Journal* 1977; **14**(4): 466–476.
14. Hou XP, Xu Q, He J, Chen SH. Composite element algorithm for unsteady seepage in fractured rock masses. *Chinese Journal of Rock Mechanics and Engineering* 2015; **34**(1): 48–56.
  15. Hyman JD, Karra S, Makedonska N, Gable CW, Painter SL, Viswanathan HS. dfnWorks: A discrete fracture network framework for modeling subsurface flow and transport. *Computers and Geosciences* 2015; **84**: 10–19.
  16. Long JCS, Remer JS, Wilson CR, Witherspoon PA. Porous media equivalents for networks of discontinuous fractures. *Water Resources Research* 1982; **18**(3): 645–658.
  17. Louis C. Rock hydraulics. In *Rock mechanics*, Muller L (ed). Springer-Verlag: New York, 1972.
  18. Narasimhan TN, Pruess K. MINC: an approach for analyzing transport in strongly heterogeneous systems. In *Groundwater flow and quality modelling*, Custodio E, Gurgui A, Ferreira JL (eds). D. Reidel Publishing Company: Boston, 1988.
  19. National Development and Reform Commission of P.R. China. Design specification for slope of hydropower and water conservancy project, DL/T 5353-2006. China Electric Power Press: Beijing, 2006.
  20. Neuman SP, Witherspoon PA. Analysis of nonsteady flow with a free surface using the finite element method. *Water Resources Research* 1971; **7**(3): 611–623.
  21. Peters R, Klavetter EA. A continuum model for water movement in an unsaturated fractured rock mass. *Water Resources Research* 1988; **24**(3): 416–430.
  22. Rinaldi M, Casagli N, Dapporto S, Gargini A. Monitoring and modelling of pore water pressure changes and riverbank stability during flow events. *Earth Surface Processes and Landforms* 2004; **29**(2), 237–254.
  23. Schwartz FW, Smith L, Crowe AS. A stochastic analysis of macroscopic dispersion in fractured media. *Water Resources Research* 1983; **19**(5): 1253–1265.
  24. Snow DT. Anisotropy permeability of fractured media. *Water Resources Research* 1969; **5**(6): 1273–1289.
  25. U.S. Army Corps of Engineers. Engineering and design stability of earth and rock-fill dams, EM 1110-2-1902. Department of the Army Corps of Engineers: Washington, 1970.
  26. U.S. Army Corps of Engineers. Engineering and design slope stability, EM 1110-2-1902. Department of the Army Corps of Engineers: Washington, 2003.
  27. Warren JE, Root PJ. The behavior of naturally fractured reservoirs. *Society of Petroleum Engineers Journal* 1963; **3**(3): 245–255.

28. Wright SG, Duncan JM. An examination of slope stability computation procedures for sudden drawdown. Waterway Experiment Station: Vicksburg, 1987.
29. Zienkiewicz OC, Mayer P, Cheung YK. Solution of anisotropic seepage by finite elements. *Journal of the Engineering Mechanics Division* 1966; **92**(1): 111–120.



## Chapter 2 Basic Considerations

### 2.1 Introduction

This chapter considers some basic problems involved in the analyses of groundwater flow in fractured media and its effects on slope stability. In the aspect of the groundwater flow in fractured media, four key issues are examined. They are: (i) flow through single fractures; (ii) flow in fractured media; (iii) composite element method; and (iv) flow in variably-saturated systems. In the aspect of the effect of groundwater flow on slope stability, two following issues are examined: (i) effects of groundwater on slope stability; and (ii) stability analysis methods. For each of these issues, a brief description is provided, as well as the existing research findings. In addition, at the end of the examination on each issue, it will be answered that “how this work will take into account or deal with this issue?”.

### 2.2 Flow through single fractures

#### 2.2.1 Classical cubic law

A single fracture is the basic element of a fracture system, hence the analysis of flow in fractured media must begin with that of flow through a single fracture. The classical view of a single fracture considers a pair of smooth, parallel plates, as shown in Figure 2.1(a). From the Navier-Stokes equations for slow, non-turbulent flow of an incompressible Newtonian fluid, equation has been derived by Snow [1969] for the volumetric flow through unit width of the smooth, parallel-plate fracture,  $q_f$ , that is:

$$q_f = \frac{\gamma_w b^3}{12\mu} J \quad (2.1)$$

where  $b$  is the fracture aperture,  $\gamma_w$  is water unit weight,  $\mu$  is the viscosity of water and  $J$  is the hydraulic gradient. Equation (2.1) is referred to as the cubic law, because the volumetric flow is proportional to the cube of the fracture aperture. Clearly, the cubic law is only applicable to the case of slow laminar flow. In case that flow be non-linear or turbulent, Equation (2.1) will no longer be applicable.

According to the cubic law and Darcy's law which relates the flow rate to the hydraulic conductivity and the hydraulic gradient, the hydraulic conductivity for a single smooth, parallel-plate fracture,  $k_f$ , can be given by:

$$k_f = \frac{\gamma_w b^2}{12\mu} \quad (2.2)$$

### 2.2.2 Correction of the cubic law

The parallel-plate model and the cubic law are attractive in predicting flow through fractures, due to the inherent simplicity. However, natural fractures often have rough walls and variable apertures that control flow and distribution of water in fracture surface, as shown in Figure 2.1(b). If the cubic law is applied to these fractures, it needs to be corrected to include the impact of the roughness.

Many researchers have proposed their own corrected formulas by experimental or theoretical research [Lomize, 1951; Louis, 1969; Neuzil and Tracy, 1981; Tsang and Witherspoon, 1981, 1983; Barton et al., 1985; Brown, 1987]. In these formulas, the cubic law's accuracy is improved by either incorporating a correction factor  $C$  or utilizing a hydraulically equivalent fracture aperture  $b_c$ , as follows:

$$q_{fc} = \frac{\gamma_w b^3}{12\mu C} J \quad \text{or} \quad q_{fc} = \frac{\gamma_w b_c^3}{12\mu} J \quad (2.3)$$

Due to the diversity of fracture rough walls and the difference between experimental conditions, the corrected formulas of the cubic law proposed are different, and they have some certain one-sidedness in analyzing flow in single rough-walled fractures. In table 1.1, there is a list of some results of  $C$  and  $b_c$  expressions.

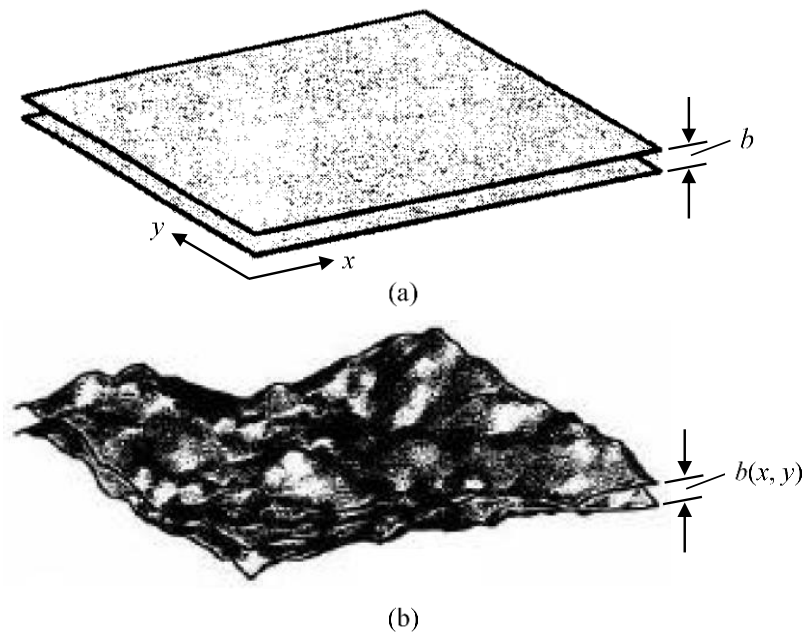


Figure 2.1 Conceptual models of a single fracture: (a) a pair of smooth, parallel plates; and (b) a pair of rough-walled surfaces [Brush, 2001]

Table 2.1 Some expressions of  $C$  and  $b_c$

Author	Expression of $C$ or $b_c$	Statement
Lomize [1951]	$C = 1 + 6.0(e / b_{\max})^{1.5}$	$e$ : absolute asperity height
Louis [1969]	$C = 1 + 8.8(e / 2b_{\max})^{1.5}$	$b_{\max}$ : maximum aperture
Neuzil and Tracy [1981]	$b_c^3 = \int_0^{\infty} b^3 f(b) db$	$f(b)$ : probability density function of
Tsang and Witherspoon [1981]	$b_c^3 = \int_0^{b_{\max}} b^3 f(b) db / \int_0^{b_{\max}} f(b) db$	aperture
Brown [1987]	$b_c = \bar{b} \sqrt{1 - 0.9 \exp(-0.56/C_v)}$	$\bar{b}$ : mean aperture $C_v$ : variable coefficient of aperture
Barton et al. [1985]	$b_c = b_m^2 / \text{JRC}^{2.5}$	$b_m$ : mechanical aperture JRC: joint roughness coefficient

Another approach to improve the cubic law's accuracy is to consider explicitly the spatial variability in aperture that results in what is known as the local cubic law [Zimmerman et al., 1991; Nicholl et al., 1999; Wang et al., 2015]. The local cubic law represents the latest development level of investigation of flow in rough-walled fractures. From the local cubic law, the volumetric flow through a single fracture varies as the cube of the fracture aperture. It has been postulated by majority of theoretical and numerical studies of single fracture flow that local flow magnitudes are well described by the Reynolds equation [David, 1993; Unger and Mase, 1993; Brown et al., 1995; Mourzenko et al., 1995], which implies that local flow magnitudes are proportional to the cube of the local aperture; and hence the name "local cubic law". However, several recent simulation studies have indicated that the local cubic law assumption might be wrong in many cases. Moreover, even if the local cubic law is adequate, it is not clear how the aperture to be used for this estimate should be measured [Berkowitz, 2002].

For both approaches, the measurement of the fracture aperture is necessary. For a single fracture used for experimental research, Hakami and Barton [1991], Hakami and Larsson [1996] and Detwiler et al. [1999] employed the transparent replicas of single fractures, and measured the aperture by the techniques of injection of fluorescent epoxy or transmitted light. Yet, these techniques are difficult to implement for measurement of the fracture aperture in situ. , the concepts of mean aperture, mechanical aperture and hydraulically equivalent aperture are proposed, as used in the corrected cubic law in Table 2.1. The laboratory or field hydraulic tests are often carried out for actual fractures. After obtaining the volumetric flow, the fracture aperture can be reversely determined according to the cubic

law, which is considered as the hydraulically equivalent aperture. This hydraulically equivalent aperture is not the real fracture aperture, but it reflects the impact of the fracture wall roughness on the discharge capacity of single fracture at a deeper level.

*In this work, fracture will be treated as a medium with the hydraulic conductivity obtained by Equation (2.2), using the hydraulically equivalent aperture.*

## **2.3 Flow in fractured media**

### **2.3.1 From single fractures to fractured media**

In Section 2.2, single fracture flow equations have been established. Consider a group of evenly spaced, parallel and identical fractures of infinite length in a matrix block. The flow magnitude through the fractured media in the direction parallel to fractures can be derived by summation of contributions from fractures and matrix (assuming that the matrix is permeable). Since the hydraulic conductivity for individual fractures is generally much higher than that for the matrix, flow through the fractured media occurs mainly along fractures. However, as the number of fractures increases and the distribution of fractures becomes irregular, zones of high and low fracture density will develop, resulting in great variation in hydraulic conductivity for the media. Such variation is due to spatial variations in fracture aperture, density, length, and fracture connectivity, and of course difference in conductivities of the fractures and the matrix. This eventually leads to a high heterogeneity, increasing difficulty of analysis of flow in fractured media.

### **2.3.2 Modelling approaches for flow in fractured media**

This section describes the main approaches used for modelling groundwater flow in fractured media. Clearly, the main issue is how to describe the heterogeneity associated with fractures. A number of modelling approaches exist, but most can be divided into three types: the equivalent porous media approach, the dual porosity approach, and the discrete fracture network approach. In the equivalent porous media approach, hydraulic properties of the fractured media are modelled using equivalent coefficients such as hydraulic conductivity and specific storage, and effective porosity to represent the volume-averaged behavior of many fractures within a rock mass. Thus, the details of individual fractures need not be known. This is in direct contrast to the discrete fracture network approach where the details of individual fractures are explicitly accounted for. In the dual porosity approach, equivalent porous media properties are separately assigned for fracture and matrix, and an exchange

function based on a simplified fracture geometry is used for transfer of water between the two porous media. The former two approach can be placed into a category of the implicit approach because individual fractures are not explicitly treated in both approaches; in contrast, the latter can be placed into a category of the explicit approach. Table 2.2 provides a concise summary of the advantages and disadvantages of each approach. It draws on discussions presented by National Research Council [1996] and Cook [2003], both of which make more exhaustive summaries of this topic.

In conclusion, each modelling approach has its own advantages and limitations. When deciding which approach to be taken, one should consider the three key factors: (i) whether the study is concerned with bulk flow; (ii) the steady or transient nature of the problem; and (iii) the scale of interest (local or regional). For flow problems concerned with bulk average volumetric behavior over larger scales, an equivalent porous media approach will usually suffice. The approach works best for steady flow systems, whereas it is inadequate for transient systems. This is because of the assumption that the flow dynamics between fractures and matrix are locally at equilibrium, and that does not match the fact that differences in the hydraulic properties of fractures and matrix can cause different response times to transient process. A dual porosity approach accounts for the disequilibrium by allowing water exchange between matrix and fracture. However, a subject of debate using this approach is how to define the exchange function representing water transfer between porous media, which strongly affects the modelling results [Huyakorn et al., 1983]. Difficulties in both the approaches can arise when working at local scales where important fractures controlling the flow system are not explicitly included in the modelling. In such cases, a discrete fracture network model may be employed as the smaller scale of the study usually permits the conducting fractures to be identified and explicitly included in the model.

### **2.3.3 The use and weakness of discrete fracture network model**

So far, the discrete fracture network model has been well developed and has gradually become an indispensable model for analyzing flow in fractured media. The discrete fracture network model can be used not only to improve our understanding of the flow dynamics in fractured media [Wang and Narasimhan, 1985], but also to derive equivalent hydraulic parameters required in continuum modelling based upon the explicit characterization of fractures [Finsterle, 2000; Wang et al., 2002; Chen et al., 2008; He et al., 2013]. Nevertheless, the use of this model has a major weakness: it requires an accurate representation of the geometry of fractures. This weakness is particularly striking in

Table 2.2 Advantages and disadvantages of each modelling approach for flow in fractured media (refer to [National Research Council,1996] and [Cook, 2003])

Model type	Advantages	Disadvantages
Equivalent porous media	(i) Simplest approach with lowest data requirements;	(i) Limited application to transient flow problems;
	(ii) If desired, high fracture density zones can be simulated as zones with higher porosity and hydraulic conductivity;	(ii) Assumes that REV <sup>†</sup> can be defined. Reliable predictions can only be made at scales greater than or equal to the scale of the assumed REV. Determination of the hydraulic parameters at these scales can be difficult.
	(iii) Most suitable for large-scale applications of steady flow.	(i) Tendency to over regularize and simplify the geometry;
Dual porosity	(i) Suitable for systems where matrix has high porosity and permeability;	(ii) Difficult to quantify the parameters needed as input to this model;
	(ii) Allows water exchange between fractures and matrix;	(iii) Needs to define an exchange function accounting for water transfer between porous media;
	(iii) Can account for different hydraulic responses in fractures and in matrix caused by transient changes.	(iv) Assumes that REV can be defined. Reliable predications can only be made at scales greater than or equal to the scale of the assumed REV.
Discrete fracture network	(i) Explicit representation of individual fractures and fracture flow;	(i) Requires the most detailed field knowledge;
	(ii) May allow flow in matrix and water exchange between matrix and fractures;	(ii) Requires powerful computational power to analyze complex fractured media, including to discretize the complex fractured areas and to solve equations with tens to hundreds of thousands of unknowns.
	(iii) Good for conceptual process understanding;	
	(iv) Useful in determining equivalent continuum parameters based upon explicit characterizations.	

<sup>†</sup>REV is a contraction of representative elementary volume.

analyzing complex, irregular domains and complicated fracture networks. Different representation approaches have been used in past studies of flow in discretely-fractured

media. A brief discussion of the existing approaches and their problems is stated in the following paragraph.

The matrix is assumed to be impermeable in some studies [Cacas et al., 1990; Mustapha and Mustapha, 2007], where flow only takes place along one-dimensional (1D) intersections of two-dimensional (2D) fractures. An impermeable matrix simplifies the fracture discretization because only the 2D fractures require discretization. However, the low-permeability matrix cannot be neglected in many cases, especially for studies involving solute transport. Therrien and Sudicky [1996] introduced a discretization approach for three-dimensional (3D) fractured media. The approach discretized the fractures by using 2D elements and discretized the matrix by using 3D elements. These 2D fracture element must be faces of neighboring matrix elements. This discretization is meaningful for simulation of flow in fractured media, because the common node approach ensures the continuity of hydraulic head at the fracture-matrix interface and no leakage terms are required to account for water exchange between fractures and matrix. Graf and Therrien [2008] developed a technique to realize such a discretization. With this technique, the matrix was first discretized into tetrahedrons, and then the embedded fractures were approximated by the faces of the tetrahedrons. However, this technique requires considerable transformations of the fractures in order to reduce complex configurations. Recently, a new and more efficient method to discretize 3D fractured media was proposed by Mustapha et al. [2011]. Using this method, the fractures were first discretized into a 2D finite element mesh with triangles and then tetrahedron elements representing matrix were generated to fill the 3D domain surrounded by the faces of the fracture elements. Unfortunately, this method still could not change the fact that the complex geometry of fractures greatly limits the mesh division.

*For the purposes of this work, the discrete fracture network model is selected, and the composite element method that requires less restraint on the mesh generation for complex fractured media will be used to realize this model.*

## **2.4 Composite element method**

### **2.4.1 Basic principle of the CEM**

The CEM is a new numerical method, developed from the FEM. In the FEM, each element represents only one material. For heterogeneous areas with multiple materials, the corresponding finite elements must be set on different material areas, which is inconvenient for mesh division. For example, if the rocks contain large numbers of fractures, or anchors,

or drainage holes, or cooling pipes, the difficulty of mesh dividing and the pre-processing workload will drastically increase. The CEM overcomes this inconvenience by setting the embedded sub-elements. In the CEM, a heterogeneous area is treated as a homogenous area for meshing. Then the generated mesh certainly will have a number of elements that contain multiple materials. For elements that contain only one material, they are ordinary finite elements and can also be considered as degraded composite elements. For elements that contain more than one materials, they are defined as composite elements, and each material area within the composite elements is defined as a sub-element. The composite element consists of multiple sub-elements and the interfaces between them.

Figure 2.2 shows two types of composite elements. In Figure 2.2(a), a closed area contained within the element is defined as a sub-element, denoted as Sub-element 1. The area in which Sub-element 1 is removed from the element is defined as another sub-element, denoted as Sub-element 2. Two sub-elements are linked through the interface. This type element is typical of an element containing an anchor bolt, or a drainage hole, or a cooling pipe. In Figure 2.2(b), a composite element is divided into four sub-elements due to the insertion of two fractures. Four sub-elements are mutually independent, and neighboring sub-elements are linked through the fracture interfaces between them. It needs to be pointed out that these two composite elements have the same outer contours as the finite elements, but their internal sub-elements can have any shapes.

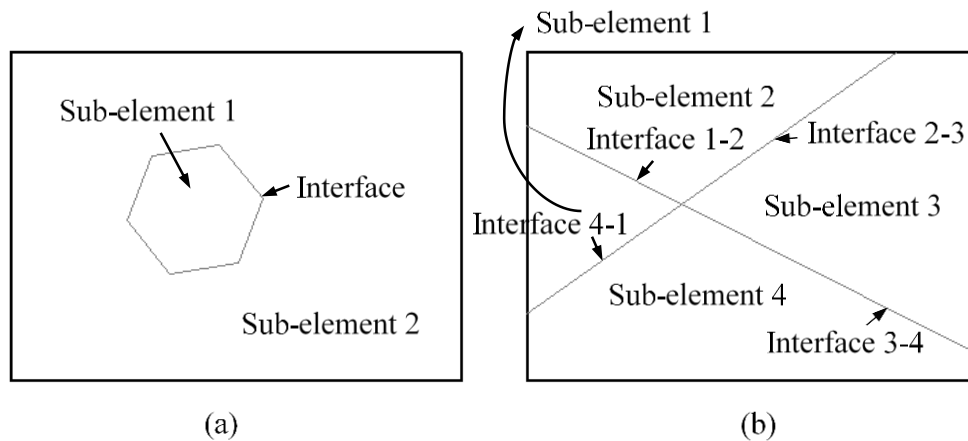


Figure 2.2 Two types of composite elements and their internal sub-elements

Theoretically, the number of sub-elements in a composite element is unlimited. For a composite element containing  $l$  sub-elements, it will be assigned to  $l$  sets of nodal variables (which refer to nodal displacements in stress-strain analysis, nodal temperatures in thermal analysis, and nodal hydraulic heads in flow analysis). Variables within each sub-element are defined by interpolation, using nodal variables of the sub-element and shape function



associated with these nodes. Variables within each interface are defined by using the variables of two adjacent sub-elements, and ensuring the continuity of the variables between the two sub-elements as well as the conservation of energy. According to the variational principle, the governing equations for each sub-element and each interface within the composite element can be derived separately. Then, these equations are integrated together to form a unified equation for the whole composite element. Solving the composite element equation means implementing simulations of all internal sub-elements and interfaces.

#### **2.4.2 Research progress of the CEM**

The CEM has been successively used for the stress-strain, thermal and flow analyses. Here are some of the existing research progress with breakthroughs. The stress and deformation of the rock mass reinforced with mortar anchor was the first to use CEM for analysis [Chen et al., 2003]. Within a composite element, the anchor bolt, the mortar and the rock were denoted by three sub-elements, respectively. The anchor—mortar contact surface and the rock—mortar contact surface were denoted by two interfaces, respectively. Through these sub-elements and interfaces, mechanical behaviors of the corresponding media and contact surfaces were accurately simulated. Chen and Qiang [2004] developed the composite element method for analyzing the stress and strain of fractured rock mass. The rock sub-elements within composite elements, formed by the incision of fractures, could have any shapes. The elasto-viscoplastic deformation of these rock sub-elements and the fracture interfaces was simulated explicitly within the composite elements. Since the cooling pipe and the drainage hole are cylindrical media similar to the anchor bolt, Chen et al. [2011] presented the composite element model for simulating the temperature field in mass concrete structure with cooling pipes; Chen et al. [2004] presented the composite element model for simulating the flow field in dam with drainage holes. Chen and Feng [2006] and Chen et al. [2010] then applied the CEM to the analysis of flow in fractured rock mass. However, their work was limited to simulation of steady, saturated flow and only simple situations where fractures are either small in number or regularly distributed were involved.

*This work continues to develop the CEM in order to analyze transient, saturated and transient, variably-saturated flow in complex, fractured media.*

### **2.5 Flow in variably-saturated systems**

The current understanding of flow processes in the fractured unsaturated zone is

limited [Hendrickx and Flury, 2001]. The difficulty inherent in measuring hydraulic properties in an unsaturated fracture has resulted in a paucity of experimental data at the fracture scale. Detailed measurements of flow through unsaturated fracture replicas [Su et al., 1999] have demonstrated the highly variable nature of the flow system dynamics in both time and space. Under partially saturated conditions, there are complex relationships between pressure, saturation and hydraulic conductivity in both the matrix and the fracture network. As a result, fractures could serve as either preferential flow pathways or as capillary barriers in the unsaturated zone [Wang and Narasimhan, 1985], depending on saturation conditions. It is therefore difficult to distinguish whether the matrix or the fractures represent the predominant flow system. In addition, given the relatively large porosity and small pore sizes in the matrix compared to the fracture, there is the potential for significant imbibition of water from the fractures into the matrix in variably-saturated flow process. The varying hydraulic properties of the matrix and fractures create a dynamic system with the fracture-matrix interaction.

Valuable insight into the hydraulic behavior of the fractured media has been derived through the use of numerical modelling tools [Kwicklis and Healy, 1993; Simunek et al., 2003; Cey et al., 2006]. Wang and Narasimhan [1985] developed a numerical model to simulate variably-saturated flow in discretely-fractured geologic material. They used the integrated finite-difference technique to solve for the drainage of a regularly fractured matrix block in three dimensions. They assumed that the fractures are rough-walled, with variable apertures characterized by a gamma probability distribution. The fracture walls were taken to be in contact when the aperture at any point in the fracture plane was smaller than a defined cutoff aperture. Effective, macroscale constitutive relationships for fracture saturation, permeability and contact area as functions of pressure head were then developed based on the aperture probability distribution function and the fact that the portions of the fractures with apertures larger than the saturation cutoff aperture would be dry. Flow along the fractures was described by a generalized cubic law and a phase-separation constriction factor was used to represent the resistance to flow caused by entrapped air. Richards' equation and Van Genuchten [1980] relationships were used to describe the flow in the matrix. Other studies that considered variably-saturated flow include those of Dykhuizen [1987] and Peters and Klavetter [1988] who developed numerical models based on the double porosity conceptualization, Therrien and Sudicky [1996] who presented a numerical model based on the discrete fracture network conceptualization, and Nitao and Buscheck [1991] who presented an analytical solution where matrix imbibition is treated as a 1D

process.

*This work aims to present a new numerical model based on the CEM and the discrete fracture network conceptualization, for the solution of variably-saturated groundwater flow in fractured media.*

## **2.6 Effects of groundwater on slope stability**

### **2.6.1 Mechanical action of groundwater**

The critical role that groundwater plays in the stability of slopes was recognized by Terzaghi [1923] in his effective stress law. He showed that the relationship between the presence of groundwater and the strength of many natural materials could be expressed in a modified form of Coulomb's law:

$$\tau = c' + \sigma_e \tan \varphi' \quad (2.4)$$

where

$$\sigma_e = \sigma_t - u \quad (2.5)$$

and  $\sigma_e$  is effective stress,  $\sigma_t$  is total stress,  $u$  is pore-water pressure,  $\tau$  is shear strength,  $c'$  is effective cohesion,  $\varphi'$  is effective angle of internal friction.

It is clear from Equations (2.4) and (2.5) that a slope stability analysis carried out in terms of effective stress requires an understanding of the distribution of the pore-water pressures in the slope, and this understanding implies a knowledge of the groundwater flow system.

### **2.6.2 Softening and erosion actions of groundwater**

Groundwater may have softening and erosion actions on slope soil or rock. On the one hand, the cohesion degree between particles as well as the friction coefficient may decrease under water lubrication, which reduces the shear strength. On the other hand, a circulating water flow in the slope may develop in response to repeated changes in the external environment, probably causing lixiviation of fine particles. This may eventually result in local instability where the toe of slope is undermined, or a block of rock is loosened.

### **2.6.3 Rapid reservoir drawdown**

Reservoir bank slopes and embankment dams may become saturated by water flow during prolonged high reservoir stages. If subsequently the reservoir level is drawn down faster than pore water can escape, unbalanced seepage forces result. Stability analyses are

routinely performed to calculate the safety factor of slopes subjected to this condition. In general, analyses for this condition are based on the conservative assumptions that: (i) the reservoir level is lowered instantaneously from the maximum to minimum pool elevation; (ii) little or no drainage occurs in the slopes while the reservoir level is being lowered. The condition that meet these two assumptions is called “sudden drawdown”. Where sudden drawdown assumption appears to be excessively conservative, considering possible drawdown rate and the permeability of proposed slope materials, analyses for relatively incompressible materials may be performed for expected drawdown rate and pore-water pressures determined from flow analyses to evaluate effective stresses.

*This work is intended to present a detailed discussion on the effects of various drawdown conditions on groundwater flow systems and slope stability. The mechanical action of groundwater, in the form of pore-water pressures, will be taken into account. The softening and erosion actions of groundwater will not be taken into account.*

## **2.7 Stability analysis methods**

### **2.7.1 Limit equilibrium methods**

Limit equilibrium methods are widely used for slope stability analysis, which looks at the sliding mass as a rigid body passing forces without deformation [Chen, 2003; Chen et al., 2005]. Based on the equilibrium conditions with respect to forces and/or moments, the reaction forces on the slip surfaces and the corresponding safety factor which represents the ratio between the driving and resisting forces can be computed. The major advantages with the limit equilibrium methods are simplicity in computation algorithm, full of experiences in parametric evaluation, and the selection of allowable safety factor. One of the major disadvantages with the limit equilibrium methods is that the deformation that in some situations could be important cannot be obtained.

Basically, the limit equilibrium analysis methods fall into two main categories: methods that deal with structurally controlled planar or wedge slides and methods that deal with circular or nearly circular failure surfaces in “homogeneous” materials. Many of these methods have been practiced for many years and can be convinced as reliable. Table 2.3 lists the limit equilibrium methods and indicates what equilibrium conditions are required for each method. Table 2.4 gives a summary of the inter-slice forces included and the assumed relationships between the inter-slice shear and normal forces. The variants of limit equilibrium methods listed in Table 2.3 (or Table 2.4) may be selectively employed with

regard to the following considerations: (i) for nearly homogenous slopes, the theoretic and experimental studies show that the most dangerous slip surface is nearly circular, and the safety factor is not sensitive when the failure surface has small deviation from the arc, and therefore, the circular slip surface may be assumed and the classical Swedish arc method or the Bishop method may be employed; (ii) for slopes dominated by discontinuities, the slip surface is usually multi-planar or curvilinear; the residual thrust method, the Sarma method, the Bishop method, and the Janbu method may be exercised [Chen, 2015].

Table 2.3 Equilibrium conditions required for each limit equilibrium method [Chen, 2015]

Method	Overall			Slice	
	Moment	Vertical force	Horizontal force	Moment	Force
Sweden arc	Yes	Yes	No	No	Yes
Bishop	No	No	Yes	No	Yes
Simplified Bishop	Yes	No	No	No	Yes
Janbu	No	No	Yes	Yes	Yes
Residual thrust method	No	No	No	No	Yes
Morgenstern-Price	Yes	Yes	Yes	Yes	Yes
Spencer	Yes	Yes	Yes	Yes	Yes
Sarma	No	No	No	No	Yes

Table 2.4 Inter-slice force characteristics and relationships for each limit equilibrium method [Chen, 2015]

Method	Inter-slice shear ( $X$ )	Inter-slice normal ( $E$ )	Inclination of $X/E$ resultant, and $X-E$ relationship
Sweden arc	No	No	No inter-slice forces
Bishop	No	Yes	Horizontal
Simplified Bishop	No	Yes	Horizontal
Janbu	Yes	Yes	Applied line of thrust and moment equilibrium of slice
Residual thrust method	Yes	Yes	Inclination of the bottom slip surface of the upper slice
Morgenstern-Price	Yes	Yes	Variable; user function
Spencer	Yes	Yes	Constant
Sarma	Yes	Yes	$X=c'+E\cdot\tan\phi'$

## 2.7.2 Numerical methods

Recently, numerical methods for slope stability analysis have become prevalent.

Methods, such as FEM, discrete element method, discontinuous deformation method, block element method and numerical manifold method, are used for such modeling. The advantage of numerical modeling over the limit equilibrium modeling is that it can be used to simulate progressive failure and ongoing displacement in addition to simple factor of safety [Chen 2006; Zhou et al. 2007]. Numerical modeling also can be used to determine the factor of safety of a complex slope in which a number of failure mechanisms (modes) can exist simultaneously or where the mechanism of failure may change as progressive failure occurs. However, realistic input information for numerical model and correct interpreting the output results are paramount for the successful computation in the context of large-scale slopes, which require well-trained skills and full understanding of the slopes concerned.

*In this work, the simplified Bishop method will be employed to compute the safety factor of homogenous slopes against circular sliding; and the Janbu method will be employed to compute the safety factor of layered slopes against planar sliding.*

## **2.8 Conclusions**

This chapter has discussed some basic problems involved in the analyses of groundwater flow in fractured media and its effects on slope stability. In the aspect of the groundwater flow in fractured media,

- First, the basic law of single fracture flow which is known as the classical cubic law, and two approaches to improving the cubic law's accuracy are introduced. The generalized cubic law based on the concept of a hydraulically equivalent fracture aperture is used more in analysis of single fracture flow. By combining the generalized cubic law with Darcy's law, the hydraulic conductivity for single fractures can be derived.
- Then, three classes of modelling approaches for flow in fractured media are expounded respectively, as well as their advantages and limitations. Compared with the continuum approaches, the discrete fracture network model has the potentiality to describe the fractures in more detail, so it is more suitable for the development of understanding of the flow dynamics in fracture-matrix systems. However, the use of this model requires to overcome a difficulty in discretization of the fractured media. The CEM employed in this thesis can well solve this difficulty.

- Next, the basic principles and the research progress of the CEM are discussed. It is particularly pointed out that the CEM has not yet been used to solve transient, saturated or variably-saturated flow problems in complex fractured media.
- Finally, the characteristics of flow in the unsaturated zone which can be different from those in the saturated zone are briefly described, as well as some recent research achievements.

In the aspect of the effect of groundwater flow on slope stability,

- First, three actions of groundwater, including mechanical, softening and erosion, are briefly described. Particular mention is made of the importance of rapid drawdown condition to slope stability analysis.
- Then, the limit equilibrium methods and numerical methods for stability analysis are introduced respectively. The limit equilibrium methods have been widely used because of the simplicity in computation algorithm

The discussion of these problems provides theoretical bases for subsequent studies.

## References

1. Barton N, Bandis S, Bakhtar K. Strength, deformation and conductivity coupling of rock joints. *International Journal of Rock Mechanics and Mining Sciences, Geomechanics Abstracts* 1985; **22**(3): 121–140.
2. Berkowitz B. Characterizing flow and transport in fractured geological media: a review. *Advances in Water Resources* 2002; **25**: 861–884.
3. Brown SR. Fluid flow through rock joints: the effect of surface roughness. *Journal of Geophysical Research: Solid Earth* 1987; **92**(B2): 1337–1347.
4. Brown SR, Stockman HW, Reeves SJ. Applicability of the Reynolds equation for modeling fluid flow between rough surfaces. *Geophysical Research Letters* 1995; **22**(18): 2537–2540.
5. Brush DJ. Three dimensional fluid flow and solute transport in rough walled fractures. Doctoral dissertation, University of Waterloo, Waterloo, 2001.
6. Cacas MC, Ledoux E, Marsily GD, Tillie B, Barbreau A, Durand E, Feuga B, Peaudecerf P. Modeling fracture flow with a stochastic discrete fracture network: calibration and validation, 1. The flow model. *Water Resources Research* 1990; **26**(3): 479–489.
7. Cey E, Rudolph D, Therrien R. Simulation of groundwater recharge dynamics in partially saturated fractured soils incorporating spatially variable fracture apertures. *Water resources research* 2006; **42**, W09413, doi: 10.1029/2005WR004589.
8. Chen SH. Computational rock mechanics and engineering. China Water and Power Press: Beijing, 2006.
9. Chen SH. Hydraulic structures. Springer Verlag: New York, 2015
10. Chen SH, Feng XM. Composite element model for rock mass seepage flow. *Journal of Hydrodynamics* 2006; **18**(2): 219–224.
11. Chen SH, Feng XM, Shahrour I. Numerical estimation of REV and permeability tensor for fractured rock masses by composite element method. *International Journal for Numerical and Analytical Methods in Geomechanics* 2008; **32**(12): 1459–1477.
12. Chen SH, Qiang S. Composite element model for discontinuous rock masses. *International Journal of Rock Mechanics and Mining Sciences* 2004; **41**(5): 865–870.
13. Chen SH, Qiang S, Chen SF. Study on the three-dimensional composite element model of bolted rock masses. *Chinese Journal of Rock Mechanics and Engineering* 2003; **22**(1):



- 1–8.
14. Chen SH, Su PF, Shahrour I. Composite element algorithm for the thermal analysis of mass concrete: Simulation of lift joint. *Finite Elements in Analysis and Design* 2011; **47**(5): 536–542.
  15. Chen SH, Xu Q, Hu J. Composite element method for seepage analysis of geotechnical structures with drainage hole array. *Journal of Hydrodynamics* 2004; **16**(3): 260–266.
  16. Chen SH, Xue LL, XU GS, Shahrour I. Composite element method for the seepage analysis of rock masses containing fractures and drainage holes. *International Journal of Rock Mechanics and Mining Sciences* 2010; **47**: 762–770.
  17. Chen ZY. Soil slope stability analysis: theory, method and programs. China Water and Power Press: Beijing, 2003.
  18. Chen ZY, Wang XG, Yang J, Jia Z, Wang YJ. Rock slope stability analysis: theory, method and programs. China Water and Power Press: Beijing, 2005.
  19. Cook PG. A guide to regional groundwater flow in fractured rock aquifers. CSIRO Land Water: Adelaide, 2003.
  20. David C. Geometry of flow paths for fluid transport in rocks. *Journal of Geophysical Research* 1993; **98**(B7): 12267–12278.
  21. Detwiler RL, Pringle SE, Glass RJ. Measurement of fracture aperture fields using transmitted light: an evaluation of measurement errors and their influence on simulations of flow and transport through a single fracture. *Water Resources Research* 1999; **35**(9): 2605–2617.
  22. Dykhuizen RC. Transport of solutes through unsaturated fractured media. *Water Resources Research* 1987; **21**(12): 1531–1539.
  23. Finsterle S. Using the continuum approach to model unsaturated flow in fractured rock. *Water Resources Research* 2000; **36**(8): 2055–2066.
  24. Graf T, Therrien R. A method to discretize non-planar fractures for 3D subsurface flow and transport simulations. *International Journal for Numerical Methods in Fluids* 2008; **56**: 2069–2090.
  25. Hakami E, Barton N. Aperture measurements and flow experiments using transparent replicas or rock joints. *Publikasjon-Norges Geotekniske Institutt* 1991; **182**: 1–8.
  26. Hakami E, Larsson E. Aperture measurements and flow experiments on a single natural fracture. *International Journal of Rock Mechanics and Mining Sciences and Geomechanics Abstracts* 1996; **33**: 395–404.
  27. He J, Chen SH, Shahrour I. Numerical estimation and prediction of stress-dependent

- permeability tensor for fractured rock masses. *International Journal of Rock Mechanics and Mining Sciences* 2013; **59**: 70–79.
28. Hendrickx JMH, Flury M. Uniform and preferential flow mechanisms in the vadose zone. In *Conceptual models of flow and transport in the fractured vadose zone*, National Research Council (ed). National Academy Press: Washington DC, 2001; pp 149–187.
  29. Huyakorn PS, Lester BH, Faust CR. Finite element techniques for modeling groundwater flow in fractured aquifers. *Water Resources Research* 1983; **19**(4): 1019–1035.
  30. Kwicklis EM, Healy RW. Numerical investigation of steady liquid water flow in a variably saturated fracture network. *Water Resources Research* 1993; **29**(12): 4091–4102.
  31. Lomize GM. Filtratsiya v treshchinovatykh porodakh. (Flow in fractured porous rocks). Gosenergoizdat: Moscow, 1951.
  32. Louis C. A study of groundwater flow in jointed rock and its influence on the stability of rock masses. In *Rock Mechanics Research Report 10*, Imperial College of Science and Technology, 1969.
  33. Mourzenko VV, Thovert JF, Adler PM. Permeability of a single fracture: validity of the Reynolds equation. *Journal de Physique II* 1995; **5**(3): 465–482.
  34. Mustapha H, Dimitrakopoulos R, Graf T, Firoozabadi A. An efficient method for discretizing 3D fractured media for subsurface flow and transport simulations. *International Journal for Numerical Methods in Fluids* 2011; **67**: 651–670.
  35. Mustapha H, Mustapha K. A new approach to simulating flow in discrete fracture networks with an optimized mesh. *SIAM Journal on Scientific Computing* 2007; **29**(4): 1439–1459.
  36. National Research Council. Rock fractures and fluid flow: contemporary understanding and applications. National Academy Press: Washington DC, 1996.
  37. Neuzil CE, Tracy JV. Flow through fractures. *Water Resources Research* 1981; **17**: 191–199.
  38. Nicholl MJ, Rajaram H, Glass RJ, Detwiler R. Saturated flow in a single fracture: Evaluation of the Reynolds equation in measured aperture fields. *Water Resources Research* 1999; **35**(11): 3361–3373.
  39. Nitao JJ, Buscheck TA. Infiltration of a liquid front in an unsaturated, fractured porous medium. *Water Resources Research* 1991; **27**(8): 2099–2112.
  40. Peters RR and Klavetter EA. A continuum model for water movement in an unsaturated

- fractured rock mass. *Water Resources Research* 1988; **24**(3): 416–430.
41. Simunek J, Jarvis NJ, Van Genuchten MT, Gardenas A. Review and comparison of models for describing non-equilibrium and preferential flow and transport in the vadose zone. *Journal of Hydrology* 2003; **272**(1): 14–35.
  42. Snow DT. Anisotropic permeability of fractured media. *Water Resources Research* 1969; **5**(6): 1273–1289.
  43. Su GW, Geller JT, Pruess K, Wen F. Experimental studies of water seepage and intermittent flow in unsaturated, rough-walled fractures. *Water Resources Research* 1999; **35**(4): 1019–1037.
  44. Terzaghi KV. Die berechnung der durchlässigkeitsziffer des tones aus dem verlauf der hydrodynamischen spannungserscheinungen. *Sitzungsberichte der Akademie der Wissenschaften in Wien, Mathematisch-Naturwissenschaftliche Klasse, Abteilung IIA* 1923; 132: 125–138.
  45. Therrien R, Sudicky EA. Three-dimensional analysis of variably-saturated flow and solute transport in discretely-fractured porous media. *Journal of Contaminant Hydrology* 1996; **23**(1): 1–44.
  46. Tsang YW, Witherspoon PA. Hydromechanical behavior of a deformable rock fracture subject to normal stress. *Journal of Geophysical Research: Solid Earth* 1981; **86**(B10): 9287–9298.
  47. Unger AJA, Mase CW. Numerical study of the hydromechanical behavior of two rough fracture surfaces in contact. *Water Resources Research* 1993; **29**: 2101–2114.
  48. Van Genuchten MT. A closed-form equation for predicting the hydraulic conductivity of unsaturated soils. *Soil Science Society of America Journal* 1980; **44**(5): 892–898.
  49. Wang JSY, Narasimhan TN. Hydrologic mechanisms governing fluid flow in a partially saturated, fractured, porous medium. *Water Resources Research* 1985; **21**(12): 1861–1874.
  50. Wang L, Cardenas MB, Slottke DT, Ketcham RA, Sharp JM. Modification of the Local Cubic Law of fracture flow for weak inertia, tortuosity, and roughness. *Water Resources Research* 2015; **51**(4): 2064–2080.
  51. Wang M, Kulatilake PHSW, Um J, Narvaiz J. Estimation of REV size and three-dimensional hydraulic conductivity tensor for a fractured rock mass through a single well packer test and discrete fracture fluid flow modeling. *International Journal of Rock Mechanics and Mining Sciences* 2002; **39**(7): 887–904.
  52. Zimmerman RW, Kumar S, Bodvarsson GS. Lubrication theory analysis of the

permeability of rough-walled fractures. *International Journal of Rock Mechanics and Mining Sciences and Geomechanics Abstracts* 1991; **28**(4): 325–331.

53. Zhou WY, Yang Q. Numerical computational methods for rock mechanics. China Electric Power Press: Beijing, 2007.

## **Chapter 3 Composite Element Method for Modelling Transient, Saturated Flow in Fractured Media with a Free Surface**

### **3.1 Introduction**

There are many different ways to classify groundwater flow. According to whether the flow elements (e.g., hydraulic head and flow velocity) change with time, flow is classified into steady flow and transient flow. According to whether the flow domain has a free surface boundary, flow is classified into confined flow and unconfined flow. According to whether the saturation within the domain is changed, flow is classified into saturated flow and variably-saturated flow. Besides, according to the type of media within the domain, flow is classified into porous media flow and fractured media flow. These classification ways make the study of groundwater flow have different emphases. In fact, steady flow, confined flow, and saturated flow can respectively viewed as a special case of transient flow, unconfined flow and variably-saturated flow. The method used for transient flow generally permits analysis of steady flow as long as the parameters associated with the time terms in the governing equations are zeroed. Also, the method for unconfined flow allows for analysis of confined flow as long as the free surface is not specified. And the method for variably-saturated flow allows for analysis of saturated flow as long as the saturation-related parameters are taken as fixed values. Thus, the method used for transient, unconfined and variably-saturated flow is the most complete method for solving groundwater flow problems.

Unconfined flow can be incorporated into variably-saturated flow because the free surface boundary in the unconfined flow essentially divides the flow domain into two zones: saturated zone where saturation is equal to one and unsaturated zone where saturation is less than one. The reason why there are still a number of studies that deal with unconfined flow is that in some cases the researchers are concerned only with flow in the saturated zone. Moreover, increasing the analysis of flow within the unsaturated zone means increasing the difficulty of solving the problem and requiring more data for the unsaturated zone. These data may include the initial state of saturation, rates of infiltration for both air and water, viscosities and densities of both fluids, capillary pressure characteristics for each part of the flow domain, relative permeability, and the absolute permeability of each part of the system [Green et al., 1970]. Since the groundwater hydrologist rarely has such data available in working in specific field problems and therefore is not able to analyze flow directly in the

unsaturated zone. Neuman and Witherspoon [1970, 1971] presented a numerical method for analyzing transient flow in porous media with a free surface. They assumed that the water flow occurred only in the saturated zone and the effect of the unsaturated zone on the transient position of the free surface was taken into account by using the concept of delayed yield which was proposed by Boulton [1954]. According to Boulton's concept, when the free surface falls, drainage is not instantaneous and some water is delayed in its downward movement. Neuman and Witherspoon [1970] established equations for the velocity of the movement of free surface, and stated that the velocity normal to itself at which the free surface falls (or rises) was equal to the velocity of water that is discharged into (or added from) the unsaturated zone normal to the free surface. Similar studies of transient saturated but unconfined flow in porous media also include Taylor and Brown [1967], Desai and Li [1983], Purkey [2006], etc. However, according to the author's knowledge, so far, there are relatively less studies on transient, saturated flow in fractured media with a free surface.

In Chapter 1 and Section 2.3 of Chapter 2, it has been explained that groundwater flow in fractured media can be simulated by either explicitly or implicitly accounting for the fractures. The distinctions between the explicit and implicit approaches as well as their advantages and disadvantages have been described in detail in the previous chapters, and are not repeated here. It is worth emphasizing that the explicit approach has a unique advantage in characterizing the heterogeneity of fractured media and is therefore adopted in this work. Wang [1993], Jing et al. [2001] and Jiang et al. [2013] studied the numerical models for simulating transient, saturated flow in discretely-fractured media with a free surface, but they almost all only considered flow in the fractures whereas ignored flow in the matrix. Therefore, it is necessary to further develop a comprehensive numerical model for simulating transient, saturated flow in the fracture-matrix systems.

The main difficulties in the explicit simulation of fractured media are: to generate a computational mesh that accurately represents the geometry of the fractured media; and to efficiently solve the discretized equations with tens to hundreds of thousands of unknowns associated with this mesh. The CEM is a new numerical method developed from the FEM. It inherits all the advantages of the FEM, for example, it can describe a range of complex geometry, boundary conditions, material properties and complicated physical processes. Meanwhile, the CEM can resolve the difficulty in discretizing the complex fractured media by interpolating the fractures into the elements. Due to the simplicity of the mesh used, the CEM usually requires less computing amount than the FEM in solving the same fractured media flow problem, which may result in higher computational efficiency. This property

has been demonstrated in many previous studies on the CEM [Chen and Feng, 2006; hen et al., 2010; Hou et al., 2015].

The purpose of this chapter is to use the CEM to develop the numerical model for simulating transient, saturated flow in fractured media with a free surface. The main contents include: (i) mathematical descriptions of transient, saturated flow problem; (ii) composite element model construction; (iii) relevant solution algorithms, including the CM pre-processing, the treatment of the free surface and the seepage face, etc.; (iv) verification example; and (v) simulations of flow problems in complicated, saturated fractured aquifers.

### 3.2 Mathematical descriptions of transient, saturated flow problem

By considering the compressibility of media skeleton, grains and pore water, and neglecting the acceleration and inertial effect, the governing equations for transient, saturated flow of groundwater can be expressed as:

$$S_s \frac{\partial h}{\partial t} = \nabla \cdot (\mathbf{k} \nabla h) - q, \quad \text{in } \Omega \quad (3.1)$$

where  $h=z+P$ ,  $h$  is hydraulic head,  $z$  is elevation head,  $P$  is pressure head,  $S_s$  is specific storage,  $q$  is any source density in flow domain  $\Omega$ ,  $t$  is the elapsed time, and  $\mathbf{k}$  is saturated hydraulic conductivity tensor.

There are four types of boundaries possible in  $\Omega$  (see Figure 3.1). They are respectively the prescribed head (Dirichlet-type) boundary  $\Gamma_1$ , the prescribed flux (Neumann-type) boundary  $\Gamma_2$ , free surface F and seepage face S. The corresponding boundary conditions are:

$$h|_{\Gamma_1} = h_1, \quad \text{on } \Gamma_1 \quad (3.2)$$

$$\mathbf{n}^T \cdot (\mathbf{k} \nabla h)|_{\Gamma_2} = -g, \quad \text{on } \Gamma_2 \quad (3.3)$$

$$\begin{cases} h|_F = z \\ \mathbf{n}^T \cdot (\mathbf{k} \nabla h)|_F = -S_y \frac{\partial h}{\partial t} \cos \theta' \end{cases}, \quad \text{on F} \quad (3.4)$$

$$h|_S = z, \quad \text{on S} \quad (3.5)$$

where  $h_1$  is the prescribed head on  $\Gamma_1$ ,  $g$  is the prescribed flux across  $\Gamma_2$ . On the free surface F, the hydraulic head is equal to the elevation head, as given by the first line in Equation (3.4). The second line in Equation (3.4) represents the velocity of the free surface. It is established based on the property that groundwater flow does not cross the free surface. So the velocity of the groundwater flow normal to the free surface must equal the velocity of

the free surface normal to itself [Li and Jiao, 2003; Mao, 2003]. A schematic diagram for the relationship is exhibited in Figure 3.1, where  $S_y$  is specific yield, defined as the ratio of the volume of water that an unconfined aquifer will release from storage by gravity to the total volume of saturated aquifer,  $\theta$  is angle of the normal direction of the free surface to the elevation direction, and  $\mathbf{n}$  is an unit vector normal to the boundaries concerned. On the seepage face S, water is in contact with air, thus  $h=z$ .

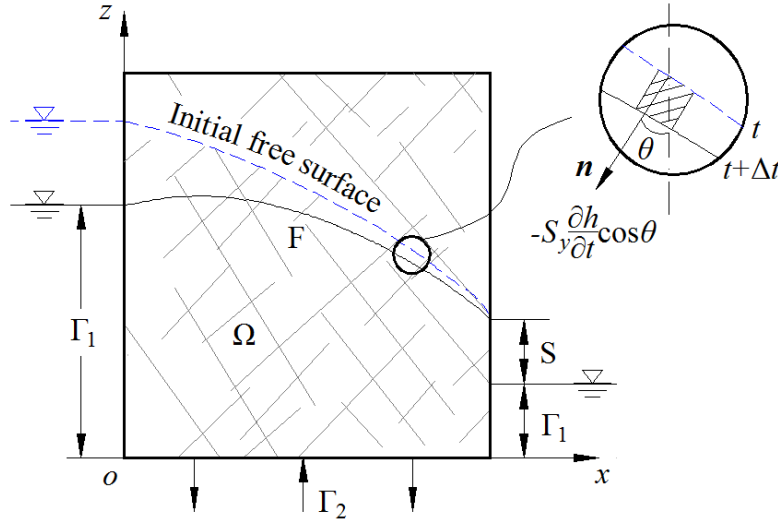


Figure 3.1 Cross section of an unconfined fractured aquifer with four types of boundaries: the prescribed head boundary  $\Gamma_1$ , the prescribed flux boundary  $\Gamma_2$ , free surface F and seepage face S

Equation (3.1) is subject to initial condition:

$$h|_{t=0} = h_0, \quad \text{in } \Omega \quad (3.6)$$

where  $h_0$  represents the initial values of hydraulic head.

According to variational principle, the solution of Equations (3.1)-(3.5) can be converted into an optimization problem of the functional as follow:

$$I(h) = \iiint_{\Omega} \left[ \frac{1}{2} (\nabla h)^T \mathbf{k} (\nabla h) + qh + S_s h \frac{\partial h}{\partial t} \right] d\Omega + \iint_{\Gamma_2} gh d\Gamma + \iint_F S_y h \frac{\partial h}{\partial t} \cos \theta d\Gamma = \min \quad (3.7)$$

And the prescribed head boundary conditions in Equations (3.2), (3.4) and (3.5) should be satisfied separately. The finite element method (FEM) is usually used to discretize the variational function in Equation (3.7) as well as the head boundary conditions. However, it is noted that the free surface and seepage face are unknown beforehand. To solve this problem, an iterative scheme [Desai, 1976; Zhang et al., 1988] is generally introduced. This study presents an iterative scheme, which is based on the initial flow method proposed by Zhang et al. [1988] to locate the free surface under steady flow condition and is modified



here to locate the shifting free surface under transient flow condition. Details on the implementation will be discussed in Section 3.4.3.

### 3.3 Composite element model construction

#### 3.3.1 Hydraulic head within composite element

The composite element method (CEM) is used to numerically formulate transient, saturated flow in fractured media with a free surface. The finite element mesh should be firstly generated to discretize the simulation domain. Then, the insertion of fractures into the mesh transforms some finite elements into composite elements by geometric calculations. Figure 3.2 shows a composite element inserted by two fracture surfaces. The composite element has the same patterns as a finite element, such as hexahedron, whereas the internal matrix sub-elements denoted by  $e_i$  ( $i=1,2,\dots$ ) can take on arbitrary shapes. The interfaces between two matrix sub-elements  $e_i$  and  $e_j$  ( $j=1,2,\dots$ ) are used to represent the fracture fragments, denoted by  $f_{ij}$  ( $i \neq j$ ).

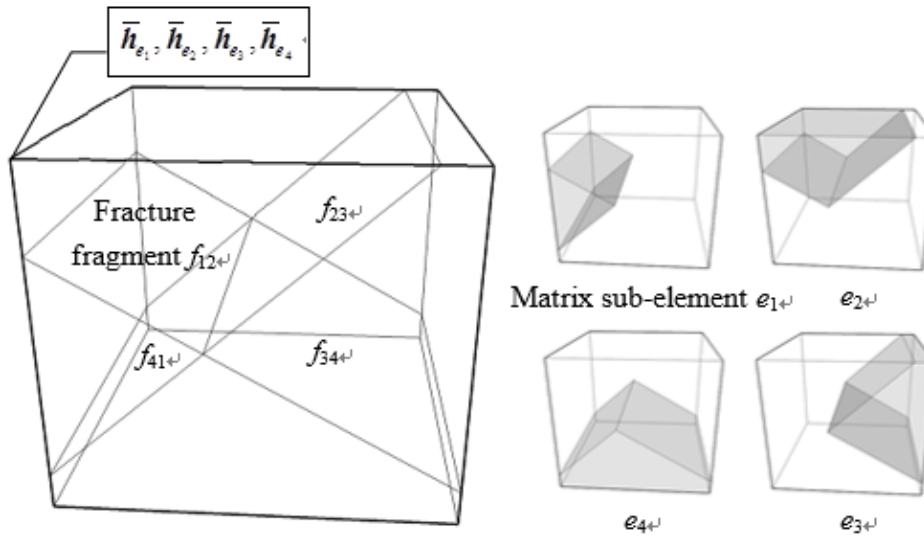


Figure 3.2 A composite element containing four matrix sub-elements and four fracture fragments

According to the CEM theory [Chen, 2006], within each matrix sub-element  $e_i$ , the hydraulic head  $h_{e_i}$  is defined as:

$$h_{e_i} = N\bar{h}_{e_i} \quad (3.8)$$

where  $\bar{h}_{e_i}$  is a set of nodal hydraulic heads for  $e_i$ , which are located on the whole element nodes, and  $N$  is shape function associated with the nodes. With respect to the composite

element in Figure 3.2, the number of nodes is four times the number of nodes of a finite element.

Within each fracture fragment  $f_{ij}$ , the hydraulic head  $h_{f_{ij}}$  is defined by using the average of  $h_{e_i}$  and  $h_{e_j}$  at the fracture fragment. And, the hydraulic gradient within the fracture fragment, normal to itself, is assumed to be constant, given that the fracture aperture is usually quite small. Thus, the hydraulic head within the fracture fragment linearly varies along its normal direction. To simplify the formula derivation, a separate coordinate system  $O-x_f y_f z_f$  for each fracture fragment is established, where  $z_f$ -axis is perpendicular to the fracture fragment and points upward,  $y_f$ -axis is in the fracture fragment and points out the direction of dip, and  $x_f$ -axis is determined by right-hand rule. Then, the hydraulic gradient along  $x_f$ -,  $y_f$ - and  $z_f$ -axis, and the derivative of hydraulic head with respect to time in  $f_{ij}$  can be expressed by:

$$\begin{aligned}
\frac{\partial h_{f_{ij}}}{\partial x_f} &= \frac{\partial \left[ \frac{1}{2} (h_{e_i} + h_{e_j}) \right]}{\partial x_f} = \frac{1}{2} \frac{\partial N}{\partial x_f} (\bar{h}_{e_i} + \bar{h}_{e_j}) \\
\frac{\partial h_{f_{ij}}}{\partial y_f} &= \frac{\partial \left[ \frac{1}{2} (h_{e_i} + h_{e_j}) \right]}{\partial y_f} = \frac{1}{2} \frac{\partial N}{\partial y_f} (\bar{h}_{e_i} + \bar{h}_{e_j}) \\
\frac{\partial h_{f_{ij}}}{\partial z_f} &= \frac{h_{e_i} - h_{e_j}}{b} = N \frac{\bar{h}_{e_i} - \bar{h}_{e_j}}{b} \\
\frac{\partial h_{f_{ij}}}{\partial t} &= \frac{\partial \left[ \frac{1}{2} (h_{e_i} + h_{e_j}) \right]}{\partial t} = \frac{1}{2} N \left( \frac{\partial \bar{h}_{e_i}}{\partial t} + \frac{\partial \bar{h}_{e_j}}{\partial t} \right)
\end{aligned} \tag{3.9}$$

### 3.3.2 Composite element formulation

By substituting Equation (3.8) into Equation (3.7), the variational principle in matrix sub-element  $e_i$  leads to:

$$\mathbf{K}_{e_i} \bar{\mathbf{h}}_{e_i} + (\mathbf{S}_{e_i} + \mathbf{Y}_{e_i}) \frac{\partial \bar{\mathbf{h}}_{e_i}}{\partial t} = \mathbf{d}_{e_i} \tag{3.10}$$

in which

$$\begin{aligned}
\mathbf{K}_{e_i} &= \iiint_{\Omega^{e_i}} (\nabla N)^T \mathbf{k}_{e_i} (\nabla N) d\Omega \\
\mathbf{S}_{e_i} &= \iiint_{\Omega^{e_i}} N^T S_{se_i} N d\Omega \\
\mathbf{Y}_{e_i} &= \iint_{F^{e_i}} N^T S_{ye_i} \cos \theta N d\Gamma \\
\mathbf{d}_{e_i} &= -\iiint_{\Omega^{e_i}} q N d\Omega - \iint_{\Gamma_2^{e_i}} g_{e_i} N d\Gamma
\end{aligned} \tag{3.11}$$

where  $\Omega^{e_i}$  is matrix sub-element domain,  $F^{e_i}$  and  $\Gamma_2^{e_i}$  are respectively free surface and the prescribed flux boundary in  $\Omega^{e_i}$ ,  $\mathbf{k}_{e_i}$ ,  $S_{se_i}$  and  $S_{ye_i}$  are respectively the hydraulic conductivity tensor, specific storage and specific yield of  $e_i$ , and  $g_{e_i}$  represents the prescribed flux across  $\Gamma_2^{e_i}$ , including the leakage flux across the fracture-matrix interface from  $f_{ij}$  to  $e_i$ , denoted as  $g_{f_{ij},e_i}$ .

Likewise, by substituting Equation (3.9) into Equation (3.7), the variational principle in fracture fragment  $f_{ij}$  leads to:

$$\begin{cases}
\mathbf{K}_{f_{ij},\ddot{u}} \bar{\mathbf{h}}_{e_i} + \mathbf{K}_{f_{ij},\ddot{u}} \bar{\mathbf{h}}_{e_j} + (\mathbf{S}_{f_{ij}} + \mathbf{Y}_{f_{ij}}) \left( \frac{\partial \bar{\mathbf{h}}_{e_i}}{\partial t} + \frac{\partial \bar{\mathbf{h}}_{e_j}}{\partial t} \right) = \mathbf{d}_{f_{ij}} \\
\mathbf{K}_{f_{ij},\ddot{u}} \bar{\mathbf{h}}_{e_i} + \mathbf{K}_{f_{ij},\ddot{u}} \bar{\mathbf{h}}_{e_j} + (\mathbf{S}_{f_{ij}} + \mathbf{Y}_{f_{ij}}) \left( \frac{\partial \bar{\mathbf{h}}_{e_i}}{\partial t} + \frac{\partial \bar{\mathbf{h}}_{e_j}}{\partial t} \right) = \mathbf{d}_{f_{ij}}
\end{cases} \tag{3.12}$$

in which

$$\begin{aligned}
\mathbf{K}_{f_{ij},\ddot{u}} &= \mathbf{K}_{f_{ij},\ddot{u}} = \frac{b}{2} \iint_{\Gamma^{f_{ij}}} \left( \frac{k_{f_{ij}x_f}}{2} \frac{\partial N^T}{\partial x_f} \frac{\partial N}{\partial x_f} + \frac{k_{f_{ij}y_f}}{2} \frac{\partial N^T}{\partial y_f} \frac{\partial N}{\partial y_f} + \frac{2k_{f_{ij}z_f}}{b^2} N^T N \right) dx_f dy_f \\
\mathbf{K}_{f_{ij},\ddot{u}} &= \mathbf{K}_{f_{ij},\ddot{u}} = \frac{b}{2} \iint_{\Gamma^{f_{ij}}} \left( \frac{k_{f_{ij}x_f}}{2} \frac{\partial N^T}{\partial x_f} \frac{\partial N}{\partial x_f} + \frac{k_{f_{ij}y_f}}{2} \frac{\partial N^T}{\partial y_f} \frac{\partial N}{\partial y_f} - \frac{2k_{f_{ij}z_f}}{b^2} N^T N \right) dx_f dy_f \\
\mathbf{S}_{f_{ij}} &= \frac{b}{4} \iint_{\Gamma^{f_{ij}}} N^T S_{sf_{ij}} N dx_f dy_f \\
\mathbf{Y}_{f_{ij}} &= \frac{b}{4} \int_{F_c^{f_{ij}}} N^T S_{yf_{ij}} \cos \theta N d\Gamma \\
\mathbf{d}_{f_{ij}} &= -\iint_{\Gamma^{f_{ij}}} g_{f_{ij}} N d\Gamma
\end{aligned} \tag{3.13}$$

where  $\Gamma^{f_{ij}}$  is fracture fragment surface,  $F_c^{f_{ij}}$  is the curve of intersection between free surface and fracture fragment,  $k_{f_{ij}x_f}$ ,  $k_{f_{ij}y_f}$  and  $k_{f_{ij}z_f}$  are the principle values of the hydraulic conductivity tensor along  $x_f$  -,  $y_f$  - and  $z_f$  -axes,  $S_{sf_{ij}}$  and  $S_{yf_{ij}}$  are

respectively specific storage and specific yield of  $f_{ij}$ , and  $g_{f_{ij}}$  is the leakage flux across the fracture-matrix interface from from  $e_i$  and  $e_j$  to  $f_{ij}$ , equal to  $-(g_{f_{ij},e_i} + g_{f_{ij},e_j})$ .

By assembling Equations (3.10) for all matrix sub-elements and Equations (3.12) for all fracture fragment within the composite element, the final composite element equation can be expressed as follows:

$$\begin{bmatrix} \mathbf{K}_{11} & \mathbf{K}_{12} & \dots & \mathbf{K}_{1l} \\ \mathbf{K}_{21} & \mathbf{K}_{22} & \dots & \mathbf{K}_{2l} \\ \vdots & \vdots & \ddots & \vdots \\ \mathbf{K}_{l1} & \mathbf{K}_{l2} & \dots & \mathbf{K}_{ll} \end{bmatrix} \begin{bmatrix} \bar{h}_{e_1} \\ \bar{h}_{e_2} \\ \vdots \\ \bar{h}_{e_l} \end{bmatrix} + \left( \begin{bmatrix} \mathbf{S}_{11} & \mathbf{S}_{12} & \dots & \mathbf{S}_{1l} \\ \mathbf{S}_{21} & \mathbf{S}_{22} & \dots & \mathbf{S}_{2l} \\ \vdots & \vdots & \ddots & \vdots \\ \mathbf{S}_{l1} & \mathbf{S}_{l2} & \dots & \mathbf{S}_{ll} \end{bmatrix} + \begin{bmatrix} \mathbf{Y}_{11} & \mathbf{Y}_{12} & \dots & \mathbf{Y}_{1l} \\ \mathbf{Y}_{21} & \mathbf{Y}_{22} & \dots & \mathbf{Y}_{2l} \\ \vdots & \vdots & \ddots & \vdots \\ \mathbf{Y}_{l1} & \mathbf{Y}_{l2} & \dots & \mathbf{Y}_{ll} \end{bmatrix} \right) \begin{bmatrix} \frac{\partial \bar{h}_{e_1}}{\partial t} \\ \frac{\partial \bar{h}_{e_2}}{\partial t} \\ \vdots \\ \frac{\partial \bar{h}_{e_l}}{\partial t} \end{bmatrix} = \begin{bmatrix} \mathbf{d}_1 \\ \mathbf{d}_2 \\ \vdots \\ \mathbf{d}_l \end{bmatrix} \quad (3.14)$$

in which

$$\begin{cases} \mathbf{K}_{ii} = \mathbf{K}_{e_i} + \sum_{j=1}^l \mathbf{K}_{f_{ij},ii} \\ \mathbf{K}_{ij} = \mathbf{K}_{f_{ij},ij} \end{cases}, \begin{cases} \mathbf{S}_{ii} = \mathbf{S}_{e_i} + \sum_{j=1}^l \mathbf{S}_{f_{ij}} \\ \mathbf{S}_{ij} = \mathbf{S}_{f_{ij}} \end{cases}, \begin{cases} \mathbf{Y}_{ii} = \mathbf{Y}_{e_i} + \sum_{j=1}^l \mathbf{Y}_{f_{ij}} \\ \mathbf{Y}_{ij} = \mathbf{Y}_{f_{ij}} \end{cases} \text{ and } \mathbf{d}_i = \mathbf{d}_{e_i} + \sum_{j=1}^l \mathbf{d}_{f_{ij}} \quad (3.15)$$

where  $l$  is the number of matrix sub-elements within the composite element. It is worth mentioning that the leakage fluxes across the fracture-matrix interface are cancelled out while superimposing the contributions at each node in the composite element. This implies that, the resulting assessment of the exchange fluxes is not biased by specification of the fracture-matrix water leakage terms. If  $l=1$ , Equation (3.14) will automatically be degenerated into the finite element equation, i.e., the coefficient matrixes contain only one sub-matrixes  $\mathbf{K}_{11} = \mathbf{K}_{e_1}$ ,  $\mathbf{S}_{11} = \mathbf{S}_{e_1}$ , and  $\mathbf{Y}_{11} = \mathbf{Y}_{e_1}$ , the nodal vectors contain only one sub-vectors  $\bar{h}_{e_1}$ , and  $\partial \bar{h}_{e_1} / \partial t$ , and the right-hand vector contains only one sub-vector  $\mathbf{d}_1$ .

Summation over all composite element and finite elements in domain yields the final system of equation, which has the following form:

$$\mathbf{K}\bar{h} + (\mathbf{S} + \mathbf{Y}) \frac{\partial \bar{h}}{\partial t} = \mathbf{d} \quad (3.16)$$

Using the implicit time difference scheme, one obtains:

$$\left( \mathbf{K} + \frac{\mathbf{S} + \mathbf{Y}}{\Delta t^{n+1}} \right) \bar{h}^{n+1} = \frac{\mathbf{S} + \mathbf{Y}}{\Delta t^{n+1}} \bar{h}^n + \mathbf{d} \quad (3.17)$$

where  $\Delta t^{n+1}=t^{n+1}-t^n$  is the time step,  $\bar{h}^{n+1}$  and  $\bar{h}^n$  are respectively the hydraulic head vectors at time nodes  $n+1$  and  $n$ .

### 3.4 Relevant solution algorithms

#### 3.4.1 CEM pre-processing

The main feature of the CEM is to simulate fractures within the composite elements. For how to seek out the composite elements and how to divide the elements into matrix sub-elements and fracture fragments, a special CEM pre-processor has been developed in previous work [Qiang, 2005]. This pre-processor consists of two functions: generating a 3D finite element mesh for the simulation domain without the fractures, and inserting the fractures into the generated mesh. As the fractures have been removed, the discretization of the simulation domain becomes simple and it can be realized by using a commonly used mesh generation technology [Qin et al., 2009]. The following paragraphs describe only the algorithms involved in inserting the fractures into a mesh.

Figure 3.3 provides the workflow of the pre-processor to insert the fracture surfaces into a finite element mesh. It contains three main modules: searching composite elements, forming sub-elements and fracture fragments within composite elements, and subdividing sub-elements and fracture fragments into multiple regular hexahedrons and quadrangles. The input data is the information of mesh topology and fracture geometry. The output result is the information needed for the CEM calculation. The algorithm of each module is briefly described as follows.

*Search composite elements.* The intersections between the fracture surface and the edges of each element are checked. If the fracture ends inside the element, it shall be stretched or trimmed toward the element's face. If the fracture surface exactly passes through the edge of element, it should be moved a little bit to implement such an intersection. The composite element is determined where no less than two edges are intersected with the fracture surface.

*Form matrix sub-elements and fracture fragments within composite elements.* In each determined composite element, the fracture fragment is formed by connecting the intersection points of the fracture surface and the element edges in clockwise (or counter clockwise) direction. On each side of the fracture fragment, the incised element faces and the fracture fragment constitute a new matrix sub-element. If there are more than one fracture surfaces intersecting the composite element, the matrix sub-elements and fracture

fragments will be further divided, in other words, the intersections between the new-inserted fracture surface and the edges of matrix sub-elements need also to be calculated. Until all fracture surfaces are inserted into the mesh, the last module will not be executed.

*Subdivide sub-elements and fragments into hexahedrons and quadrangles.* The purpose of the subdivision is to make the sub-elements and fragments becoming aggregates of several regular bodies and faces. In this way, when calculating the integral terms of the matrix sub-elements and the fracture fragments (respectively in Equations (3.11) and (3.13)), they can be derived by superimposing the integrals over respective internal regular hexahedrons and quadrangles.

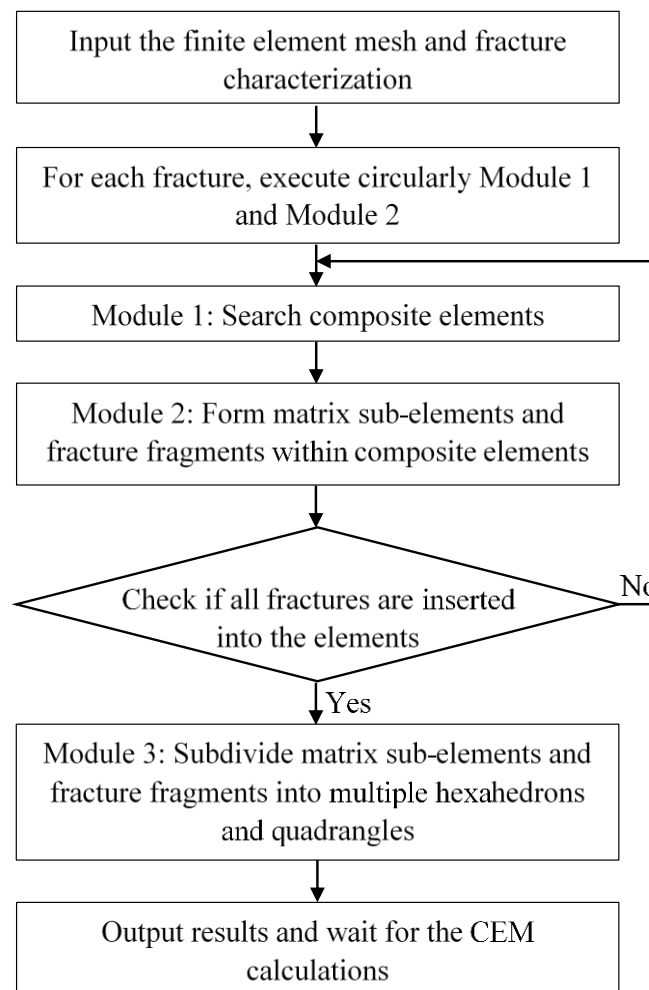


Figure 3.3 Workflow of the pre-processor to insert the fracture surfaces into the generated mesh

### 3.4.2 Numerical integral calculation

The Gaussian integral is adopted to calculate the coefficient matrixes (i.e.,  $\mathbf{K}$ ,  $\mathbf{S}$  and  $\mathbf{Y}$ ) and right-hand vectors (i.e.,  $\mathbf{d}$ ) in Equations (3.11) and (3.13). As mentioned above, the matrix sub-elements and fracture fragments have been divided into multiple hexahedrons

and quadrangles. Thus, it is required to first calculate the integrals over these hexahedrons and quadrangles, and then to sum them to obtain the integrals over entire sub-elements and fracture fragments.

For a volume integral, the basic formula of the Gaussian integral [Zhu, 1998] is:

$$\iiint_{\Omega} A(x, y, z) d\Omega = \sum_{i=1}^n \sum_{j=1}^n \sum_{m=1}^n a_i b_j c_m A(\xi, \eta, \zeta) |J| \quad (3.18)$$

where  $A(x, y, z)$  represents the integrand function over  $\Omega$ ,  $o-\xi\eta\zeta$  is the local coordinate system obtained by coordinate transformation from  $o-xyz$ ,  $i, j$ , and  $m$  are the serial numbers of the Gaussian points in  $\xi, \eta$ , and  $\zeta$  directions,  $n$  is the number of the Gaussian points taken in each direction, thus the total number of the Gaussian points in the integral area  $\Omega$  is  $n^3$ ,  $A(\xi, \eta, \zeta)$  is the integrand function value at the Gaussian point,  $a_i, b_j$ , and  $c_m$  are the weight coefficients in  $\xi, \eta$ , and  $\zeta$  directions, and  $J$  is the Jacobian matrix generated by the coordinate transformation, expressed as:

$$J = \begin{bmatrix} \frac{\partial x}{\partial \xi} & \frac{\partial y}{\partial \xi} & \frac{\partial z}{\partial \xi} \\ \frac{\partial x}{\partial \eta} & \frac{\partial y}{\partial \eta} & \frac{\partial z}{\partial \eta} \\ \frac{\partial x}{\partial \zeta} & \frac{\partial y}{\partial \zeta} & \frac{\partial z}{\partial \zeta} \end{bmatrix} = \begin{bmatrix} \frac{\partial N}{\partial \xi} \bar{x} & \frac{\partial N}{\partial \xi} \bar{y} & \frac{\partial N}{\partial \xi} \bar{z} \\ \frac{\partial N}{\partial \eta} \bar{x} & \frac{\partial N}{\partial \eta} \bar{y} & \frac{\partial N}{\partial \eta} \bar{z} \\ \frac{\partial N}{\partial \zeta} \bar{x} & \frac{\partial N}{\partial \zeta} \bar{y} & \frac{\partial N}{\partial \zeta} \bar{z} \end{bmatrix} \quad (3.19)$$

where  $\bar{x}$ ,  $\bar{y}$ , and  $\bar{z}$  are respectively a set of nodal coordinates in  $x, y$ , and  $z$  directions, and  $N$  is shape function which is the same as that in Equation (3.8). The method of the Gaussian integral for the volume integral and for the area integral is identical except for the difference in dimensionality; hence the formula for the area integral is omitted here.

It should be noted that the shape function used in the composite element, which is for either the coordinate function or the hydraulic head function, is defined relative to the whole element, whereas the Gaussian points in a small hexahedron of the sub-element or in a small quadrangle of the fracture fragment are defined relative to the hexahedron or quadrangle itself. For the whole composite element, these Gaussian points can be any points within the element, and their local coordinates are unknown in advance. Therefore, the local coordinates of the Gaussian points need to be first reversely calculated according to their global coordinates, and then the shape function and the Jacobian matrix at these Gaussian points are determined. This is the difference between the CEM and FEM in dealing with the numerical integral. Details on the numerical integral method in the CEM can be found in the literature [Feng, 2006].

### 3.4.3 Treatment of boundary conditions

As in the FEM, the Dirichlet-type and Neumann-type boundary conditions are treated by assigning the fixed heads and fluxes onto the nodes forming the boundaries. However, within the composite element containing multiple sub-elements and multiple sets of nodes, only the sets of nodes related to the boundary are imposed to have the fixed head or flux.

The initial flow method [Zhang et al., 1988] is introduced to locate the transient position of the free surface. In each time step, the “initial load vector”  $\mathbf{Q}$  is calculated by the following equation to correct the free surface:

$$\mathbf{Q} = \tilde{\mathbf{K}}\bar{\mathbf{h}}^n + \frac{\tilde{\mathbf{S}}}{\Delta t^{n+1}}(\bar{\mathbf{h}}^{n+1} - \bar{\mathbf{h}}^n) \quad (3.20)$$

where  $\tilde{\mathbf{K}}$  and  $\tilde{\mathbf{S}}$  indicate the matrixes obtained by accumulating the contributions of the Gaussian points in the unsaturated zone (where the elevation is greater than the hydraulic head). Add  $\mathbf{Q}$  into the right-hand vector in Equation (3.17), leading to the resulting calculating equations:

$$\left( \mathbf{K} + \frac{\mathbf{S} + \mathbf{Y}}{\Delta t^{n+1}} \right) \bar{\mathbf{h}}^{n+1} = \frac{\mathbf{S} + \mathbf{Y}}{\Delta t^{n+1}} \bar{\mathbf{h}}^n + \mathbf{d} + \mathbf{Q} \quad (3.21)$$

It should be noted that this iterative procedure is carried out on the assumption that all the other boundaries (including the prescribed head boundary, the prescribed flux boundary, and seepage face) are known. However, in most cases, the seepage face is unknown beforehand. Before the iteration begins, the boundary conditions on the potential seepage face should be predesignated. The results after iteration should be checked to remain consistent with the predesignated conditions. If there is an inward flux into the domain at the node on the seepage face, the node will be turned into a no-flux one in next iteration. If the hydraulic head at the node on the no-flux boundary is greater than its elevation, the node will be turned into a seepage face node in next iteration. All the nodes forming the potential seepage face are adjusted until each of them achieves convergence. This procedure to locating seepage face was proposed by Neuman [1973] and later modified by Cooley [1983].

The convergent criterion for the iterative scheme is established as follow:

$$\|\bar{\mathbf{h}}^{n+1,m+1} - \bar{\mathbf{h}}^{n+1,m}\|_{\infty} < \varepsilon \|\bar{\mathbf{h}}^{n+1,m+1} - \bar{\mathbf{h}}^n\|_{\infty} \quad (3.22)$$

where  $\bar{\mathbf{h}}^{n+1,m+1}$ ,  $\bar{\mathbf{h}}^{n+1,m}$  are respectively the hydraulic head vectors at iteration  $m+1$ ,  $m$  and at time node  $n+1$ ,  $\bar{\mathbf{h}}^n$  is the calculated hydraulic head vector at the previous time node  $n$ ,  $\varepsilon$  is tolerance error and  $\|\cdot\|_{\infty}$  is the infinite norm operator. If Equation (3.22) is satisfied within



the specified maximum number of iterations, the value of  $\bar{h}^{n+1,m+1}$  is accepted as the solution to Equation (3.21) at time node  $n+1$  and the next time step proceeds. Or else, the time step will be reduced by half and the calculation will be restarted at the new time step.

#### 3.4.4 Solving large sparse symmetric equations

The resulting system of equations, i.e., Equation (3.21), is solved by an iterative solver combining symmetric successive over relaxation and preconditioned conjugate gradient which has been developed and shown to be efficient and robust for solving large, sparse and symmetrical linear equations [Lin, 1997].

### 3.5 Verification example

The formulation and solution algorithms mentioned above have been implemented into a computer program CEM\_SATFLOW for simulating transient, saturated flow in fractured media with a free surface. To verify the program, a synthetic example is used below.

#### 3.5.1 Flow in a synthetic fractured rock mass

The cubic mass shown in Figure 3.4 is 10 m in width, and there are six orthogonal, connected fractures with aperture of 1 mm in the mass. The initial state of flow throughout the domain is steady with the hydraulic head  $h_0=10$  m. The origin of coordinates is located on left bottom corner. In case 1: at time  $t \geq 0$ , the hydraulic head  $h=20$  m is imposed at left side ( $x=0$ ) and the hydraulic head  $h=10$  m remains unchanged at right side ( $x=10$  m). In case 2: at time  $t \geq 0$ , the hydraulic head at  $x=10$  m is suddenly lowered to zero and this side becomes potential seepage face, whereas the hydraulic head at  $x=0$  is equal to 10 m. The else sides are no-flux boundaries. To verify the accuracy, the results calculated by composite element model presented in this chapter will be compared with those by the well-tested, FEM-based software COMSOL.

The required parameters are: for matrix, the hydraulic conductivity is  $10^{-10} \text{ m}\cdot\text{s}^{-1}$ , the specific storage is  $10^{-5} \text{ m}^{-1}$  and the specific yield is 0.001; and for fractures, the hydraulic conductivity is  $10^{-5} \text{ m}\cdot\text{s}^{-1}$ , which is five orders of magnitude higher than matrix, the specific storage is  $10^{-5} \text{ m}^{-1}$  and the specific yield is 0.01. The domain is discretized using 12 nodes in each of the directions, for a total of 1,728 nodes and 1,331 elements (see Figure 3.5(a)). Fractures are then incorporated into the mesh by the pre-processor. There are 602 composite elements to be identified, which contain two, four or eight matrix sub-elements. In the composite elements a set of nodal heads are assigned for each matrix sub-element. The total

number of nodal hydraulic heads is 4,096. A constant time step of 1 h is used. In case 2 involving unconfined flow, the tolerance error of the convergent criterion is prescribed to be 0.001 and the prescribed maximum number of iterations is 50.

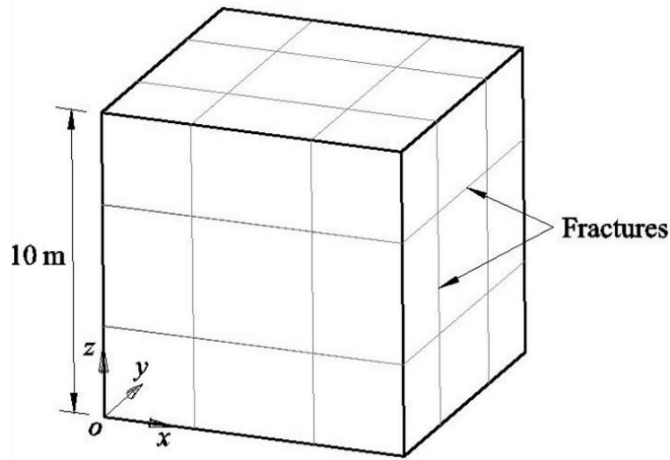


Figure 3.4 Synthetic fractured rock mass

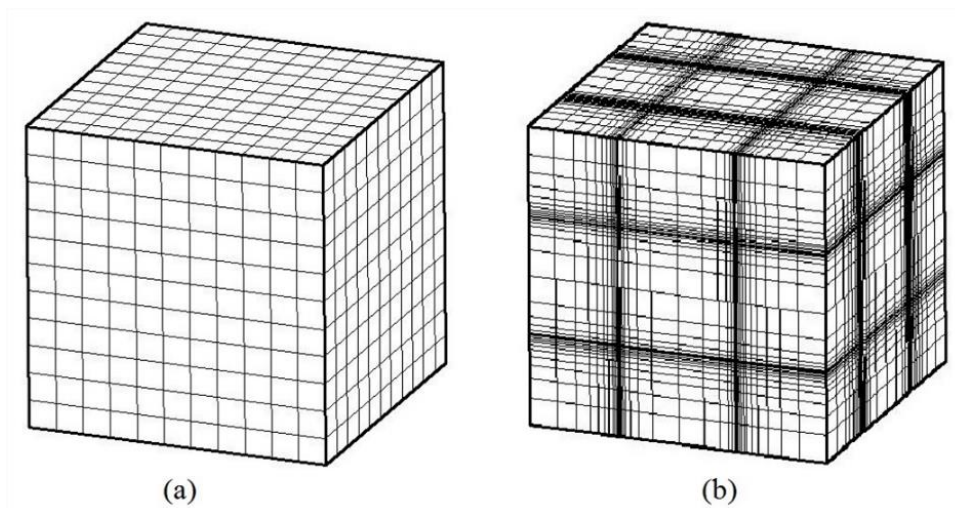


Figure 3.5 Two computational meshes respectively used in (a) composite element model, and (b) COMSOL

Simulation by COMSOL based on the FEM is meanwhile performed to verify the present composite element model. The thin-layer elements with large area-thickness ratio are employed to discretize fractures. To ensure the quality of the finite element mesh used in COMSOL, the nodal spacing is smaller near fractures and gradually larger further from fractures. This results in a domain with a total of 6,624 nodes and 5,324 elements (see Figure 3.5(b)). Obviously, the unknowns to be calculated using COMSOL are more than those using composite element model. However, it is noted that COMSOL does not provide the simulation of saturated but unconfined flow. As an alternative, the Richards' Equation Module [COMSOL AB, 2011] for simulating variably-saturated flow is adopted. The

description of transient, variably-saturated flow in fractured media will be provided in next chapter. Now the readers just need to know when the capillary effect is not significant or only significant near the free surface, the simulation results using the two flow equations are close. The additionally required parameters for COMSOL are: for matrix, the saturated water content and residual water content are respectively assumed to be 0.01 and 0.001; and for fractures, the saturated water content and residual water content are respectively 0.2 and 0.01. The constitutive relations (saturation–pressure head and relative permeability–saturation) for fractures and matrix are assumed to be the same, and evaluated by Van Genuchten–Mualem (VGM) model with the fitting parameters  $\alpha=2\text{ m}^{-1}$ ,  $n=2$  and  $m=0.5$ .

### ***Case 1: transient, saturated flow under confined condition***

The simulation of transient, saturated flow under confined condition is carried out up to a time value equal to 100 h. The total CPU time for 100 time steps using composite element model is 1.15 min on the Intel Xeon X5660, 2.80GHz, and the COMSOL is 2.60 min. Figure 3.6 shows the evolution of the hydraulic head on vertical profile  $y=5\text{ m}$  using composite element model. The nearly identical results using COMSOL are obtained and not shown here. It is clearly seen from Figure 3.6 that the responses of fracture flow and matrix flow to the change of the left side are different. Due to high permeability of fractures, the growth of the hydraulic head in fractures propagates much faster than that in matrix. At the initial stage, e.g.,  $t=1\text{ h}$ ,  $5\text{ h}$ ,  $15\text{ h}$  and  $25\text{ h}$ , matrix flow with lower hydraulic head values is separated by fractures flow. Water flows down the hydraulic gradient, from fractures to surrounding matrix. Until about  $t=95\text{ h}$  a disequilibrium does not vanish, and the new steady flow is formed. The evolution of the hydraulic head in Figure 3.6 illustrates that (i) preferential flow occurs along fractures, and (ii) the interactions between fracture flow and matrix flow play an important role in the process of water flow to the final equilibrium following the change of hydraulic conditions.

Figure 3.7 compares the distributions of the hydraulic head along the horizontal centerline ( $y=5\text{ m}$ ,  $z=5\text{ m}$ ) at different times obtained with composite element model and COMSOL. Excellent agreements are shown. The hydraulic head values at fractures (at  $x=3\text{ m}$  and  $x=7\text{ m}$ ) are greater than those in surrounding matrix. At final time, a uniform distribution of head varying from 20 m to 10 m is achieved.

### ***Case 2: transient, saturated flow under unconfined condition***

The simulation of transient, saturated flow under unconfined condition is firstly

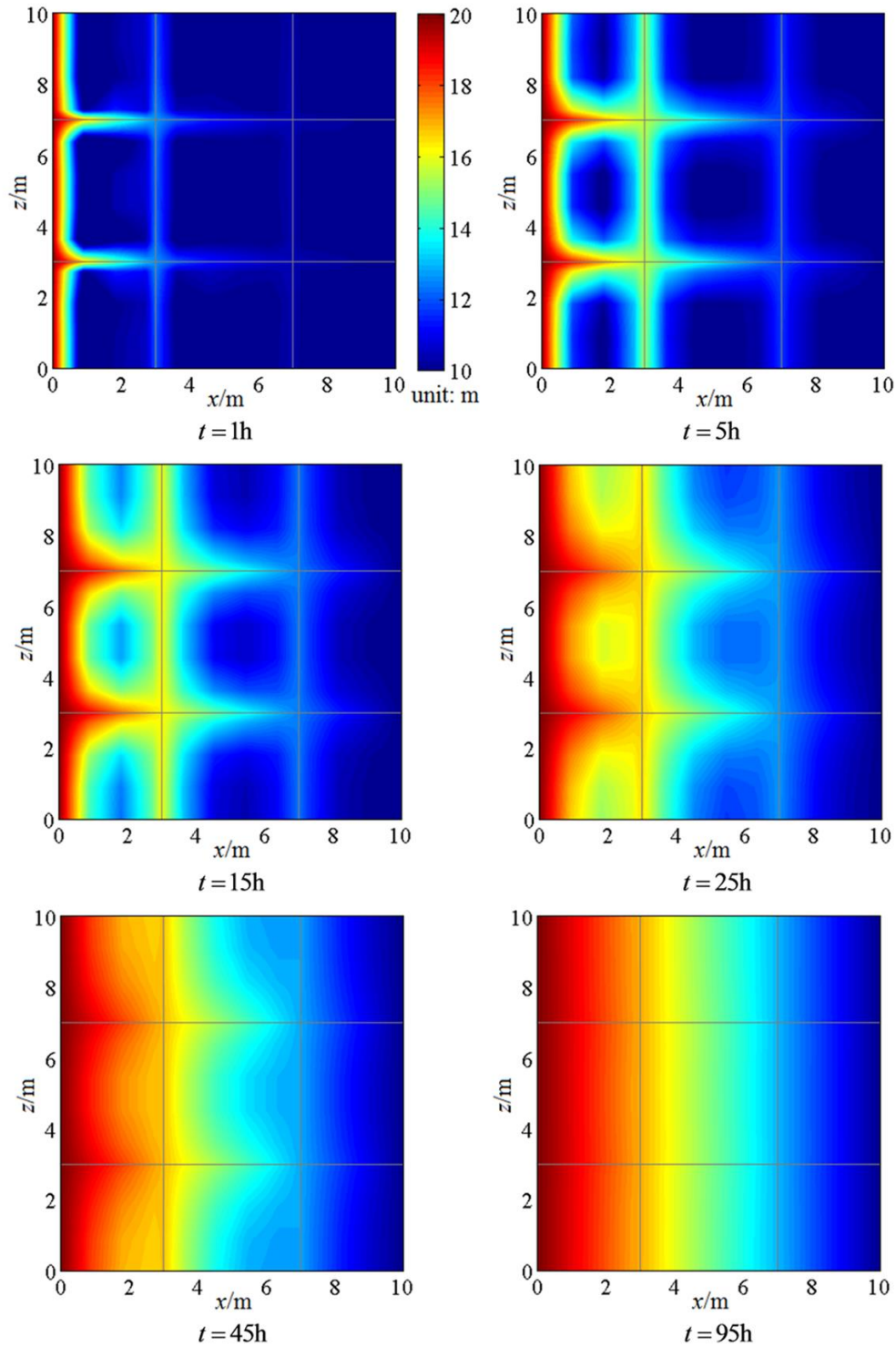


Figure 3.6 Evolution of the hydraulic head on the profile  $y=5$  m using composite element model in case 1

performed up to 10 d with the constant time step of 1 h, and afterwards, is extended to a time value of 1000 d with the constant time step of 10 d. For each time step the iterative process will continue until the prescribed convergence criterion is satisfied or the number of iterations reaches the prescribed maximum. The total CPU time for 339 time steps using

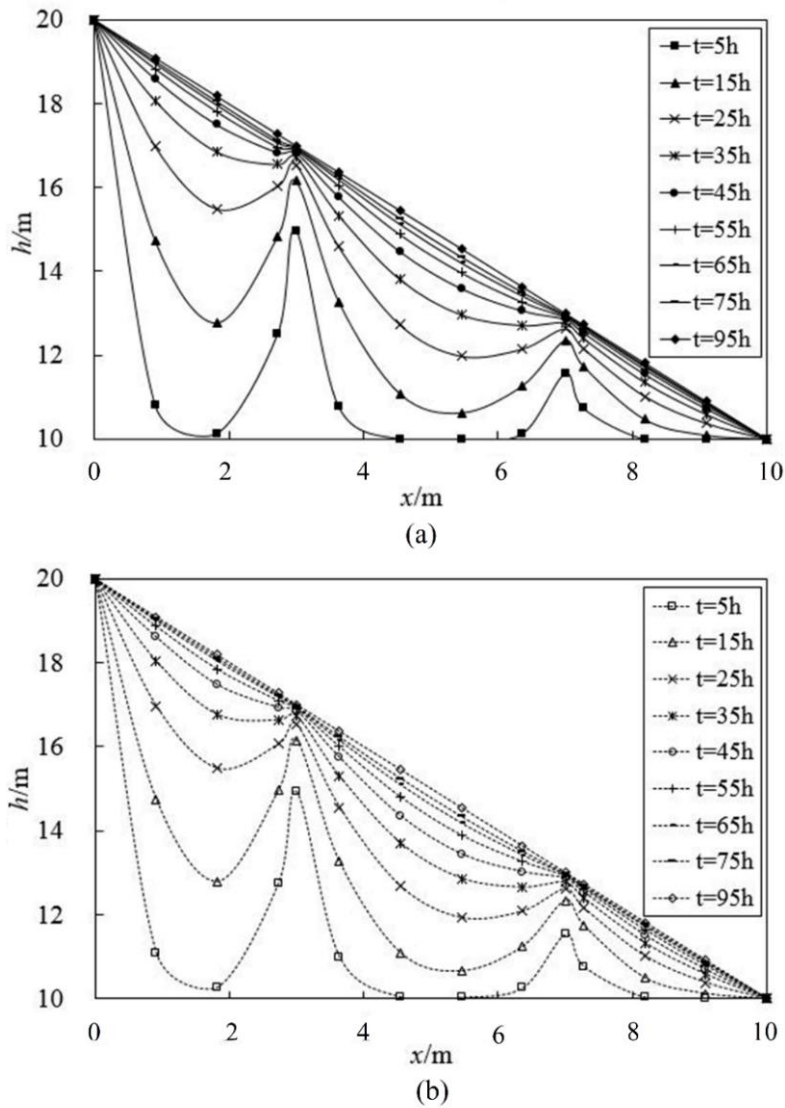


Figure 3.7 Comparisons of the hydraulic head distributions along the centerline at different times obtained with (a) composite element model, and (b) COMSOL in case 1

composite element model is 8.75 min. The convergence of the iteration occurred typically after three to five iterations within most time steps. While using COMSOL, the CPU time is 20.05 min. Figure 3.8 shows the evolution of the hydraulic head on  $y=5$  m using composite element model, in which free surfaces are depicted by solid lines. For comparison purpose, the free surfaces obtained with COMSOL are drawn by dotted lines. It can be seen from Figure 3.8 that there are some disagreements in the free surfaces obtained with composite element model and COMSOL. This can be explained by the use of different governing equations and therefore different solution procedures. Even so, the whole development of the hydraulic head field as well as the shifting of free surface with time appears much the same. Initially, the free surface drops only at fractures but remains at the top of the domain in most of matrix. At about  $t=10$  d, the hydraulic head close to the bottom is nearly steady,

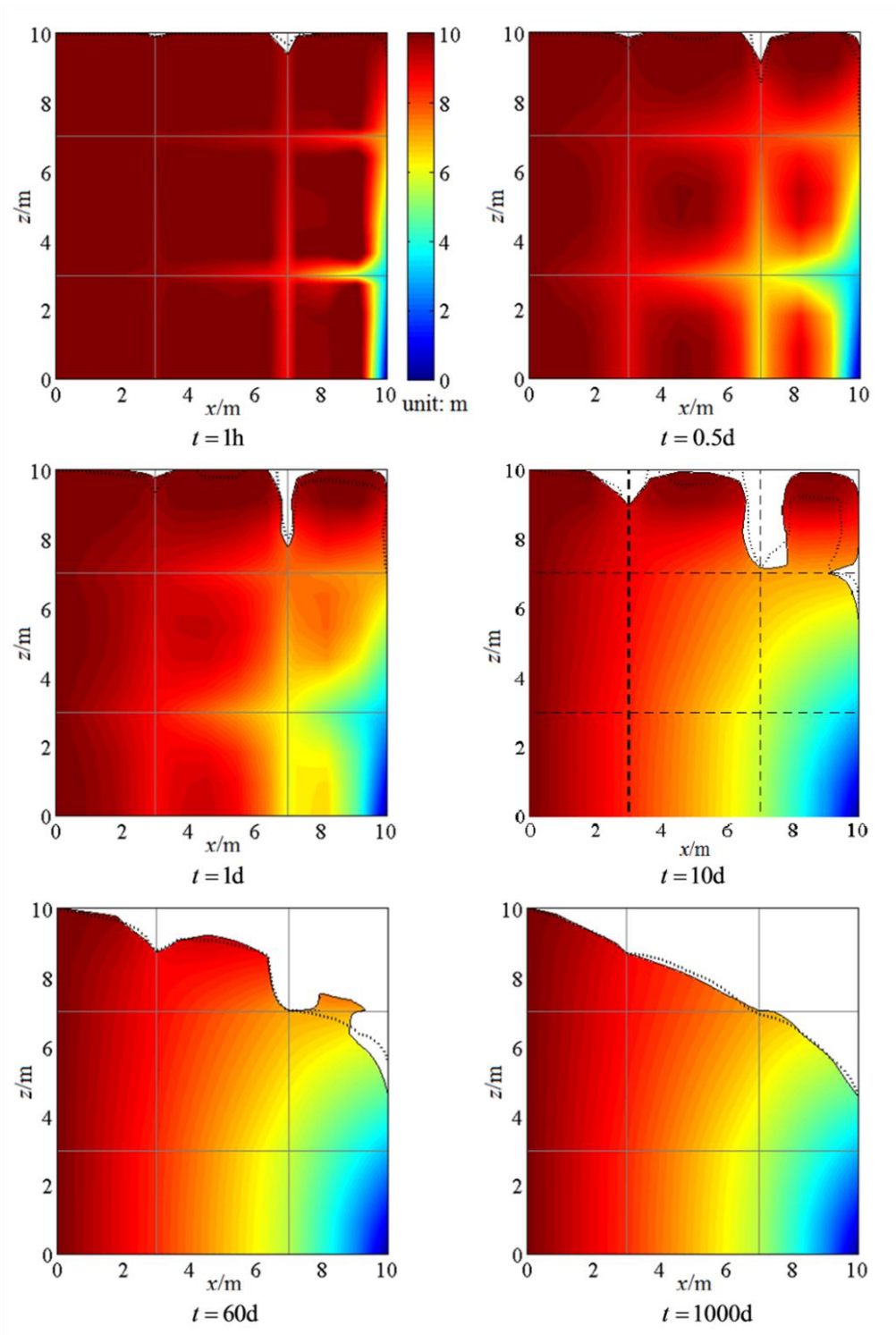


Figure 3.8 Evolution of the hydraulic head on the profile  $y=5$  m using composite element model in case 2

but the shifting of free surface still goes on. A relatively smooth free surface would be achieved at  $t=1000$  d.

Figure 3.9 presents fluxes of inflow, outflow and drainage in the domain obtained with composite element model and COMSOL. They are roughly consistent with each other. The

cause of bringing the difference has been explained above. In the end of transient flow, a steady flux equal to  $0.02 \text{ m}^3 \cdot \text{d}^{-1}$  is expected to be achieved, corresponding to the new steady state. It is worthwhile pointing out that in case 2, the less time is spent on the CPU running using composite element model than COMSOL. This is because on the one hand, the less amount of nodal heads are to be calculated using composite element model; and on the other hand, the governing equations of saturated unconfined flow is known to be less complicated than those of variably-saturated flow used in COMSOL.

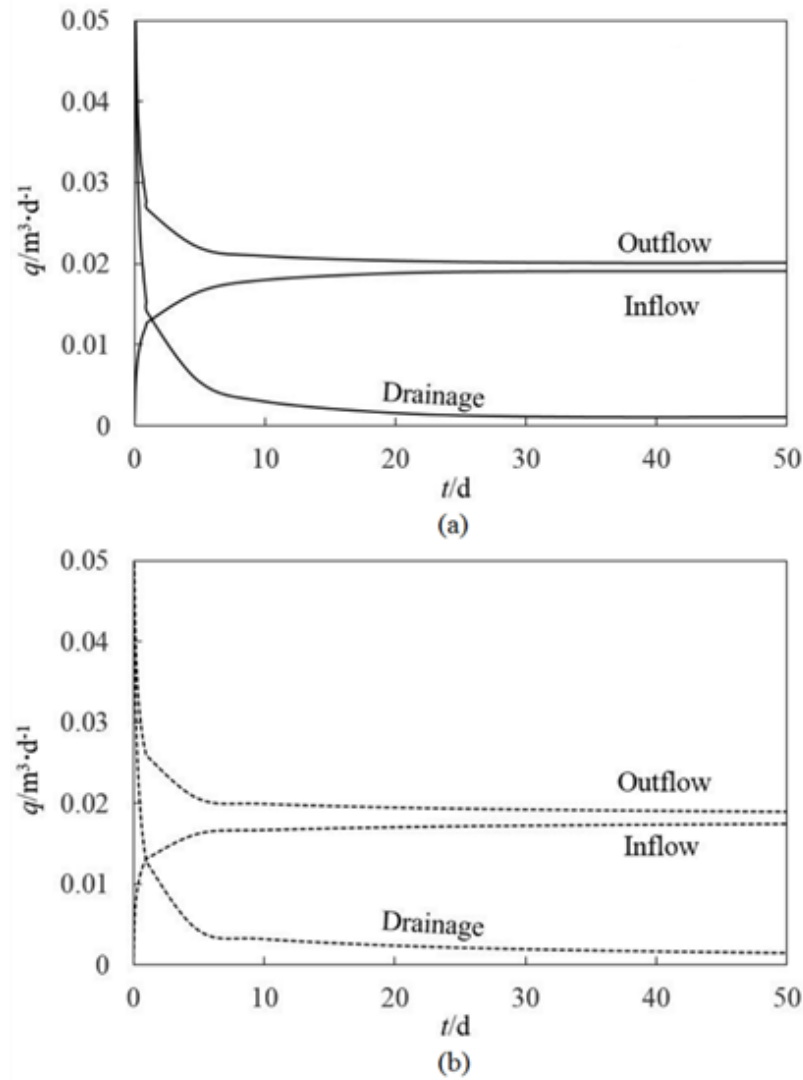


Figure 3.9 Comparisons of inflow, outflow and drainage fluxes in the domain obtained with (a) composite element model, and (b) COMSOL in case 2

### 3.6 Simulations of flow problems in complicated, saturated fractured aquifers

#### 3.6.1 Flow in a 2D fracture network

A two-dimensional aquifer containing a stochastic fracture network is analyzed in this

example. The problem involves groundwater flow through the fractured aquifer to the pumping wells, and was presented by Woodbury and Zhang [2001] who used the finite element method combining the Lanczos reduction technique for modelling transient, saturated flow. A direct comparison with results published in the literature can directly be made. Figure 3.10 shows the geometry of the problem. The simulation domain is 200 m in the  $x$ -axis, 100 m in the  $z$ -axis and a unit thickness in the  $y$ -axis. Fracture characteristics described by Woodbury and Zhang [2001] are used in this study. There are two orthogonal groups of fractures in the aquifer: one being parallel to the  $x$ -axis and the other parallel to the  $z$ -axis. Both groups of fracture have the same aperture equal to  $3.0 \times 10^{-5}$  m.

The boundary conditions for the problem consist of a specified hydraulic head of 10 m along the entire right side ( $x=200$  m) and the lower half left side ( $x=0$ ,  $z=0-50$  m). The top and bottom boundaries are impermeable. Initially, the hydraulic head throughout the domain is equal to 10 m. Two pumping wells are located in the aquifer, the first at  $x=139.89$  m,  $z=77$  m with a pumping rate equal to  $200 \text{ m}^3 \cdot \text{y}^{-1}$ , and the second at  $x=62.68$  m,  $z=48.17$  m with a pumping rate equal to  $150 \text{ m}^3 \cdot \text{y}^{-1}$ . The whole simulation domain is assumed under confined condition. For fractures, the hydraulic conductivities are given by cubic law. Thus, the hydraulic conductivities of fractures are equal to  $2.3196 \times 10^4 \text{ m} \cdot \text{y}^{-1}$ . The specific storage of fractures is  $10^{-3} \text{ m}^{-1}$ . For matrix, the transmissivity and storage coefficient are  $3.1536 \times 10^{-2} \text{ m}^2 \cdot \text{y}^{-1}$  and 0.03 respectively.

The simulation domain is discretized into a regular finite element mesh containing 13,284 elements and 27,058 nodes. By incorporating fractures into the mesh, 5,905 composite elements are determined, and the remaining 7,379 are original finite elements. The total number of nodal heads are 61,234. A constant time step of 0.01 y is used and the simulated time period is 3 y. Hence a total of 300 time steps are calculated.

The CPU time using the composite element model is 34.93 min. Figure 3.10 shows the hydraulic head distribution after three-year pumping obtained with the composite element model. It can be seen that there is preferential flow down the fractures. The lowest hydraulic head in the domain occurs at the locations of the pumping wells. With the increase in distance to the wells, the hydraulic head gradually increases to external boundary head of 10 m. These results are basically consistent with those reported in literature [Woodbury and Zhang, 2001]. But due to the use of relatively sparse computational mesh in this study, the degree of preferential flow down fractures obtained with the composite element model appears to be a little less prominent. By refining the mesh or increasing the number of Gaussian points in matrix sub-elements and fracture fragments, the accuracy will be



improved and approaches that of the finite element approximation. This feature has also been discovered by Chen et al. [2010] and other researchers [He and Chen, 2006]. However, the readers should be reminded that when using the CEM, less effort is made on dividing the computational mesh because fractures are taken into account separately. A relatively simple, regular mesh which means the less number of unknowns to be calculated can always be available if the accuracy is satisfied, even for a very complicated problem. In such problems, the use of the composite element model would be highly advantageous. Oppositely, the finite element approximation becomes difficult to implement in terms of the discretization for fractures. Analysis of the next problem will demonstrate this advantage of the composite element model.

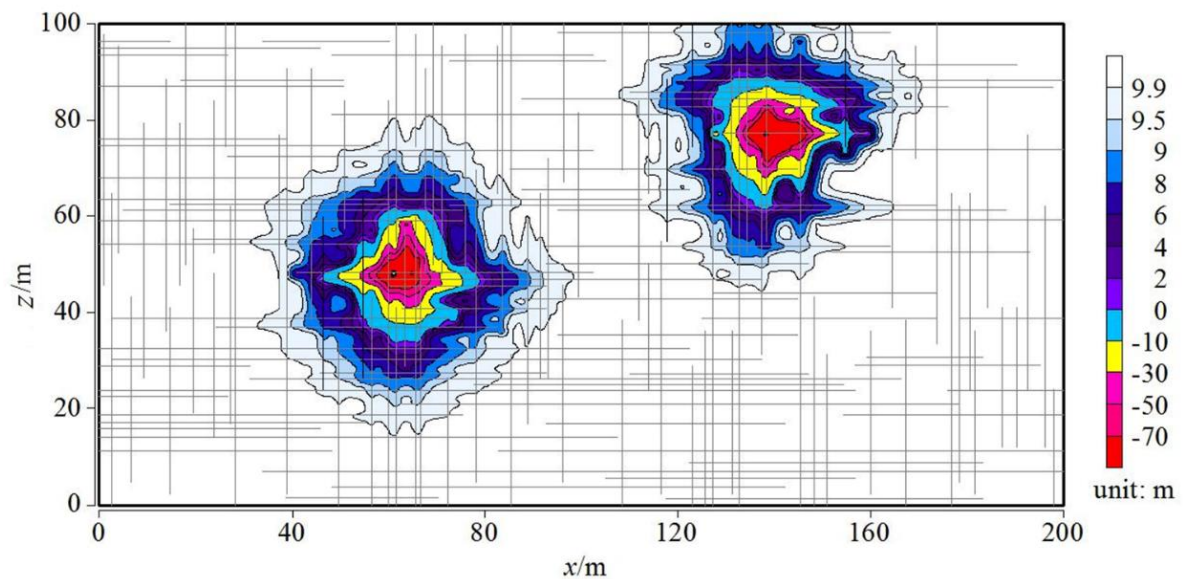


Figure 3.10 Hydraulic head distribution in the domain after three-year pumping obtained with the composite element model

### 3.6.2 Transient groundwater flow in a rock slope following reservoir rapid impounding

The last example concerns a field-scale problem of transient flow of groundwater in a fractured rock slope after reservoir rapid impoundment. The geometry of rock slope and computational mesh are shown in Figure 3.11, where a unit thickness is taken into account. According to the field geological survey [Jiang et al., 2013], the slope is seated on the fresh or slightly weathered plagioclase granite. The magnitude of hydraulic conductivity for rock matrix is  $10^{-12} \text{ m}\cdot\text{s}^{-1}$ . There are four groups of fractures in the rock slope, whose statistical parameters and probability models are listed in Table 3.1. The stochastic fracture networks are generated by the Monte Carlo method, one of which containing 1,817 fractures is

analyzed here (see Figure 3.11(a)).

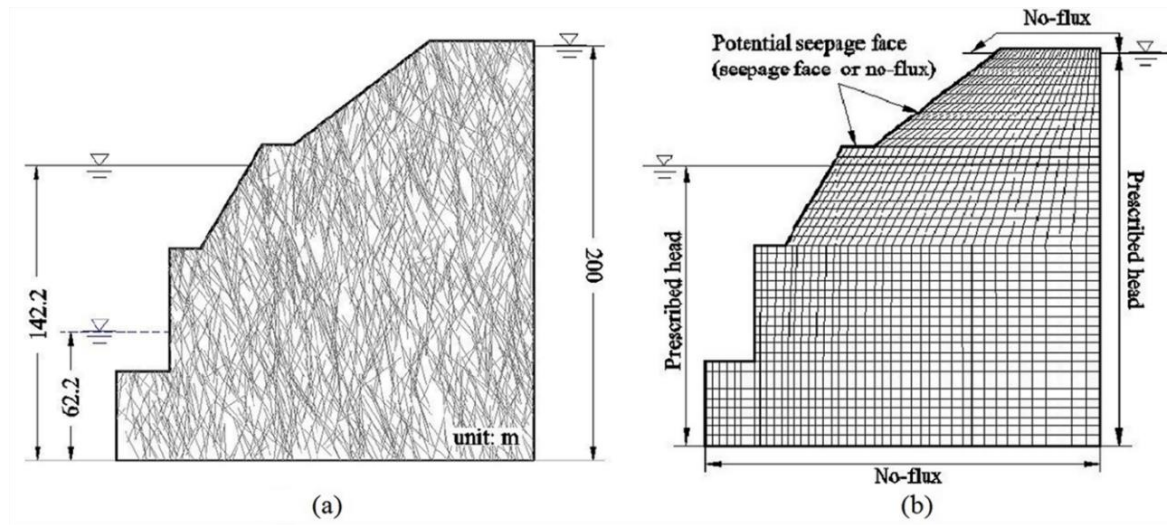


Figure 3.11 Fractured rock slope: (a) geometry, and (b) computational mesh

Table 3.1 Parameters of four groups of fractures and their probability models

Fracture group	Length/m			Dip angle/°			Aperture/mm			Mean spacing/m
	Mean values	Variance	Probability model	Mean values	Variance	Probability model	Mean values	Variance	Probability model	
1	25.97	0.52	Normal	74.27	10.00	Normal	0.20	0.10	Lognormal	2.18
2	31.00	0.92	Normal	110.00	15.00	Normal	0.15	0.75	Lognormal	1.30
3	17.52	0.52	Normal	110.43	10.00	Normal	0.20	0.10	Lognormal	3.56
4	11.13	0.92	Normal	65.49	15.00	Normal	0.15	0.75	Lognormal	7.39

The hydraulic conductivities for fractures in group 1 and group 4 are assumed to be  $1.3 \times 10^{-5} \text{ m}\cdot\text{s}^{-1}$ , and for fractures in group 2 and group 3 are  $2.1 \times 10^{-4} \text{ m}\cdot\text{s}^{-1}$ . Of all the fractures the specific storage and the specific yield are equal to  $10^{-6} \text{ m}^{-1}$  and 0.01, respectively. The specific storage and the specific yield of rock matrix are assumed to be  $10^{-5} \text{ m}^{-1}$  and 0.001, respectively. Suppose groundwater level at right side of the slope equal to 200 m. The left side is submerged by reservoir water. An initial steady flow is developed under a lower reservoir level equal to 62.2 m. The corresponding boundary condition is that the hydraulic head at the lower left side is equal to be 62.2 m, and the higher left side is the potential seepage face. At a certain point in time the slope is subjected to reservoir rapid impounding. The reservoir level is suddenly rise to 142.2 m. Distribution of groundwater flow in the fractured rock slope is changed.

The slope is discretized into 1,504 elements and 3,184 nodes (see Figure 3.11(b)). By executing the CEM pre-processing program, 1,494 composite elements are sought out. The total number of unknowns in the system is 103,686. A steady flow simulation using the

composite element model is firstly performed. Based on the results of initial steady hydraulic head, simulation of transient flow up to the time value of 1000 d is carried out. The time discretization adopted is the same as case 2 in simply synthetic example. For the iteration procedure, the convergence criterion is 0.01 and the maximum number of iterations is 30.

The total CPU time taken to solve steady flow is 34.18 min and to solve transient flow is 8 h 11.60 min. Figure 3.12 shows the distribution of the hydraulic head in the rock slope before and after reservoir rapid impounding. It is seen from Figure 3.12 that at  $t=0$ , the hydraulic head smoothly varies from 62.2 m at left side to 200 m at right side. After the reservoir level is raised to 142.2 m it begins to grow. Meanwhile, the free surface shifts upward, resulting in a gradually expanded saturated zone. Figure 3.13 shows the velocity vectors of groundwater in the slope. At the initial time, the groundwater velocities adjacent to reservoir point out of the slope because the reservoir level is lower than the free surface in slope. Water flows into the slope after the rise of reservoir level, which has been clearly indicated by the profile of groundwater velocity vectors at  $t=10$  d, where there are some inward velocity vectors. These inward velocity vectors mostly vanish at  $t=100$  d. The groundwater velocities keep decreasing until the end of the simulated period. It is found that they are heterogeneous in the fractured rock slope. The velocities at fractures are greater than those at rock matrix. These results illustrate that fractures dominate groundwater flow, and rock matrix with relatively large porosity play a major role of storing water that flows down fractures. The interactions between the two flow systems are varying temporally and spatially.

### **3.7 Conclusions**

A composite element model for simulating transient, saturated flow in fractured media with a free surface has been constructed. The model has the following features: (i) fractures do not need to be discretized into specific elements but are inserted into elements representing matrix according to their geometric positions, thereby forming the composite elements containing both matrix sub-elements and fracture fragments; (ii) in each composite element, governing equations for matrix sub-element and of fracture fragment are respectively established, and they are linked through the fracture-matrix interface, finally constituting an integrated composite element equation; and (iii) the composite element equation has the same form as the conventional finite element one, thus the techniques used

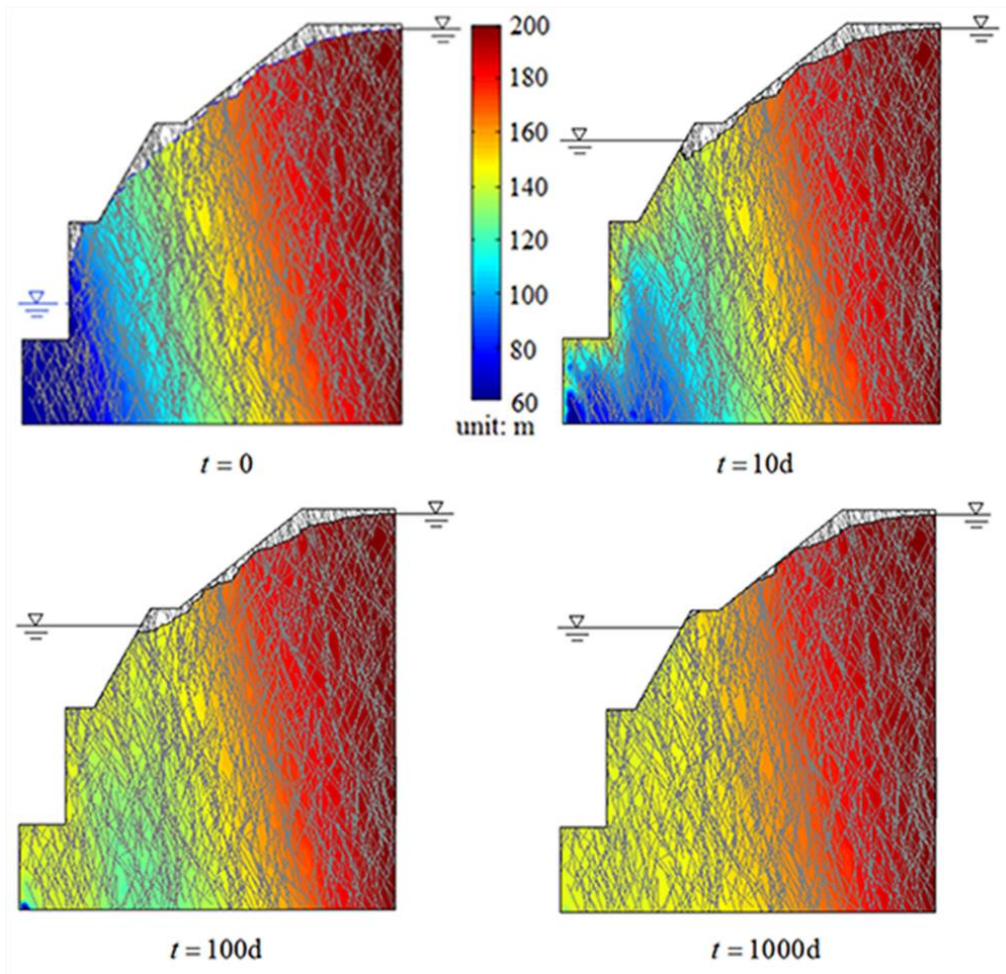


Figure 3.12 Evolution of the hydraulic head in the fractured rock slope using the composite element model

to solve the finite element equation can be directly applied into the composite element solution. Specifically, when superimposing the contributions from matrix sub-elements and fracture fragments at each node in the composite element the leakage fluxes across the fracture-matrix interface achieve self-balancing. Therefore, no special calculation is needed to consider the fracture-matrix interaction.

The effectiveness of the composite element model was firstly verified by a simply synthetic example. Results were compared with those obtained with the well-tested, FEM-based COMSOL. Unlike the composite element model, fractures need to be individually discretized while using COMSOL, increasing the complexity of the computational mesh. The impact of the mesh complexity would be embodied in time consumption of the solution. In the first case concerning transient, saturated flow under confined condition, the difference in CPU time using the composite element model and COMSOL was not obvious. Also, excellent agreements between the two results were shown. For the second case concerning

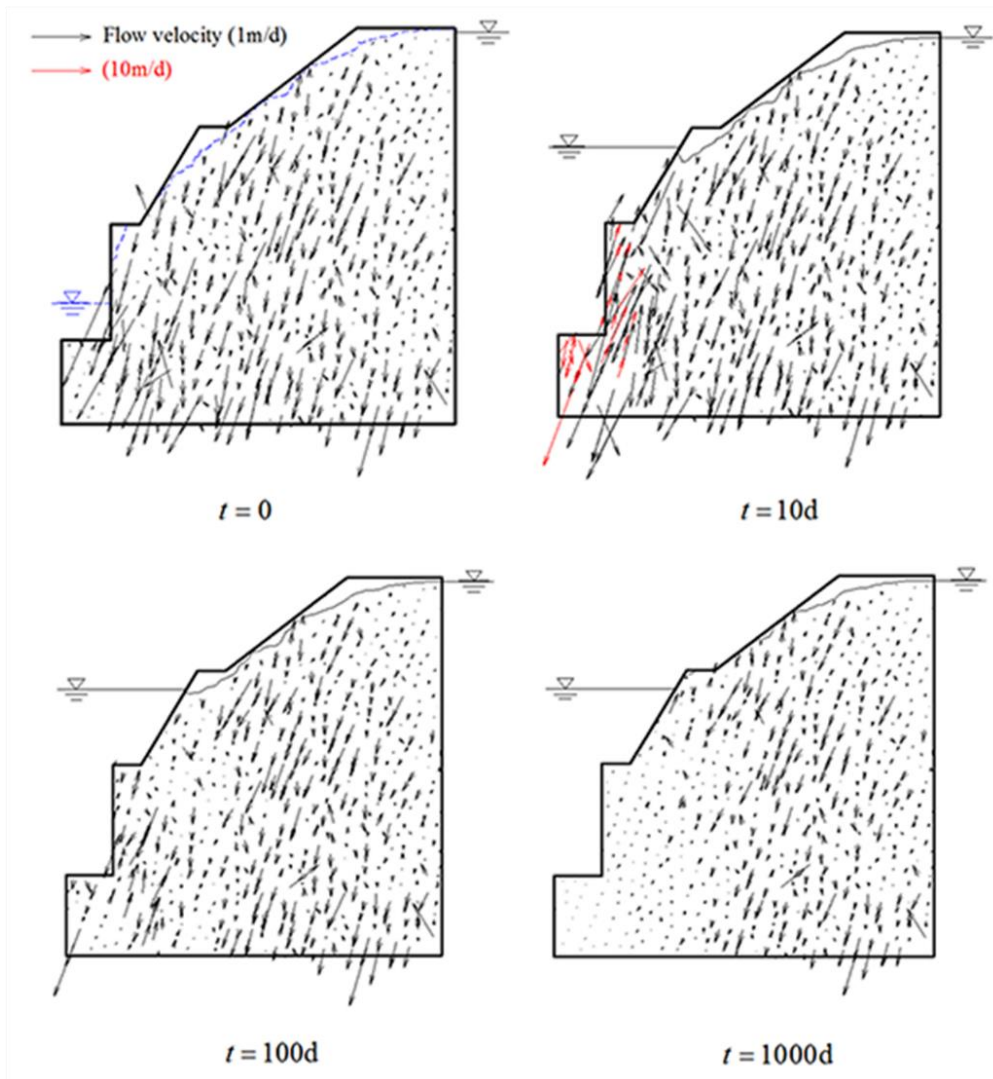


Figure 3.13 Groundwater velocity vectors in the fractured rock slope obtained with the composite element model

transient, saturated flow under unconfined condition, the simulation of transient, variably-saturated flow was constrainedly implemented in COMSOL because COMSOL could not provide that of transient, saturated but unconfined flow. Naturally, there were some disagreements in the results obtained with the composite element model constructed in this chapter and COMSOL, but a basic fact could be confirmed that the velocity of the free surface at fractures was greater than in matrix and much longer time than the case under confined condition was needed to reach the final equilibrium. It needs to be particularly mentioned that in practice, when the capillary effect in the unsaturated zone is not significant, the use of equations of transient, saturated flow with a shifting free surface takes precedence over the use of equations of transient, variably-saturated flow, not only because of the less nonlinearity of governing equations but also because of the easier accessibility to the

specific yield compared to the constitutive relations under variably-saturated condition.

The CEM pre-processing program for automatic discretization of the simulation domain has been introduced. In fact, only matrix domain is discretized. Fractures are later incorporated into the generated mesh. In this way, the intersection calculations with each small, regular element are mainly performed, which are believed to be more efficient than the generation of specific elements for fractures. In the first illustrative problem that was described by *Woodbury and Zhang* [2001], the distribution of the fracture network was not very complicated because two groups of fractures were orthogonal. The simulation results were nearly consistent with those reported in the literature. To highlight the advantage of the composite element model, the problem concerning a rock slope containing four groups of randomly distributed fractures was discussed. The results of the hydraulic head and groundwater velocity demonstrated that fractures with high permeability are dominant flow pathways, while rock matrix with relatively large porosity have a capacity for storing water that flows down fractures.

## References

1. Boulton NS. Unsteady radial flow to a pumped well allowing for delayed yield from storage. *International Association of Scientific Hydrology Publication* 1954; **37**: 472–477.
2. Chen SH. Computational rock mechanics and engineering. China Water and Power Press: Beijing, 2006.
3. Chen SH, Feng XM. Composite element model for rock mass seepage flow. *Journal of Hydrodynamics* 2006; **18**(2): 219–224.
4. Chen SH, Xue LL, Xu GS, Shahrour I. Composite element method for the seepage analysis of rock masses containing fractures and drainage holes. *International Journal of Rock Mechanics and Mining Sciences* 2010; **47**(5): 762–770.
5. COMSOL AB. Subsurface Flow Module User's Guide (version 4.2a), 2011.
6. Cooley RL. Some new procedures for numerical solution of variably saturated flow problems. *Water Resources Research* 1983; **19**(5): 1271–1285.
7. Desai CS. Finite element residual schemes for unconfined flow. *International Journal for Numerical Methods in Engineering* 1976; **10**(6): 1415–1418.
8. Desai CS, Li GC. A residual flow procedure and application for free surface flow in porous media. *Advances in Water Resources* 1983; **6**(1): 27–35.
9. Feng XM. Study on the composite element method for the seepage field and characteristics of the fractured rock masses. Doctoral dissertation, Wuhan University, Wuhan, 2006.
10. Green DW, Dabiri H, Weinaug CF, Prill R. Numerical modeling of unsaturated groundwater flow and comparison of the model to a field experiment. *Water Resources Research* 1970; **6**(3): 862–874.
11. He Z, Chen S. Study on bolted rock mass by hierarchical composite element method. *Chinese Journal of Rock Mechanics and Engineering* 2006; **25**(8): 1698–1704.
12. Hou XP, Xu Q, He J, Chen SH. Composite element algorithm for unsteady seepage in fractured rock masses. *Chinese Journal of Rock Mechanics and Engineering* 2015; **34**(1): 48–56.
13. Jiang Q, Yao C, Ye Z, Zhou C. Seepage flow with free surface in fracture networks. *Water Resources Research* 2013; **49**(1): 176–186.
14. Jing L, Ma Y, Fang Z. Modeling of fluid flow and solid deformation for fractured rocks

- with discontinuous deformation analysis (DDA) method. *International Journal of Rock Mechanics and Mining Sciences* 2001; **38**(3): 343–355.
15. Li H, Jiao JJ. Influence of the tide on the mean watertable in an unconfined, anisotropic, inhomogeneous coastal aquifer. *Advances in Water Resources* 2003; **26**(1): 9–16.
  16. Lin SZ. Improved iterative format of symmetric successive over relaxation-preconditioned conjugated gradient method. *Chinese Journal of Numerical Methods and Computer Applications* 1997; **12**(4): 266–270.
  17. Mao CX. Seepage computation analysis and control. China Water and Power Press: Beijing, 2003.
  18. Neuman SP. Saturated-unsaturated seepage by finite elements. *Journal of the Hydraulic Division, American Society of Civil Engineers* 1973; **99**: 2233–2250.
  19. Neuman SP, Witherspoon PA. Variational principles for confined and unconfined flow of ground water. *Water resources research* 1970; **6**(5): 1376–1382.
  20. Neuman SP, Witherspoon PA. Analysis of nonsteady flow with a free surface using the finite element method. *Water Resources Research* 1971; **7**(3), 611–623.
  21. Purkey DR, Wallender WW, Islam N, Fogg GE, Sivakumar B. Describing near surface, transient flow processes in unconfined aquifers below irrigated lands: a deforming finite element model for heterogeneous aquifers. *Journal of hydrology* 2006; **330**(3), 435–443.
  22. Qiang S. Study on the three-dimensional elastic-viscoplastic composite element method. Doctoral dissertation, Wuhan University, Wuhan, 2005.
  23. Qin WX, Zhang YA, Qiang S, Wang YJ. Pre-process of two-dimensional composite element method for discontinuous rock masses. *Chinese Journal of Changsha University of Science and Technology (Natural Science)* 2009; **6**(1): 29–35.
  24. Taylor RL, Brown CB. Darcy flow solutions with a free surface. *Journal of the Hydraulics Division* 1967; **93**(2): 25–33.
  25. Wang EZ. Seepage calculation method in fissure networks on vertical section. *Hydrogeology Engineering Geology* 1993; **20**(4): 27–29.
  26. Woodbury A, Zhang K. Lanczos method for the solution of groundwater flow in discretely fractured porous media. *Advances in Water Resources* 2001; **24**(6): 621–630.
  27. Zhang YT, Chen P, Wang L. Initial flow method for seepage analysis with free surface. *Chinese Journal of Hydraulic Engineering* 1988; **8**: 18–26.
  28. Zhu BF. The finite element method theory and applications. China Water and Power Press: Beijing, 1998.



# Chapter 4 Composite Element Method for Modelling Transient, Variably-Saturated Flow in Fractured Media

## 4.1 Introduction

In recent years, problems involving groundwater flow in variably-saturated fractured media have received increasing attention. One primary reason for this is the need to evaluate the suitability of a site for near surface disposal of highly radioactive waste. Another reason is the need to evaluate the impact of an existing waste disposal site on surrounding groundwater system and its environment [Huyakorn and Thomas, 1984]. Both types of evaluation require a thorough understanding of groundwater flow in variably-saturated fractured media. Due to the difference of hydraulic characteristics between fractures and matrix, and the complexity of the geometric configurations of natural fractured media, the groundwater flow regimes can be very complicated. The computer simulation using numerical models is the most effective and indispensable research means.

Similar to the saturated flow, the variably-saturated flow in fractured media may be simulated using either the implicit approaches including the equivalent porous media approach and the dual porosity approach or the explicit approach that is the discrete fracture network approach. However, the appropriateness of using the implicit approaches for simulations of variably-saturated flow in fractured media appears to be less than that of using the implicit approaches for simulations of saturated flow in fractured media. This is due to the fact that the differences in the capillary pressure characteristics and the hydraulic conductivities between fractures and matrix often result in a high degree of heterogeneity in the unsaturated fracture-matrix flow systems. Field and laboratory experiments in natural unsaturated fractured rock masses have demonstrated strong evidence of channeling and obviously preferential flow paths in individual fractures and in fracture networks [Neretnieks et al., 1982; Neretnieks, 1993]. Thus, the explicit approach is considered to be conceptually preferable than the implicit approaches for simulations of variably-saturated flow in fractured media.

A number of discrete fracture network models have been developed in the literature [Rasmussen and Evans, 1989; Cacas et al., 1990; Mustapha and Mustapha, 2007; Erhel et al., 2009; Berrone et al., 2013; Hyman et al, 2015], but most of them did not account for flow in matrix. Cey et al. [2006] in their study on infiltration processes in fractured soils

indicated that the incorporation of matrix flow is necessary even in situations where fracture dominated flow occurs. The model that is currently widely accepted and applied is the discretely-fractured porous media model proposed by Therrien and Sudicky [1996] based on the control volume finite element method [Therrien et al., 2005]. In this model, fractures are discretized into 2D elements; the porous matrix are discretized into 3D elements; and the two elements have common nodes at the fracture-matrix interface. In other words, the fractures are forcibly discretized to the faces of the adjacent porous matrix elements. Therrien and Sudicky [1996] established the finite element equations for variably-saturated flow in fractured media on the basis of this mesh. According to the author's understanding, it is not easy to generate such a mesh, especially if the number of fractures is large or their distribution is complex. The geometric characteristics of the fracture network strongly restrict the mesh generation. Although Mustapha et al. [2011] has presented a relatively efficient method to discretize the fractured media, there is still a need to remove or replace the locally complex geometric configurations of fractured media. More details on the discretization method of Mustapha et al. [2011] has been presented in Section 2.3.3 of Chapter 2.

As mentioned many times earlier, the CEM has a unique advantage in dealing with the discretization of the fractured media. Moreover, its capability to simulations of transient saturated flow problems in fractured media has been demonstrated in Chapter 3. As a continuation of Chapter 3, this chapter studies the application of CEM to solution of transient, variably-saturated flow in fractured media. The main contents include: (i) mathematical descriptions of transient, saturated flow problem; (ii) composite element model development, including the establishment of the constitutive relations for matrix and fractures and the fracture-matrix interaction area factor, and the formulation of the CEM; (iii) key techniques for improving numerical accuracy and efficiency, including under-relaxation iteration, mass matrix lumping, and adaptive time stepping techniques; (iv) verification examples; and (v) simulations of flow problems in complicated, variably-saturated fractured aquifers.

## 4.2 Mathematical descriptions of transient, variably-saturated flow problem

A modified Richards' equation is used to describe transient, variably-saturated flow, as follow:

$$(S_w S_s + C) \frac{\partial h}{\partial t} = \nabla \cdot (k_r \mathbf{k} \nabla h) - q, \quad \text{in } \Omega \quad (4.1)$$

where  $S_w = \theta/\theta_s$  is saturation,  $\theta$  is water content,  $\theta_s$  is saturated water content which is equal to the porosity,  $C = \theta_s \cdot dS_w/dh$ ,  $C$  is specific moisture capacity,  $k_r = k_r(S_w)$  is relative permeability, and the remaining parameters have the same meanings as mentioned above. Equation (4.1) is subjected to boundary conditions as given in Equations (3.2)-(3.3) and initial conditions in Equation (3.6).

The variational principle can convert the solution of Equation (4.1) together with boundary conditions into a functional optimization problem below:

$$I(h) = \iiint_{\Omega} \left[ \frac{1}{2} (\nabla h)^T k_r k (\nabla h) + qh + (S_w S_s + C) h \frac{\partial h}{\partial t} \right] d\Omega + \iint_{\Gamma_2} gh d\Gamma = \min \quad (4.2)$$

Unlike that in transient, saturated but unconfined flow, the free surface in transient, variably-saturated flow is no longer the unknown boundary to be determined but is directly achieved as part of the solution of Equation (4.2). Collection of the points at which  $P=0$  forms the free surface.

### 4.3 Composite element model development

#### 4.3.1 Constitutive relations for matrix and fractures

In order to solve the variably-saturated flow equation, the constitutive relations, i.e., saturation–pressure head and relative permeability–saturation relations, must be established. Generally, the Van Genuchten [1980] and Brooks-Corey [1964] models are adopted to describe the constitutive relations for matrix. The saturation–pressure head relations in the two models are respectively expressed as:

$$\text{VG: } S_e(P) = \begin{cases} \left(1 + |\alpha P|^n\right)^{-m}, & P < 0 \\ 1, & P \geq 0 \end{cases} \quad (4.3)$$

$$\text{BC: } S_e(P) = \begin{cases} |\alpha P|^{-n}, & P < -1/\alpha \\ 1, & P \geq -1/\alpha \end{cases} \quad (4.4)$$

where  $S_e = (\theta - \theta_r)/(\theta_s - \theta_r)$  is effective saturation,  $\theta_r$  is residual water content,  $\alpha$ ,  $n$  and  $m$  are the fitting parameters. Then based on theory of Mualem [1976], the relative permeability–saturation relations are respectively given by:

$$\text{VGM: } k_r(S_e) = \begin{cases} S_e^{0.5} \left[1 - \left(1 - S_e^{1/m}\right)^m\right]^2, & P < 0 \\ 1, & P \geq 0 \end{cases} \quad (4.5)$$

$$\text{BCM: } k_r(S_e) = \begin{cases} S_e^{2/n+2.5}, & P < -1/\alpha \\ 1, & P \geq -1/\alpha \end{cases} \quad (4.6)$$

where  $m=1-1/n$ . Vogel et al. [2001] have pointed out that when  $n$  is small, i.e.,  $n < 1.5$  (which is typical of fine-grained soil), the use of the VGM model may induce numerical instability. To eliminate the instability they put forward the modified forms of Equations (4.3) and (4.5), as follows:

$$\text{Modified VG: } S_e^*(P) = \begin{cases} \left(1 + |\alpha P|^n\right)^{-m}, & P < P_{\min} \\ 1, & P \geq P_{\min} \end{cases} \quad (4.7)$$

$$\text{Modified VGM: } k_r(S_e) = \begin{cases} S_e^{0.5} \left[ \frac{1 - F(S_e^*)}{1 - F(1)} \right]^2, & P < P_{\min} \\ 1, & P \geq P_{\min} \end{cases} \quad (4.8)$$

where  $P_{\min}$  is the prescribed minimum pressure head, and

$$\begin{aligned} F(S_e^*) &= (1 - S_e^{*1/m})^m \\ S_e^* &= (\theta - \theta_r) / (\theta_m - \theta_r) \\ \theta_m &= \theta_r + (\theta_s - \theta_r) \cdot [1 + (2\alpha)^n]^m \end{aligned} \quad (4.9)$$

Note that the parameters  $P_{\min}$  and  $\theta_{\min}$  have no real physical meaning and are just used to modify the shapes of the saturation and relative permeability curves. In this study, the VGM and modified VGM models are respectively used for matrix with  $n < 1.5$  and  $n \geq 1.5$ .

Natural fractures have variable apertures that are expected to be important for their hydraulic properties under variably-saturated condition, where the capillary pressure (negative pressure) is the function of pore size. A number of researches have been made on the relationship between the variable aperture of a single fracture and its hydraulic parameters. The research methodologies cover laboratory measurement (e.g., [Reitsma and Kueper, 1994], [Persoff and Pruess, 1995]), theoretical analysis (e.g., [Wang and Narasimhan, 1985], [Zhou et al., 1998]) and numerical experiment (e.g., [Pruess and Tsang, 1990], [Vandersteen et al., 2003]). The following is a brief description of each of the methodologies.

Reitsma and Kueper [1994] made use of a laboratory technique to investigate the relation between fluid saturation and capillary pressure of a rough-walled limestone fracture. In their experiment, oil and water were respectively used as non-wetting and wetting phase. The measured capillary pressure curves were represented by the standard constitutive relations including the VGM and BCM models. Wang and Narasimhan [1985] constructed a general statistical theory for flow along the fractures and generated the synthetic

expressions describing the relations between fracture saturation, hydraulic conductivity and pressure head based on aperture distributions. Pruess and Tsang [1990] used a stochastically generated network of the variable fracture aperture to numerically investigate two-phase flow through a rough-walled fracture. Results were obtained according to the invasion percolation model for determining the relations of saturation–pressure head and relative permeability–saturation.

In this study, the constitutive relations for fractures are based on the work of Wang and Narasimhan [1985]. In addition, the VGM model or the tabular data will also be used to describe the constitutive relations for the fractures in some examples.

### 4.3.2 Fracture-matrix interaction area factor

In contrast to the saturated zone in which water move rapidly along fractures, the fractures with apertures larger than the size of matrix pores will desaturate first during the drainage process, and the bulk of water will be through interconnected pores in the matrix. Under this condition, as water moves from one matrix block to another, the drained or unsaturated portions of the fractures will reduce the area available for water flow from one matrix block to another matrix block. Wang and Narasimhan [1985] explained this phenomenon and suggested using an effective area factor to account for the changes of the fracture-matrix interaction area when the fractures desaturate. In developing the composite element model, the effective area factor will be taken into account. Details on the implementation will be discussed in the next section.

### 4.3.3 Composite element formulation

The composite element equation for transient, variably-saturated flow in fractured media is derived by the variational analysis. Similar to that in Section 3.3.2, by substituting Equation (3.8) into Equation (4.2), the variational principle within matrix sub-element  $e_i$  can result in:

$$\mathbf{K}_{e_i} \bar{\mathbf{h}}_{e_i} + \mathbf{C}_{e_i} \frac{\partial \bar{\mathbf{h}}_{e_i}}{\partial t} = \mathbf{d}_{e_i} \quad (4.10)$$

in which

$$\begin{aligned} \mathbf{K}_{e_i} &= \iiint_{\Omega^{e_i}} (\nabla N)^T k_{re_i} \mathbf{k}_{e_i} (\nabla N) d\Omega \\ \mathbf{C}_{e_i} &= \iiint_{\Omega^{e_i}} N^T (S_{we_i} S_{se_i} + C_{e_i}) N d\Omega \\ \mathbf{d}_{e_i} &= -\iiint_{\Omega^{e_i}} q N d\Omega - \iint_{\Gamma_2^{e_i}} g_{e_i} N d\Gamma \end{aligned} \quad (4.11)$$

where  $k_{re_i}$ ,  $S_{we_i}$  and  $C_{e_i}$  are respectively relative permeability, saturation and specific moisture capacity of  $e_i$ .

By substituting Equation (3.9) into Equation (4.2), the variational principle within fracture fragment  $f_{ij}$  can result in:

$$\begin{cases} \mathbf{K}_{f_{ij},ii} \bar{\mathbf{h}}_{e_i} + \mathbf{K}_{f_{ij},ij} \bar{\mathbf{h}}_{e_j} + \mathbf{C}_{f_{ij}} \left( \frac{\partial \bar{\mathbf{h}}_{e_i}}{\partial t} + \frac{\partial \bar{\mathbf{h}}_{e_j}}{\partial t} \right) = \mathbf{d}_{f_{ij}} \\ \mathbf{K}_{f_{ij},ji} \bar{\mathbf{h}}_{e_i} + \mathbf{K}_{f_{ij},ij} \bar{\mathbf{h}}_{e_j} + \mathbf{C}_{f_{ij}} \left( \frac{\partial \bar{\mathbf{h}}_{e_i}}{\partial t} + \frac{\partial \bar{\mathbf{h}}_{e_j}}{\partial t} \right) = \mathbf{d}_{f_{ij}} \end{cases} \quad (4.12)$$

in which

$$\begin{aligned} \mathbf{K}_{f_{ij},ii} = \mathbf{K}_{f_{ij},jj} &= \frac{b}{2} \iint_{\Gamma^{f_{ij}}} k_{rf_{ij}} \left( \frac{k_{f_{ij}x_f}}{2} \frac{\partial \mathbf{N}^T}{\partial x_f} \frac{\partial \mathbf{N}}{\partial x_f} + \frac{k_{f_{ij}y_f}}{2} \frac{\partial \mathbf{N}^T}{\partial y_f} \frac{\partial \mathbf{N}}{\partial y_f} + \frac{2k_{f_{ij}z_f}}{b^2} \mathbf{N}^T \mathbf{N} \right) dx_f dy_f \\ \mathbf{K}_{f_{ij},ij} = \mathbf{K}_{f_{ij},ji} &= \frac{b}{2} \iint_{\Gamma^{f_{ij}}} k_{rf_{ij}} \left( \frac{k_{f_{ij}x_f}}{2} \frac{\partial \mathbf{N}^T}{\partial x_f} \frac{\partial \mathbf{N}}{\partial x_f} + \frac{k_{f_{ij}y_f}}{2} \frac{\partial \mathbf{N}^T}{\partial y_f} \frac{\partial \mathbf{N}}{\partial y_f} - \frac{2k_{f_{ij}z_f}}{b^2} \mathbf{N}^T \mathbf{N} \right) dx_f dy_f \\ \mathbf{C}_{f_{ij}} &= \frac{b}{4} \iint_{\Gamma^{f_{ij}}} \mathbf{N}^T \left( S_{wf_{ij}} S_{sf_{ij}} + C_{f_{ij}} \right) \mathbf{N} dx_f dy_f \\ \mathbf{d}_{f_{ij}} &= - \iint_{\Gamma^{f_{ij}}} g_{f_{ij}} \mathbf{N} d\Gamma \end{aligned} \quad (4.13)$$

where  $k_{rf_{ij}}$ ,  $S_{wf_{ij}}$  and  $C_{f_{ij}}$  are respectively relative permeability, saturation and specific moisture capacity for  $f_{ij}$ . As mentioned above, water flow between two adjacent matrix sub-elements is only through the portions of the fracture fragment that remain saturated. Thus, the integral area corresponding to the normal hydraulic conductivity of the fracture fragment (i.e.,  $k_{f_{ij}z_f}$ ) should be multiplied by the effective area factor to reflect the change of the fracture-matrix interaction area with the saturation or the pressure head.

By assembling Equations (4.11) for all matrix sub-elements and Equations (4.13) for all fracture fragment within the composite element, the final composite element equation can be expressed as:

$$\begin{bmatrix} \mathbf{K}_{11} & \mathbf{K}_{12} & \cdots & \mathbf{K}_{1l} \\ \mathbf{K}_{21} & \mathbf{K}_{22} & \cdots & \mathbf{K}_{2l} \\ \vdots & \vdots & \ddots & \vdots \\ \mathbf{K}_{l1} & \mathbf{K}_{l2} & \cdots & \mathbf{K}_{ll} \end{bmatrix} \begin{bmatrix} \bar{\mathbf{h}}_{e_1} \\ \bar{\mathbf{h}}_{e_2} \\ \vdots \\ \bar{\mathbf{h}}_{e_l} \end{bmatrix} + \begin{bmatrix} \mathbf{C}_{11} & \mathbf{C}_{12} & \cdots & \mathbf{C}_{1l} \\ \mathbf{C}_{21} & \mathbf{C}_{22} & \cdots & \mathbf{C}_{2l} \\ \vdots & \vdots & \ddots & \vdots \\ \mathbf{C}_{l1} & \mathbf{C}_{l2} & \cdots & \mathbf{C}_{ll} \end{bmatrix} \begin{bmatrix} \frac{\partial \bar{\mathbf{h}}_{e_1}}{\partial t} \\ \frac{\partial \bar{\mathbf{h}}_{e_2}}{\partial t} \\ \vdots \\ \frac{\partial \bar{\mathbf{h}}_{e_l}}{\partial t} \end{bmatrix} = \begin{bmatrix} \mathbf{d}_1 \\ \mathbf{d}_2 \\ \vdots \\ \mathbf{d}_l \end{bmatrix} \quad (4.14)$$

in which

$$\begin{cases} \mathbf{C}_{ii} = \mathbf{C}_{e_i} + \sum_{j=1}^l \mathbf{C}_{f_{ij}} \\ \mathbf{C}_{ij} = \mathbf{C}_{f_{ij}} \end{cases} \quad (4.15)$$

and the expressions of  $\mathbf{K}_{ii}$ ,  $\mathbf{K}_{ij}$  and  $\mathbf{d}_i$  are the same as given in Equation (3.15). Equation (4.14) can be abbreviated as:

$$\mathbf{K}\bar{\mathbf{h}} + \mathbf{C} \frac{\partial \bar{\mathbf{h}}}{\partial t} = \mathbf{d} \quad (4.16)$$

Using the implicit time difference scheme, Equation (4.16) becomes:

$$\left( \mathbf{K} + \frac{\mathbf{C}}{\Delta t^{n+1}} \right) \bar{\mathbf{h}}^{n+1} = \frac{\mathbf{C}}{\Delta t^{n+1}} \bar{\mathbf{h}}^n + \mathbf{d} \quad (4.17)$$

## 4.4 Key techniques for improving numerical accuracy and efficiency

### 4.4.1 Under-relaxation iteration

Since the material hydraulic conductivity (referring in particular to  $k_r$ ) and storage properties (referring in particular to  $S_w$  and  $C$ ) are the functions of the hydraulic head, the composite element equations are nonlinear and an iterative scheme is required for the solution process. The Picard method is commonly applied, in which the hydraulic head calculated from the previous time node is directly used to define the material properties at current time node. It is found that numerical instability often occurs in the calculated hydraulic head while using the Picard method. Tan et al. [2004] have pointed out that the incorporation of under-relaxation technique in the iterative process can improve the convergence efficiency and stability, and it has been used in this implementation. The specific iteration steps are as follows:

*Step 1:* In each time step, the initial hydraulic head is estimated by the linear extrapolation approach:

$$\begin{cases} \bar{\mathbf{h}}^{n+1,0} = \bar{\mathbf{h}}^n, & n = 0 \\ \bar{\mathbf{h}}^{n+1,0} = \bar{\mathbf{h}}^n + \frac{\Delta t^{n+1}}{\Delta t^n} (\bar{\mathbf{h}}^n - \bar{\mathbf{h}}^{n-1}), & n \geq 1 \end{cases} \quad (4.18)$$

When  $n=0$ ,  $\bar{\mathbf{h}}^n$  indicates the initial condition for transient analysis.

*Step 2:* Then, in each iteration, an under-relaxation technique is used, whereby the material properties are defined at the midpoint of the time step, that is, the average of the hydraulic heads calculated from the previous time node and from the previous iteration at

the current time node. The definition of this hydraulic head is expressed as:

$$\bar{\mathbf{h}}^{n+1/2,m+1} = (\bar{\mathbf{h}}^n + \bar{\mathbf{h}}^{n+1,m})/2 \quad (4.19)$$

where  $\bar{\mathbf{h}}^{n+1/2,m+1}$  is the hydraulic head vector used to defined the material properties at iteration  $m+1$  and time node  $n+1$ . Equation (4.19) is not strictly applied to define  $dS_w/dh$  (contained in  $C$ ). The chord slope rather than the tangent slope of the saturation–pressure head curve is believed to be more robust, whereby  $dS_w/dh$  is estimated by the ratio of the change in saturations to the change in hydraulic heads from the previous time node to the previous iteration at current time node. When the two hydraulic heads are nearly identical,  $dS_w/dh$  is calculated from the tangent slope of the saturation–pressure head curve at  $\bar{\mathbf{h}}^{n+1/2,m+1}$  in Equation (4.19)

*Step 3:* If Equation (3.22) is satisfied within the specified maximum number of iterations,  $\bar{\mathbf{h}}^{n+1} = \bar{\mathbf{h}}^{n+1,m+1}$ ; otherwise the time step is reduced and the calculation will be restarted.

#### 4.4.2 Mass matrix lumping

It is found that the coefficient matrix due to  $C/\Delta t^{n+1}$  of Equation (4.17) would be ill-conditioned if  $\Delta t^{n+1}$  is very small, thus affecting the accuracy of the solutions. To solve this problem, a mass matrix lumping technique is employed, whereby the non-diagonal elements of the mass matrix  $C$  are centralized to the diagonal elements. The matrixes  $C_{e_i}$  and  $C_{f_{ij}}$  in Equations (4.11) and (4.13) are replaced by the expressions:

$$\begin{aligned} C_{e_i} &= \iiint_{\Omega^{e_i}} (S_{w_{e_i}} S_{s_{e_i}} + C_{e_i}) N d\Omega \\ C_{f_{ij}} &= \frac{b}{4} \iint_{\Gamma^{f_{ij}}} (S_{w_{f_{ij}}} S_{s_{f_{ij}}} + C_{f_{ij}}) N dx_f dy_f \end{aligned} \quad (4.20)$$

#### 4.4.3 Adaptive time stepping

An adaptive time stepping scheme proposed by Forsyth and Sammon [1986] has been incorporated into the solution procedure. After obtaining the hydraulic heads at time nodes  $n$  and  $n-1$ ,  $\bar{\mathbf{h}}^n$  and  $\bar{\mathbf{h}}^{n-1}$ , the next time step  $\Delta t^{n+1}$  in Equation (4.17) is determined according to:

$$\Delta t^{n+1} = \frac{h^*}{\|\bar{\mathbf{h}}^n - \bar{\mathbf{h}}^{n-1}\|_{\infty}} \Delta t^n \quad (4.21)$$

where  $h^*$  is the expected value of the hydraulic head change within a time step. When the hydraulic head experiences a relatively small change, the use of Equation (4.21) allows the



selection of the greater time step to achieve efficiency. If the iteration cannot converge within the prescribed maximum number of iterations, half of the time step will be taken into account.

## 4.5 Verification examples

The composite element formulation and the key techniques described above have been implemented into the computer program CEM\_UNSATFLOW for simulating transient, variably-saturated flow in fractured media. Three examples are now presented to verify the program. The first example involves one-dimensional infiltration into dry soils which was widely used in previous numerical studies [Celia et al., 1990; Rathfelder and Abriola, 1994; Lehmann and Ackerer, 1998]. The results obtained with the present composite element model are compared with the semi-analytical solution developed by Philip [1957]. The second example uses the one that has been described in Section 3.5. The results recalculated by the present composite element model are compared with those presented in Chapter 3, and with those obtained from COMSOL. The last example involves the vertical drainage of a 3D fractured tuff column and was presented by Wang and Narasimhan [1985]. Results obtained with the present model are compared to results published in Wang and Narasimhan [1985].

### 4.5.1 1D infiltration into dry soil

The length of the soil profile is taken to be 30 cm. Initially, the pressure head throughout the profile is -1000 cm. At time  $t \geq 0$ , water infiltrates steadily through the upper boundary. The boundary conditions are as follows: the hydraulic heads at upper boundary and at lower boundary are -75 cm and -1000 cm respectively.

The required parameters are: the saturated hydraulic conductivity is 0.00922 cm/s, the saturated water content and the residual water content are 0.368 and 0.102, and the specific storage is 0. The VGM model is used to describe the constitutive relations with the fitting parameters  $\alpha = 0.0335 \text{ m}^{-1}$  and  $n=2$ . The profile is discretized using a uniform element size of 0.25 cm. All the elements are finite elements. The time step is fixed to be 50 s. The tolerance error is prescribed to be  $10^{-6}$  and the prescribed maximum number of iterations is 100. Simulation of transient, variably-saturated flow is carried out up to a time value equal to 6 h. There are a total of 432 time steps to be calculated.

Figure 4.1 presents the distributions of the pressure head along depth at time  $t=6$  h obtained by implementing the Picard and under-relaxation iterative schemes. These results

are compared with the semi-analytical solution of Philip [1957]. It can be seen from Figure 4.1 that there is good agreement between the results obtained by the Picard and under-relaxation iterative schemes. However, compared with the results of the Picard iteration, the calculated pressure head distribution using the under-relaxation iteration is closer to Philip's solution. Compare the numbers of iterations required to achieve convergence when using the two iterative schemes, shown in Figure 4.2. It is clear that when using the under-relaxation iterative scheme, convergence occurs almost within ten iterations in each time step; however, when using the Picard method, it takes more than ten iterations to achieve convergence. From the above, it can be concluded that the under-relaxation iterative scheme not only provides the higher computational efficiency but also yields the more accurate results than the commonly-used Picard method.

#### **4.5.2 Flow in a synthetic fractured rock mass**

The composite element model developed in this chapter is used to recalculate case 2 in the example described in Section 3.5. The results are compared with those calculated by COMSOL and those given in Chapter 3. Figure 4.3 shows the evolution of the hydraulic head and the free surface with time on section  $y=5$  m. For comparison, the free surfaces obtained by COMSOL are also plotted in Figure 4.3, shown by dotted lines. It is observed from Figure 4.3 that the free surfaces calculated by the present composite element model are very close to the free surfaces obtained from COMSOL. Figure 4.4 compares three sets of inflow, outflow and drainage fluxes respectively obtained by the composite element models developed in Chapter 3 and in Chapter 4, and COMSOL. As can be seen from Figure 4.4, the composite element model developed in this chapter produces the results that are closer to the COMSOL results than the model in Chapter 3. This results are expected, because both the present composite element model and COMSOL are based on the Richards' equation to simulate transient, variably-saturated flow in the fractured rock mass. The results also prove the accuracy of the present composite element model.

#### **4.5.3 Vertical drainage of a fractured tuff column**

The composite element model is used to simulate transient, variably-saturated flow problem in the Yucca mountain tuff, which was described by Wang and Narasimhan [1985]. The tuff matrix contains two groups of vertical fractures and one group of horizontal fractures. The aperture and spacing for vertical fractures are 0.24 mm and 0.22 m, and for horizontal fractures are 0.31 mm and 0.48 m. The three groups of fractures are mutually

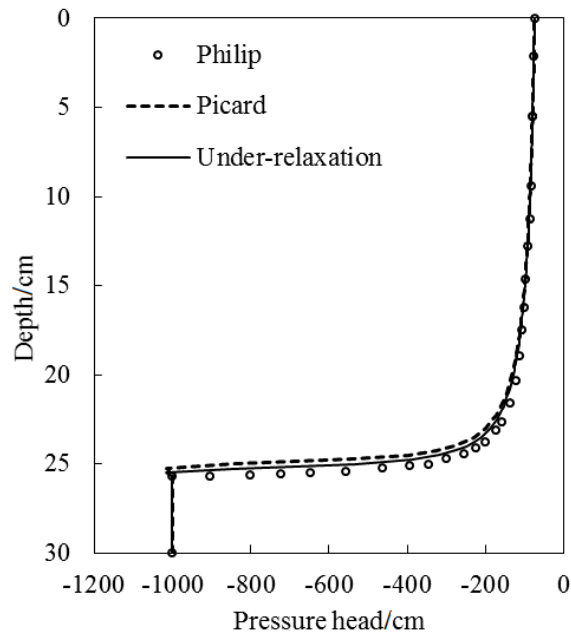


Figure 4.1 Distributions of the pressure head along depth at  $t=6$  h

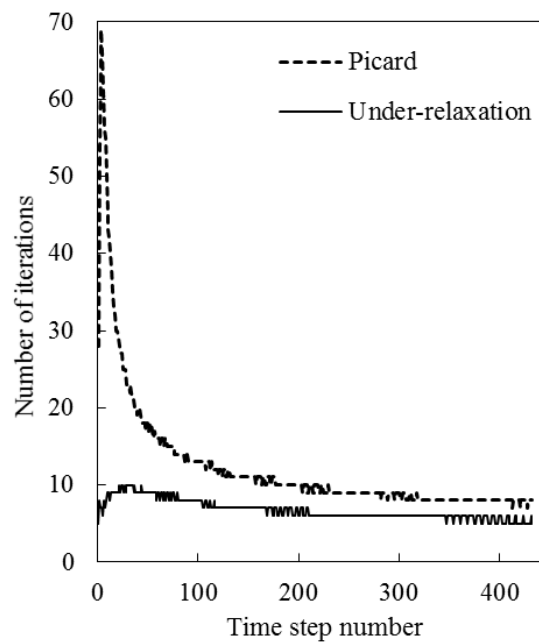


Figure 4.2 Number of iterations in each time step required to achieve convergence

orthogonal and partition the matrix into blocks, as shown in Figure 4.5. Due to the symmetry of the system, only one vertical column is taken into account. The dimension of the column is  $0.44 \text{ m} \times 0.44 \text{ m} \times 1.44 \text{ m}$ . The column is initially saturated, the flow was static and the pressure head is everywhere zero. At  $t \geq 0$ , the pressure head at the bottom is reduced to  $-112 \text{ m}$ , and all other boundaries are impermeable. Under this condition, transient flow in the column is triggered and the saturated state is transitioned to the unsaturated state. The simulation results will be compared with those reported in Wang and Narasimhan [1985].

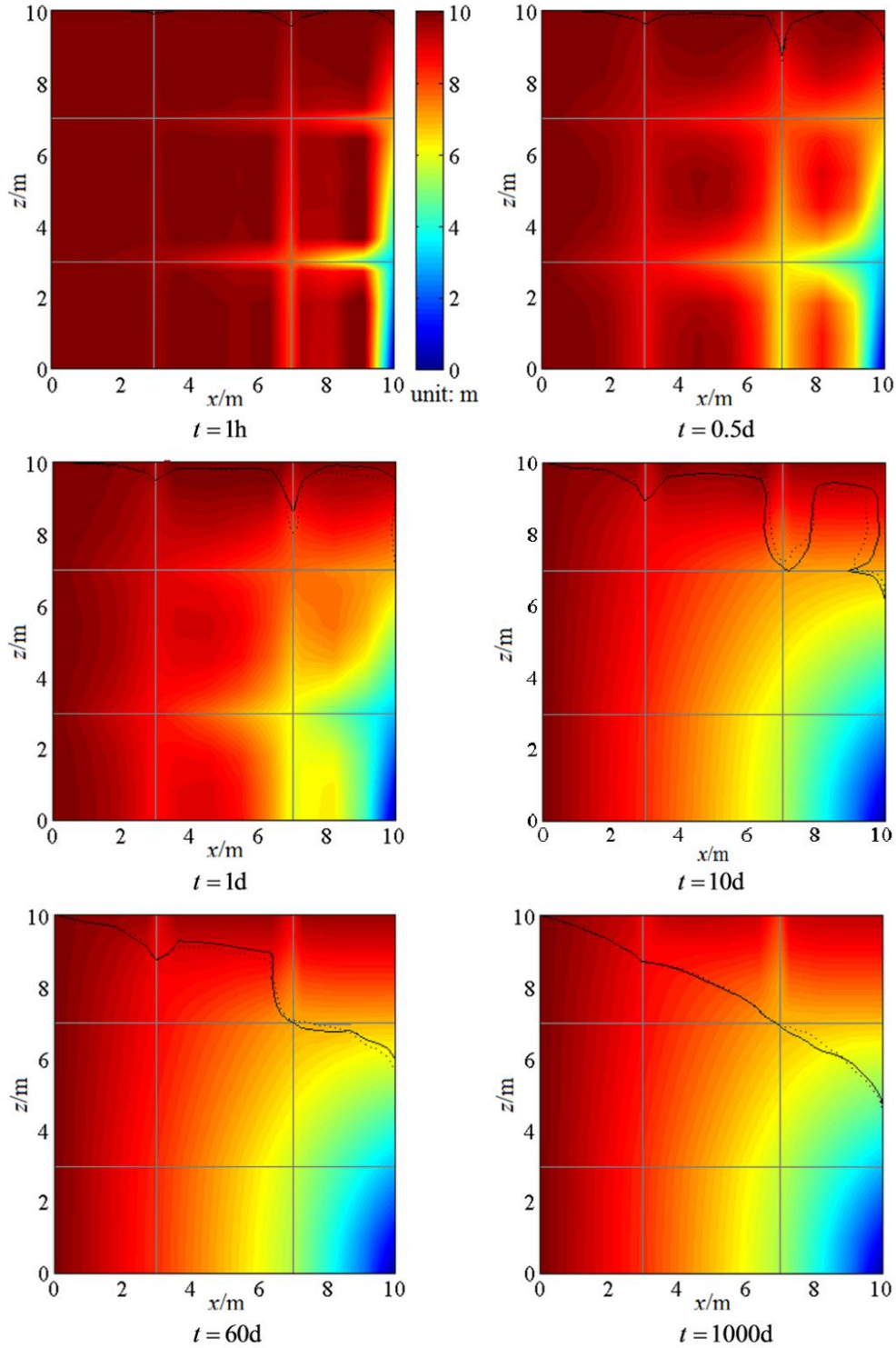


Figure 4.3 Evolution of the hydraulic head on the profile  $y=5$  m using composite element model in case 2 (recalculated by simulating transient, variably-saturated flow)

The required parameters are as follows: for tuff matrix, the saturated hydraulic conductivity is  $3.24 \times 10^{-10}$  m/s, the saturated and residual water contents are 0.09 and  $8.64 \times 10^{-5}$ , respectively, the specific storage is  $10^{-6} \text{ m}^{-1}$ , and the constitutive relations for matrix are described by the VGM model; for vertical fractures, the saturated hydraulic

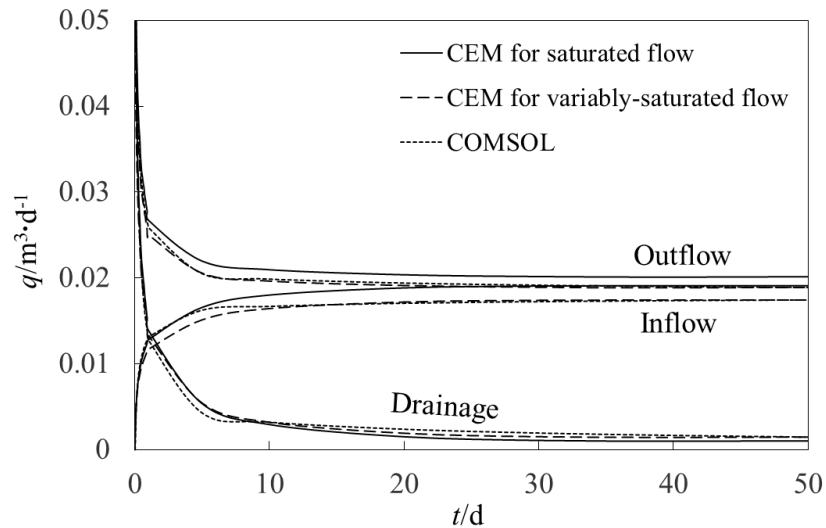


Figure 4.4 Comparisons of inflow, outflow and drainage fluxes in the domain obtained with the two composite element models respectively developed in Chapter 3 and in Chapter 4 and COMSOL

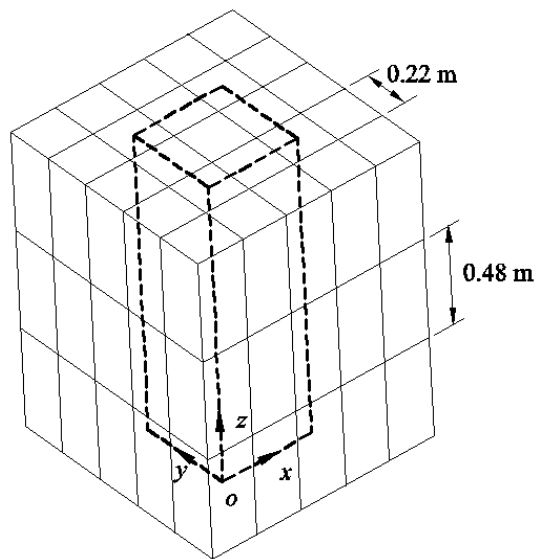
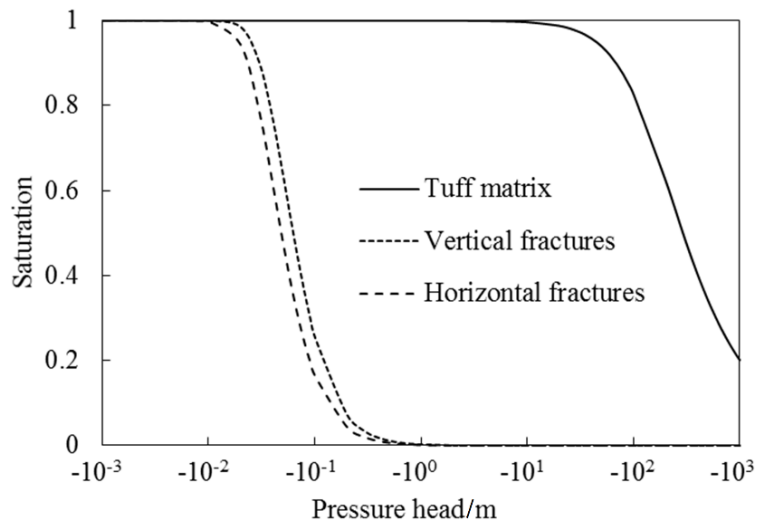
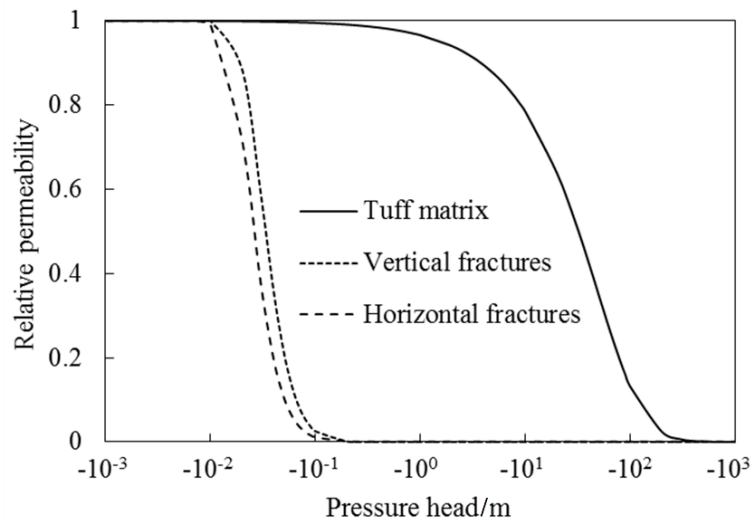


Figure 4.5 A fractured tuff column

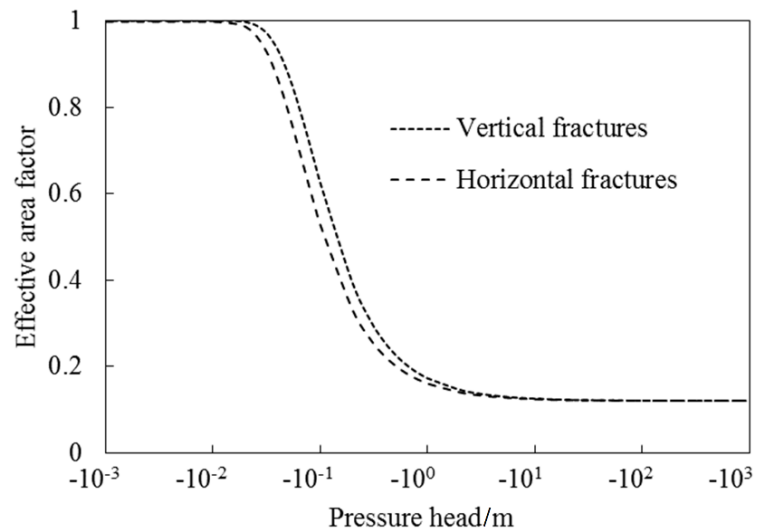
conductivities are  $4.71 \times 10^{-2}$  m/s and for horizontal fractures, the saturated hydraulic conductivities are  $7.85 \times 10^{-2}$  m/s, given by Equation (2.2). The saturated water content for fractures is 1.0, and the specific storage for fractures is  $4.4 \times 10^{-6}$  m<sup>-1</sup>. Wang and Narasimhan [1985] derived the relations between fracture saturation, relative permeability, effective area factor and pressure head from an aperture distribution model. These relations are compiled into the program CEM\_UNSATFLOW to accurately calculate the hydraulic conductivities of the fractures and the effective area of the fracture-matrix interaction. To facilitate the readers to read, the constitutive relations and effective area factor are plotted in Figure 4.6.



(a)



(b)



(c)

Figure 4.6 Relations between (a) saturation, (b) relative permeability, and (c) effective area factor and pressure head

The column is discretized using 25 nodes along  $x$ - and  $y$ -axes and 32 nodes along  $z$ -axis, and thus a computational mesh with 20,000 elements and 22,308 nodes is generated. By running the CEM pre-processor, 4,130 composite elements are found. The total number of nodes for all composite and finite elements is 33,300. Using the adaptive time stepping scheme, the expected value of the hydraulic head change for a single time step is 1.0 m. The tolerance error is 0.01. The simulation of transient, variably-saturated flow is carried out up to the final time value equal to  $10^5$  y.

Two cases of flow in the column are simulated: flow in a fractured tuff column (case 1); and flow in a tuff matrix column without fractures (case 2). In case 1 and case 2, a total of 283 and 222 time steps are respectively required to reach the final time value. The comparisons of the results obtained with the present model (shown by lines) and those of Wang and Narasimhan [1985] (shown by symbols) are presented in Figures 4.7(a) and 4.7(b), which respectively present the variations of the pressure head with time at four different points in the above two cases. The four points are located on section  $y=0.22$  m, of which A lies at the center of the matrix block, B lies at the middle of the vertical fracture, C and D are at the middles of the upper and lower horizontal fractures respectively. It can be seen from Figure 4.7 that there is a very good agreement between the results obtained and those reported by Wang and Narasimhan [1985]. At the initial moment, the pressure head at all observation points is only slightly reduced. Starting from a certain time node, the pressure head begins to decrease significantly. The time at which the pressure head begins to decrease significantly in case 1 is later than in case 2, which indicates that the presence of the fractures delays the propagation of the pressure head change in the column. When  $t \geq 10^{-2}$  y, the variation curves of the pressure head are basically the same in both cases. This means that as the saturation decreases flow will be mainly controlled by the matrix. At the point D closer to the bottom, the pressure head is less than the pressure heads at other three points. At the points A and B with the same elevation, the pressure heads are approximately identical.

## **4.6 Simulation of flow problem in complicated, variably-saturated fractured aquifer**

### **4.6.1 Transient flow in an aquitard-aquifer system under recharge and pumping**

The distribution of fractures in realistic aquifers are usually random and complex. The problem of groundwater flow in a 3D aquitard-aquifer system containing a complex fracture

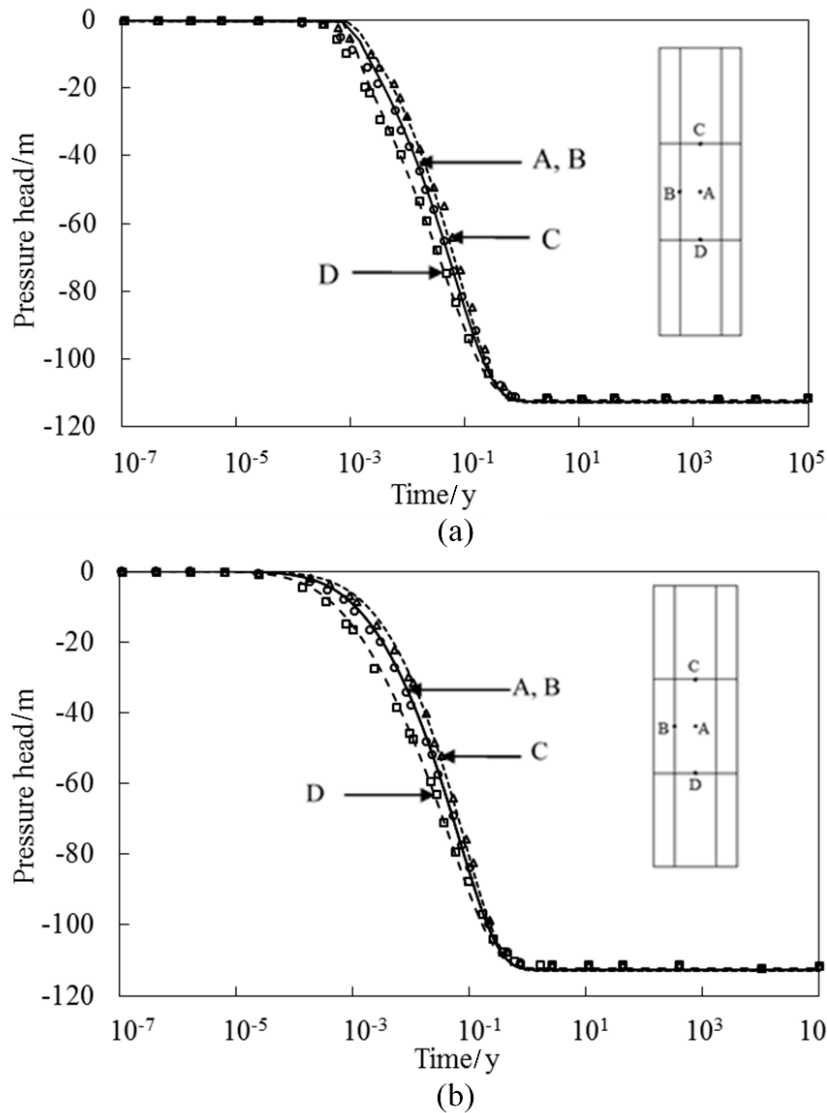


Figure 4.7 Variations of the pressure head with time at four given points in (a) case 1, and (b) case 2

network, described by Therrien and Sudicky [1996], is used to demonstrate the capability of the present composite element model. The system is comprised of a 10-m-thick aquitard overlying a 3-m-thick aquifer. The horizontal extent of the domain is 90 m in the  $x$ -direction and 90 m in the  $y$ -direction. The aquitard contains three mutually orthogonal groups of stochastic fracture. Assume that the fracture surfaces are rectangular in shape, and all vertical fractures originate at the top of the aquitard. The statistical parameters and probability models for the distribution of fractures are given in Table 4.1. Using the Monte Carlo method, one stochastic fracture network that contains 337 fractures is generated, as shown in Figure 4.8. Some of the vertical fractures fully penetrate the aquitard and the others do not. Additionally, there is a fully-penetrating pumping well in the center (at  $x=45$  m and  $y=45$  m) of the aquifer.



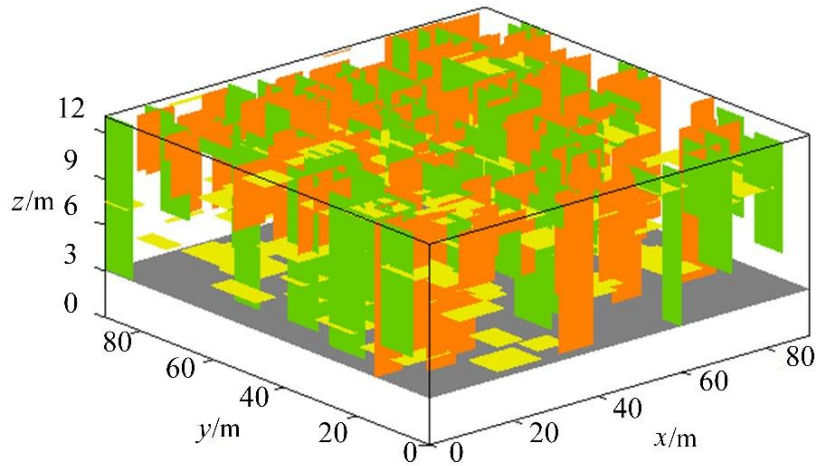


Figure 4.8 A aquitard-aquifer system

Table 4.1 Parameters of three groups of fractures and their probability models

Fracture group	Length/m			Width/m			Location	Dip direction /°	Dip angle /°	Aperture /μm	Number
	Mean value	Variance	Probability model	Mean value	Variance	Probability model					
1	8.0	2.0	Lognormal	8.0	2.0	Lognormal	Uniform	0	0	30	127
2	8.0	2.0	Lognormal	5.4	5.4	Negative exponential	Uniform	0	90	35	108
3	8.0	2.0	Lognormal	6.0	6.0	Negative exponential	Uniform	90	90	25	102

Suppose that steady flow has already been formed in the system prior to the start of pumping. The corresponding boundary conditions are: the recharge flux across the upper boundary of aquitard is equal to  $1.0 \times 10^{-4}$  m/d; the hydraulic heads at  $x=0$  and  $x=90$  m are 9.05 m and 8.85 m, respectively; and the other boundaries are no-flux boundaries. The pumping starts at  $t \geq 0$  and the pumping rate in the well is fixed at  $175 \text{ m}^3/\text{d}$ . In the meantime, the recharge flux across the upper boundary is reduced to  $5.0 \times 10^{-5}$  m/d, and the other boundary conditions remain unchanged. The composite element model developed in this chapter is firstly used to simulate steady, variably-saturated flow in the system in order to obtain the initial hydraulic head distribution; and is then used to simulate transient, variably-saturated flow under the effect of pumping. To simplify the simulation difficulty, the groundwater flux distribution along the well is assumed to be uniform. That is, the nodal fluxes along the well screen are identical, and their sum equals the total pumping rate.

For the aquitard, the saturated hydraulic conductivity is  $1.0 \times 10^{-10}$  m/s, the porosity is 0.4 and the specific storage is  $10^{-3} \text{ m}^{-1}$ ; and for the aquifer, the saturated hydraulic

conductivity is  $1.0 \times 10^{-4}$  m/s which is six orders of magnitude larger than the aquitard matrix, the porosity is 0.35 and the specific storage is  $10^{-4}$  m<sup>-1</sup>. The saturated hydraulic conductivities for the three groups of fractures are  $6.57 \times 10^{-4}$  m/s,  $8.94 \times 10^{-4}$  m/s and  $4.56 \times 10^{-4}$  m/s respectively, as given by Equation (2.2). The constitutive relations used to describe variably-saturated flow in the aquitard, aquifer, and fractures are presented in Table 4.2. During the numerical simulation, if the computed pressure head falls between the given two data points in Table 4.2, the corresponding saturation is determined by the linear interpolation method. Similarly, if the computed saturation falls between the given two data points in Table 4.2, the corresponding relative permeability is determined by the linear interpolation method.

Table 4.2 Tabular data describing the saturation–pressure head and relative permeability–saturation relations

Material	Saturation–pressure head		Relative permeability–saturation	
	Pressure head/m	Saturation	Saturation	Relative permeability
Aquitard	-100	0.26	0	0
	-60	0.31	0.352	$10^{-5}$
	-10	0.557	0.465	$10^{-4}$
	-6.5	0.65	0.61	$10^{-3}$
	-4.5	0.7	0.76	$10^{-2}$
	-2.3	0.8	0.9	$1.2 \times 10^{-1}$
	-0.1	0.985	0.945	$3.4 \times 10^{-1}$
	0	1.0	1	1
Aquifer	-100	0.02	0	0
	-12	0.1	0.185	$10^{-4}$
	-3.5	0.2	0.28	$10^{-3}$
	-1	0.35	0.428	$1.2 \times 10^{-2}$
	-0.5	0.57	0.648	$1.1 \times 10^{-1}$
	-0.35	0.725	0.81	$3.7 \times 10^{-1}$
	-0.1	0.917	0.888	$5.8 \times 10^{-1}$
	0	1.0	1	1
Fracture	-1.5	0.29	0.2399	0
	-0.225	0.29	0.24	$1.7 \times 10^{-3}$
	-0.15	0.3	0.33	$2.51 \times 10^{-2}$
	0	1.0	1	1

The discretization of the domain is such that 40 nodes are used along  $x$ -axis, 40 nodes

along  $y$ -axis and 11 nodes along  $z$ -axis. This yields a total of 20,172 nodes and 17,600 elements, of which 5,418 are composite elements. The total number of nodes for all the composite elements and finite elements is 35,594. In the transient, variably-saturated flow simulation, the expected value of the hydraulic head change in an individual time step is 0.01 m and the tolerance error is 0.01. The simulation will end if a time value is exceeding 600 d.

Due to the presence of fractures, the recharge flux distribution at the nodes on the top surface of the system is not uniform. To simulate this property, the redistribution elements proposed by Therrien and Sudicky [1996] are used on this top surface. These redistribution elements have very thin thickness and adequately high hydraulic conductivity so that the water entering as recharge redistributes itself by flowing laterally on the surface in the regions where vertical hydraulic conductivity is low. The thickness of the redistribution elements is taken as 0.05 m and the hydraulic conductivity value is designated as  $1.25 \times 10^{-5}$  m/s. This combination of thickness and hydraulic conductivity produces a transmissivity that allows optimal flux redistribution for the system. It is found that a further increase in the transmissivity value of the redistribution elements does not affect the results.

The initial, steady hydraulic head distribution at section  $y=45$  m is shown in Figure 4.9(a). The hydraulic head pattern is seen to be irregular in the aquitard due to the presence of the fractures. The same type of erratic hydraulic head pattern was found by Therrien and Sudicky [1996]. It can also be seen that groundwater will generally flow from the fractures into the matrix except in the case of those fractures that extend downward to intersect the more permeable, underlying aquifer.

The distribution of the hydraulic head at  $y=45$  m after 500 d pumping are presented in Figure 4.9(b). It can be observed from Figure 4.9(b) that groundwater flows toward the pumping well and the minimum hydraulic heads occur at the pumping well. Figure 10 shows the location of the free surface after 500 d pumping. The reader is reminded that prior to pumping, the system is fully saturated and that the free surface is located near the top of the aquitard. It can be seen that the combined effect of pumping and the reduced recharge rate has caused desaturation of the upper portion of the fractures that intersect the top of the aquitard, with greater perturbations in the free surface occurring near those fractures that fully penetrate the aquitard. This enhanced decline of the free surface is due to the drawdown in the aquifer from pumping which propagates along the fully-penetrating fractures. The desaturation occurs firstly in the fractures and then extends laterally to the surrounding matrix. As fractures desaturate, they are no longer acting as the preferential

flow pathways and become barriers to water flow. In this case, groundwater flow tends to be through matrix pores.

The above results are consistent with those reported in the literature [Therrien and Sudicky, 1996]. It is worth emphasizing again that the present composite element model places the fractures into the elements, thus greatly reducing the difficulty of the mesh generation. When analyzing multiple random fracture networks, the use of the composite element model does not require to regenerate the computational mesh, but rather to find the new composite elements by running the CEM pre-processor.

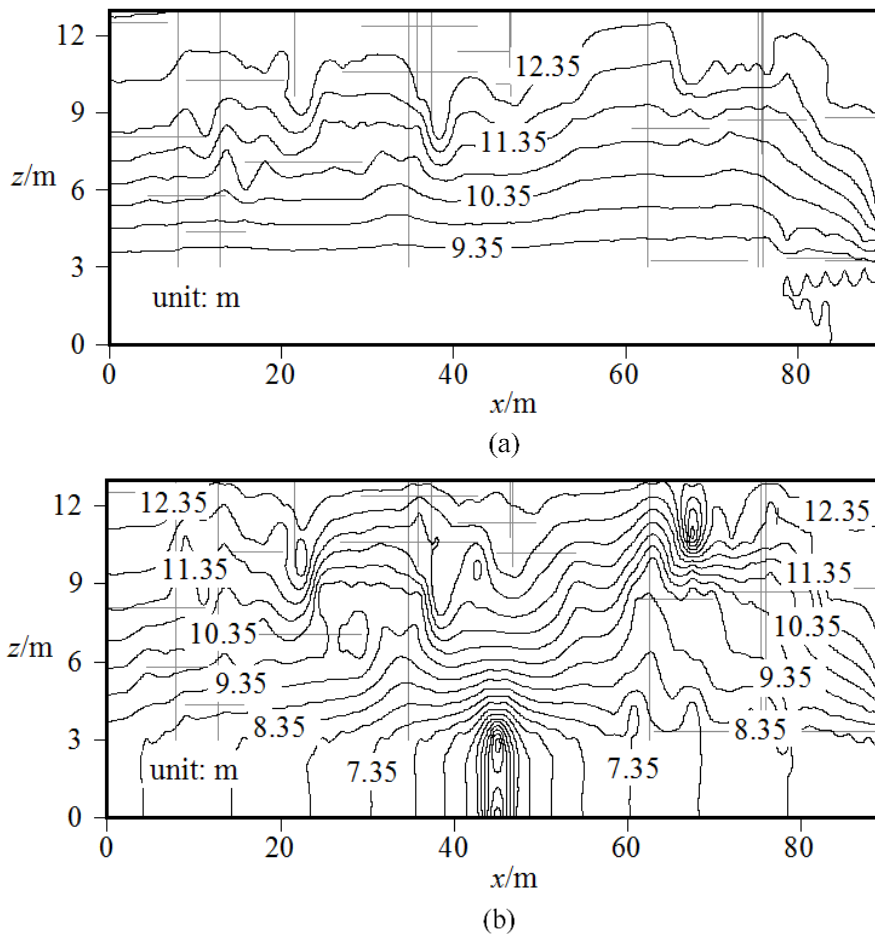


Figure 4.9 Contours of the hydraulic head at  $y=45$  m (a) initially, and (b) after 500 d pumping

## 4.7 Conclusions

The composite element model has been further developed to simulate transient, variably-saturated flow in fractured media. In order to solve the variably-saturated flow equation, an iterative scheme with under-relaxation has been adopted. The nonlinearity involved in the variably-saturated flow problem is resulted from the nonlinear relations

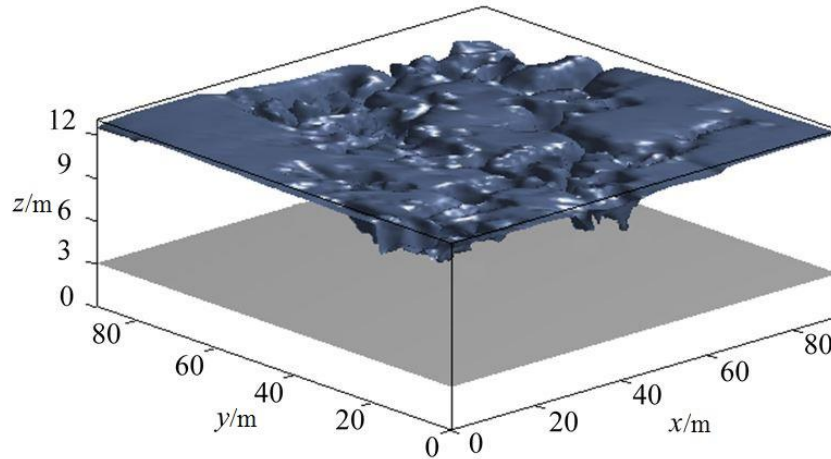


Figure 4.10 Location of the free surface after 500 d pumping

between the saturation, relative permeability and the pressure head, which is different the nonlinearity resulted from the unknown free surface boundary in the saturated, unconfined flow problem. In this chapter, the techniques of mass matrix lumping and adaptive time stepping are specially incorporated to improve the accuracy and efficiency of the solution process.

The effectiveness of the composite element model and the solution algorithms has been verified by three examples. Firstly, the one-dimensional infiltration problem in dry soil was analyzed using the composite element model. The comparisons between the under-relaxation iterative scheme, the Picard method and the semi-analytical solution showed that the under-relaxation iterative scheme had better computational accuracy and efficiency than the Picard method. Then, the composite element model together with the proposed key techniques was applied into the synthetic example that had been discussed in Chapter 3. The results obtained by the present composite element model were closer to the COMSOL results than those in Chapter 3. This results were expected, because both the present model and COMSOL were based on the Richards' equation to simulate transient, variably-saturated flow in fractured media. Finally, an example of the vertical drainage of a fractured tuff column described by Wang and Narasimhan [1985] was presented. The validity of the present model is further validated by comparing with the results obtained by other numerical simulator.

The problem of transient flow in an aquitard-aquifer system under pumping was simulated using the developed composite element model. The simulation results clearly showed the complexities of variably-saturated flow in the fractured system. The complexities were mainly manifested in the facts that: (i) the fracture interconnectivity could create erratic hydraulic head distribution patterns; and (ii) depending on the

relationships between saturation, relative permeability and pressure head for the fractures and the matrix, groundwater flow could be controlled by either the fractures or the matrix. These results illustrated the necessity for an explicit and coupled simulation of the flow processes occurring in both the fractures and the matrix.

## References

1. Berrone S, Pieraccini S, Scialo S. A PDE-constrained optimization formulation for discrete fracture network flows. *SIAM Journal on Scientific Computing* 2013; **35**(2): B487–B510
2. Brooks RH, Corey AT. Hydraulic properties of porous media. *Colorado State University, Hydro Paper* 1964; **3**: 27.
3. Cacas MC, Ledoux E, Marsily GD, Tillie B, Barbreau A, Durand E, Feuga B, Peaudecerf P. Modeling fracture flow with a stochastic discrete fracture network: calibration and validation, 1. The flow model. *Water Resources Research* 1990; **26**(3): 479–489.
4. Celia MA, Bouloutas ET, Zarba RL. A general mass-conservative numerical solution for the unsaturated flow equation. *Water Resources Research* 1990; **26**(7): 1483–1496.
5. Cey E, Rudolph D, Therrien R. Simulation of groundwater recharge dynamics in partially saturated fractured soils incorporating spatially variable fracture apertures. *Water resources research* 2006; **42**, W09413, doi: 10.1029/2005WR004589.
6. Erhel J, De Dreuzy JR, Poirriez B. Flow simulation in three-dimensional discrete fracture networks. *SIAM Journal on Scientific Computing* 2009; **31**(4): 2688–2705.
7. Forsyth PA, Sammon PH. Practical considerations for adaptive implicit methods in reservoir simulation. *Journal of Computational Physics* 1986; **62**(2): 265–281.
8. Huyakorn PS, Lester BH, Faust CR. Finite element techniques for modeling groundwater flow in fractured aquifers. *Water Resources Research* 1983; **19**(4): 1019–1035.
9. Hyman JD, Karra S, Makedonska N, Gable CW, Painter SL, Viswanathan HS. dfnWorks: A discrete fracture network framework for modeling subsurface flow and transport. *Computers and Geosciences* 2015; **84**: 10–19.
10. Lehmann F, Ackerer PH. Comparison of iterative methods for improved solutions of the fluid flow equation in partially saturated porous media. *Transport in Porous Media* 1998; **31**(3): 275–292.
11. Mualem Y. A new model for predicting the hydraulic conductivity of unsaturated porous media. *Water Resources Research* 1976; **12**(3): 513–522.
12. Mustapha H, Dimitrakopoulos R, Graf T, Firoozabadi A. An efficient method for discretizing 3D fractured media for subsurface flow and transport simulations. *International Journal for Numerical Methods in Fluids* 2011; **67**: 651–670.

13. Mustapha H, Mustapha K. A new approach to simulating flow in discrete fracture networks with an optimized mesh. *SIAM Journal on Scientific Computing* 2007; **29**(4): 1439–1459.
14. Neretnieks I. Solute transport in fractured rock—applications to radionuclide waste repositories. In *Flow and contaminant transport in fractured rock*, Bear J, Tsang CF, de Marsily G (eds). Academic Press Inc.: San Diego, 1993; pp 39–127.
15. Neretnieks I, Eriksen T, Tahtinen P. Tracer movement in a single fissure in granitic rock: some experimental results and their interpretation. *Water resources research* 1982; **18**(4), 849–858.
16. Persoff P, Pruess K. Two-phase flow visualization and relative permeability measurement in natural rough-walled rock fractures. *Water Resources Research* 1995; **31**(5): 1175–1186.
17. Philip JR. The theory of infiltration: 1. the infiltration equation and its solution. *Soil Science* 1957; **83**(5): 345–358.
18. Pruess K, Tsang YW. On two-phase relative permeability and capillary pressure of rough-walled rock fractures. *Water Resources Research* 1990; **26**(9): 1915–1926.
19. Rasmussen TC, Evans DD. Fluid flow and solute transport modeling through three-dimensional networks of variably saturated discrete fractures, NUREG/CR-5239. U.S. Nuclear Regulatory Commission: Washington, 1989.
20. Rathfelder K, Abriola LM. Mass conservative numerical solutions of the head-based Richards equation. *Water Resources Research* 1994; **30**(9): 2579–2586.
21. Reitsma S, Kueper BH. Laboratory measurement of capillary pressure–saturation relationships in a rock fracture. *Water Resources Research* 1994; **30**(4): 865–878.
22. Tan TS, Phoon KK, Chong PC. Numerical study of finite element method based solutions for propagation of wetting fronts in unsaturated soil. *Journal of geotechnical and geoenvironmental engineering* 2004; **130**(3): 254–263.
23. Therrien R, McLaren RG, Sudicky EA, Panday SM. HydroGeoSphere: a three-dimensional numerical model describing fully-integrated subsurface and surface flow and solute transport. Groundwater Simulations Group, University of Waterloo: Waterloo, Canada, 2005.
24. Therrien R, Sudicky EA. Three-dimensional analysis of variably-saturated flow and solute transport in discretely-fractured porous media. *Journal of Contaminant Hydrology* 1996; **23**(1): 1–44.
25. Van Genuchten MT. A closed-form equation for predicting the hydraulic conductivity



- of unsaturated soils. *Soil Science Society of America Journal* 1980; **44**(5): 892–898.
26. Vandersteen K, Carmeliet J, Feven J. A network modeling approach to derive unsaturated hydraulic properties of a rough-walled fracture. *Transport in Porous Media* 2003; **50**(3): 197–221.
27. Vogel T, Van Genuchten MT, Cislserova M. Effect of the shape of the soil hydraulic functions near saturation on variably-saturated flow predictions, *Advances in Water Resources* 2000; **24**(2): 133–144.
28. Wang JSY, Narasimhan TN. Hydrologic mechanisms governing fluid flow in a partially saturated, fractured, porous medium. *Water Resources Research* 1985; **21**(12): 1861–1874.
29. Zhou CB, Ye ZT, Xiong WL. A study on unsaturated hydraulic conductivity of rock joints. *Chinease Journal of Hydraulic Engineering* 1998; **3**: 22–25.

# Chapter 5 Investigation of Stability of Homogeneous Soil Slopes Under Drawdown Conditions

## 5.1 Introduction

A large number of engineering practices have shown that the reservoir drawdown can have a significant impact upon the stability of slopes adjacent to the reservoir. During the drawdown of reservoir level, pore water in slope soils or rocks drains from the slope. But when the soil or rock hydraulic conductivity is weak, pore water cannot drain soon so that the decline of the free surface within the slope lags behind the lowering of the reservoir level. In this case, transient flow that is detrimental to slope stability results. The seepage forces generated by transient flow reduce the effective stress between soil or rock particles, thus reducing the shear strength on the potential slip surface and endangering the stability of slope. Moreover, the faster the reservoir drawdown, the more obvious the hysteresis of the free surface decline, and the greater the impact on slope stability. In actual engineering, it is essential to prevent the occurrence of slope instability due to the rapid drawdown of reservoir.

Many scholars attempted to establish the index that judges the rate of reservoir drawdown and to use the index to evaluate the effect of reservoir drawdown on slope stability [Gu, 2000]. In their studies, the reservoir drawdown is divided into rapid drawdown and slow drawdown. The rapid drawdown is considered to endanger the stability of slope, and the slow drawdown is considered not to affect the stability of slope. Schnitte and Zeller as early as 1957 proposed the index  $k/(S_y v)$ , where  $k$  is hydraulic conductivity,  $v$  is drawdown rate, and  $S_y$  is specific yield which indicates the amount of water that saturated soils will release from storage by gravity. They obtained the following conclusions through experiment: when  $k/(S_y v) \leq 0.1$ , the drawdown is considered “rapid” because the decline of the free surface is very slow; when  $k/(S_y v) > 10$ , the drawdown is considered “slow” because the free surface is brought down nearly simultaneously with the reservoir level. Systakov in 1960 pointed out that the judgment index should also include the slope ratio  $m$ , and concluded that: when  $k/(m^2 S_y v) < 0.05$ , the drawdown can be identified “rapid”. Besides, some scholars [Shi and Zheng, 2003; Zheng et al., 2004; Liu et al., 2005; Duan and Xie, 2009] established the relationship between  $k/(S_y v)$  and the height of the free surface after drawdown by analyzing transient flow within slope. For the homogenous earth dam and the

core wall dam with poor drainage conditions in the upstream slope, the following conclusions are drawn in Chen [2015]: when  $k/(S_y v) \leq 0.1$ , the height of the free surface at end of drawdown is greater than 90% of total drawdown level, so “rapid” drawdown is considered; when  $k/(S_y v) > 60$ , the drawdown is called “slow” because the height of the free surface is less than 10% of total drawdown level; when  $0.1 < k/(S_y v) \leq 60$ , the height of the free surface is between 10% and 90% of total drawdown level, so the drawdown is termed “moderate”. The above are actually based on the relative height of the free surface after drawdown to define “rapid”, “slow” and “moderate” drawdown, respectively.

However, the reservoir drawdown ultimately affects the stability of slope, therefore the judgment of the rate of reservoir drawdown should even more be linked with the stability of slope. Consider such a fact that: when the reservoir drawdown just causes a slight reduction in the slope safety factor (denoted by  $SF$ ) and  $SF$  is still greater than 1.0 after drawdown, the effect of reservoir drawdown can usually be ignored; on the contrary, when the drawdown results in a significant reduction in  $SF$  and  $SF$  is reduced below 1.0 after drawdown, the stability of slope under this drawdown needs to be given special attention. Obviously, the former situation occurs when the drawdown is “slow”; and the latter situation occurs when the drawdown is “rapid”. From the perspective of ensuring slope stability, the “rapid” and “slow” drawdown can be redefined as follows: rapid drawdown causes  $SF$  to reduce beyond the acceptable range; and slow drawdown does not. This definition is more explicit than the previous one that is based on the relative height of the free surface. In the slope stability analysis, only the drawdown condition that is judged as “rapid” drawdown needs to be checked.

From the above discussion on the judgment of the rate of reservoir drawdown, it is not difficult to find that the factors that influence slope stability include: reservoir drawdown rate, hydraulic parameters ( $k$  and  $S_y$ ) of slope material, slope geometry, drainage condition and shear strength parameters. Although there have been some understandings about the influence of these factors on the free surface during drawdown, there is still a lack of quantitative description of the ultimate influence of these factors on the slope safety factor. The use of specific index, such as  $k/(S_y v)$ , to evaluate the impact of reservoir drawdown and even to establish the quantitative relationship between the index and the resulting slope behaviors are of great practical significance for the design and reinforcement of the reservoir slope. These are the intentions for performing this investigation.

The main task of this investigation is to quantify the influences of various reservoir drawdown rates, material hydraulic and strength parameters, and slope geometries on slope

stability safety factor. The results of the investigation are used to produce the criterion for judging rapid drawdown and slow drawdown. Unlike those in the “old” criterion given by Chen [2015], the rapid drawdown and slow drawdown in this “new” criterion are distinguished according to the relative reductions of the  $SF$  they cause. It should be noted that the objects investigated in this chapter are limited to the case where the homogeneous soil slopes are subjected to potential circular sliding failures. The other types of slopes and possible failure modes, such as layered rock slopes and potential planar sliding failures, will be discussed in the next chapter.

In this investigation, the transient flow in the slope is first simulated by applying the CEM. Using the pore-water pressures obtained by transient flow modelling, the limit equilibrium stability analyses are subsequently conducted to evaluate the variation of the safety factor of slopes during drawdown. These two analyses are treated in a completely uncoupled manner, similar to the approach adopted by Desai [1977]. However, advances have been made recently to fully couple flow and deformation analyses including consolidation of slope media with the numerical technique [Berilgen, 2007; Pinyol et al., 2008], but this approach is often costly at the expense of computation time and complicated numerical implementation. Thus, the uncoupled transient flow and stability analyses approach is preferred here due to its simplicity and effectiveness.

The main contents in this chapter include: (i) theories and approaches used for this investigation, including the analyses of transient flow and slope stability, and the design specifications for allowable  $SF$  and acceptable reduction in  $SF$  of reservoir slopes; (ii) investigation of drawdown in homogeneous soil slopes, involving the decline of the free surface within slopes and the variation in  $SF$  of slopes during drawdown; and (iii) charts for quick judgment of rapid drawdown in homogeneous soil slopes.

## **5.2 Theories and approaches used for this investigation**

### **5.2.1 Analysis of transient flow in a 2D slope**

The numerical model of transient, saturated flow with a free surface established in Chapter 3 is used to simulate the transient flow in the slope under reservoir drawdown condition. Take the slope of the unit thickness to study. The boundary conditions are as follows: the hydraulic head on the slope face below the reservoir level is equal to the water level elevation; the slope face above the reservoir level is potential seepage face; and the other boundaries are impermeable. Assume that the slope is initially fully saturated and that

the hydraulic head is everywhere equal to full reservoir level elevation.

For the homogenous, isotropic and non-deforming soils, the hydraulic conductivity at arbitrary points can be described by a constant  $k$  and the specific storage  $S_s$  is equal to 0. Equations (3.1) can be reduced to the following expression:

$$\nabla \cdot (\nabla h) = 0, \quad \text{in } \Omega \quad (5.1)$$

which is well known as Laplace's equation. It is clear that the solution to Equation (5.1) is independent of the value of the hydraulic parameters. The influence of the parameters on transient flow simulation is reflected in the solution to the free surface equation as follow:

$$\mathbf{n}^T \cdot (k \nabla h) \Big|_F = -S_y \frac{\partial h}{\partial t} \cos \theta, \quad \text{on F} \quad (5.2)$$

Equations (5.2) may explain why the decline of the free surface during drawdown depends on the index  $k/(S_y v)$ . The index  $k/(S_y v)$  is used below to systematically investigate the influence of various drawdown rates and material hydraulic parameters on transient flow in homogeneous soil slopes.

### 5.2.2 Analysis of slope stability with respect to circular sliding

The simplified Bishop's method [Bishop and Morgenstern, 1960] is used for slope stability analysis. Figure 5.1 shows the forces acting on a slice through the sliding mass enclosed by a circular slip surface. Note that the sliding mass is partially submerged by reservoir. In order to be able to directly utilize the simplified Bishop's formula for the safety factor, a substitution approach proposed by Chen [2003] is used to convert the mass with partial submergence to the one without submergence. Using this approach, the reservoir water line is extended to intersect the circular slip surface (as shown by dotted line). Thus the sliding mass is divided into two parts: above and below the reservoir level. For the part below, the external hydrostatic force acting on the slope face is equivalent to the resultant force of the water weight in the same volume as this part of sliding mass and the static pore-water pressures acting on the slip surface of this part below. As such, the formula for solving the safety factor  $SF$  can be expressed by:

$$SF = \frac{1}{\sum W' \sin \psi} \sum \left\{ \left[ c' \delta + (W' - U' \cos \psi) \tan \phi' \right] \frac{\sec \psi}{1 + \tan \psi \cdot \tan \phi' / SF} \right\} \quad (5.3)$$

where  $W' = W - W_w$ ,  $W$  is the total weight of a slice,  $W_w$  is the weight of water in the part of the slice below reservoir level (as shown by the shaded area in Figure 5.1),  $U' = U - U_s$  is the resultant force of the excess pore-water pressures on the slice base, equal to the resultant

force of the pore-water pressures  $U$  minus the resultant force of the static pore-water pressures  $U_s$ ,  $\psi$  is the angle between the slice base and the horizontal plane and  $\delta$  is the slice width. The rest of forces acting on the slice include the horizontal forces on the left and right sides  $E_n$ ,  $E_{n+1}$ , the normal force on the slice base  $N$  and the shear force along the slice base  $T$ .

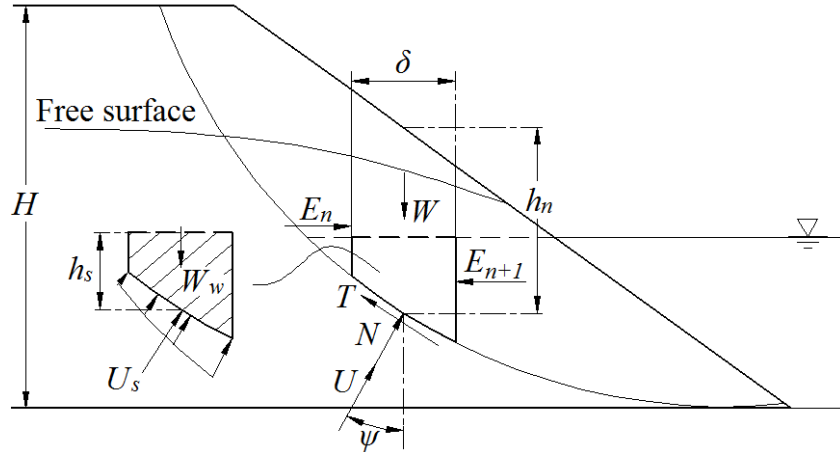


Figure 5.1 Forces acting on a slice through the sliding mass enclosed by a circular slip surface

To illustrate the parameters influencing  $SF$ , the expressions of  $W=\gamma\delta h_n$ ,  $W_w=\gamma_w\delta h_s$ ,  $U=u\delta/\cos\psi$  and  $U_s=\gamma_w\delta h_s/\cos\psi$ , where  $\gamma$  is unit weight of sliding mass, assumed to be uniform,  $h_n$  is the slice height,  $h_s$  is the submergence depth and  $u$  ( $u=P\cdot\gamma_w$ ) is the pore-water pressure, are substituted into Equation (5.3) and the linear dimensions are expressed as ratios of the slope height  $H$ . As a result, Equation (5.3) becomes:

$$\frac{SF}{\tan\phi'} = \frac{1}{\sum\left(\frac{h_n}{H} - \frac{\gamma_w}{\gamma} \frac{h_s}{H}\right)\sin\psi} \sum \left\{ \left[ \frac{c'}{\gamma H \tan\phi'} + \left( \frac{h_n}{H} - \frac{\gamma_w}{\gamma} \frac{h_s}{H} - \frac{u - \gamma_w h_s}{\gamma H} \right) \right] \frac{\sec\psi}{1 + \tan\psi \cdot \frac{\tan\phi'}{SF}} \right\} \quad (5.4)$$

From Equation (5.4), it is concluded that  $SF/\tan\phi'$  depends on the strength parameter combination  $c'/(\gamma H \tan\phi')$  and the pore-water pressure in dimensionless form  $u/(\gamma H)$ , for the given slope geometry and drawdown condition.

A limit equilibrium stability analysis program SLOPE/W [GEO-SLOPE/W International Ltd., 2008] is employed, adopting Bishop Simplified method. In SLOPE/W, the pore-water pressures or pressure heads at discrete points are specified from the results of transient flow simulation using the CEM; the circular slip surfaces are specified by the grid and radius approach, and the final slip surface is the one that yields the lowest safety

factor.

### 5.2.3 Design specifications for allowable $SF$ and acceptable reduction in $SF$

In several design specifications, the allowable safety factors which are the minimum required safety factors of reservoir slopes are designated. Table 5.1 is taken from “Design specification for slope of hydropower and water conservancy project, DL/T 5353-2006” set by National Development and Reform Commission of P.R. China [2006]. In Table 5.1, the reservoir slopes are divided into three grades from high to low: I, II and III, based upon its belonging pivotal project grade, the position of the slope in the pivot, the project service life and the harm extent of a failure. The permanent situation mainly refers to the normal operation condition, corresponding to longer-term steady flow under various reservoir levels between maximum storage and dead reservoir level. The temporary situation include the construction, repair conditions and other temporary condition during operation, corresponding to transient flow under a temporary change of water environment. As for the two situations, the design safety factors from limit equilibrium analysis cannot be lower than the values specified in Table 5.1.

It is noticed from Table 5.1 that the design safety factors applying to the temporary situation are generally lower than those applying to the permanent situation. Taking I-grade slope for example, the upper bound of the design safety factors for temporary situation (1.15) is about 8% lower than that for permanent situation (1.25). For II-grade slope, it is about 4% reduction in the upper bound of the design safety factor from permanent (1.15) to temporary situation (1.10). This reveals that the slope is allowed to have less safety margin against a temporary situation, e.g., rapid drawdown of reservoir. In case that the reservoir drawdown causes more than 8% or 4% reduction in the critical safety factor of I-grade or II-grade slopes (compared to the safety factor under permanent situation), it becomes the control condition for the design of slope; otherwise, the reservoir drawdown can be neglected and the permanent situation dominates the design of slope. Taking into account the aforementioned division for the drawdown conditions, this percentage can be taken as the critical value of the relative reduction in the safety factor caused by rapid drawdown and slow drawdown. Note that these safety factors should represent the minimum or critical safety factors in respective conditions.

In this study, rapid drawdown and slow drawdown are judged by examining whether or not the relative reduction in the minimum safety factor exceeds 4%. It is apparent that the judgment basis is relatively strict for I-grade slope which allows a maximum of 8%

reduction in the minimum safety factor for slow drawdown. Additionally, for III-grade slope, the design safety factors applying to permanent and temporary situations are the same and relatively low, so the reservoir drawdown must be checked in any case and can be considered always “rapid”.

Table 5.1 Allowable safety factors for slopes at reservoir area [National Development and Reform Commission of P.R. China, 2006]

Grade of slope at reservoir area	Working status	
	Permanent situation (normal operation)	Temporary situation (construction, repair or other temporary situation during operation)
I	1.25-1.15	1.15-1.05
II	1.15-1.05	1.10-1.05
III	1.05-1.00	1.05-1.00

### 5.3 Investigation of drawdown in homogeneous soil slopes

A drawdown problem in a homogenous soil slope is illustrated in Figure 5.2, showing the free surface and a potential slip surface. The slope is located on the impervious foundation and the origin of coordinates is on the left bottom. The left boundary is impermeable. Some basic parameters are defined in Figure 5.2, including the reservoir drawdown level  $H_D$ , the relevant lowering of the free surface at left boundary  $\Delta H_D$ , the slope crest width  $L$  and slope ratio  $m$  ( $m=\cot\beta$ , where  $\beta$  is slope angle). Considering the initial reservoir level at the slope crest, with a constant drawdown rate  $v$  the reservoir level drops along slope face. The transient flow in the slope is triggered, changing the slope safety factor. In the followings, the slope geometries are relative slope crest width  $L/H=1.2$  and slope ratio  $m=2$ .

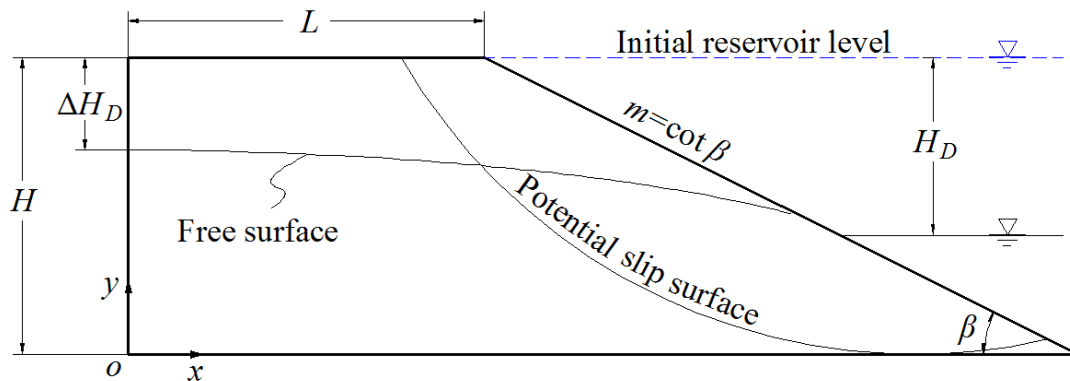


Figure 5.2 A drawdown problem in a homogenous soil slope



### 5.3.1 The decline of the free surface within slopes during drawdown

The representative values of  $k/(S_y v)$  are selected based on the field and laboratory measurements for various types of geological materials summarized by Singhal and Gupta [2010], shown in Table 5.2. The minimum and maximum values,  $k/S_y=0.05$  m/d and  $k/S_y=500$  m/d, respectively correspond to a weak pervious soil with  $k=0.0005$  m/d and  $S_y=0.01$  (typically, a clayed soil), and a strong pervious soil with  $k=50$  m/d and  $S_y=0.1$  (typically, a gravel soil). Consider the drawdown rate  $v$  equal to 0.5 m/d. Thus the value of  $k/(S_y v)$  ranges from 0.1 to 1000. The transient, saturated flow simulation arrives at the one-to-one correspondence between  $k/(S_y v)$  and the evolution of the free surface (and the pore-water pressure distribution) with different relative drawdown levels  $H_D/H$ .

Table 5.2 Input parameters for drawdown analyses of homogeneous soil slopes shown in Figures 5.3 and 5.5

Parameters	Values						Unit
$k/S_y$	0.05	0.5	5	50	500	–	m/d
$k/(S_y v)$ for $v=0.5$ m/d	0.1	1	10	100	1000	–	–
$c'/\gamma H$	0.01	0.05	0.1	0.2	0.3	0.36	–
$c'/(\gamma H \tan \phi')$ for $\phi'=20^\circ$	0.03	0.14	0.27	0.55	0.82	1.00	–

Figure 5.3 presents the calculated free surfaces under conditions of  $k/(S_y v)=0.1, 1, 10, 100$  and 1000. It can be observed from Figure 5.3 that the decline of the free surface lags behind obviously the lowering of the reservoir level when  $k/(S_y v)$  is smaller, for instance  $k/(S_y v)=0.1, 1$  and 10. As  $k/(S_y v)$  increases, the free surface declines at a growing velocity and stabilizes nearly instantaneously to the new reservoir level under condition of  $k/(S_y v)=1000$ . These results can be easily understood, because the larger value of  $k/(S_y v)$  means the relatively stronger hydraulic conductivity  $k$  of slope soils, less delayed yield from storage  $S_y$ , and slower reservoir drawdown rate  $v$ , which are all beneficial to quick decline of the free surface following the lowering of reservoir level.

The relative height of the free surface at left boundary,  $(H_D - \Delta H_D)/H_D$ , and at end of drawdown (i.e.,  $H_D/H=1$ ) can be achieved from Figure 5.3. The relation between  $k/(S_y v)$  and  $(H_D - \Delta H_D)/H_D$  at end of drawdown is depicted in Figure 5.4. The Bezier curve is used to fit and interpolate the data point. This relation, of course, is negative. According to the definitions of rapid drawdown, slow drawdown and moderate drawdown given by Chen [2015], the following conclusions can be drawn: (i) when  $k/(S_y v) \leq 1$ , the reservoir drawdown is judged as rapid drawdown due to  $(H_D - \Delta H_D)/H_D \geq 90\%$ ; (ii) when  $k/(S_y v) > 370$ , the reservoir

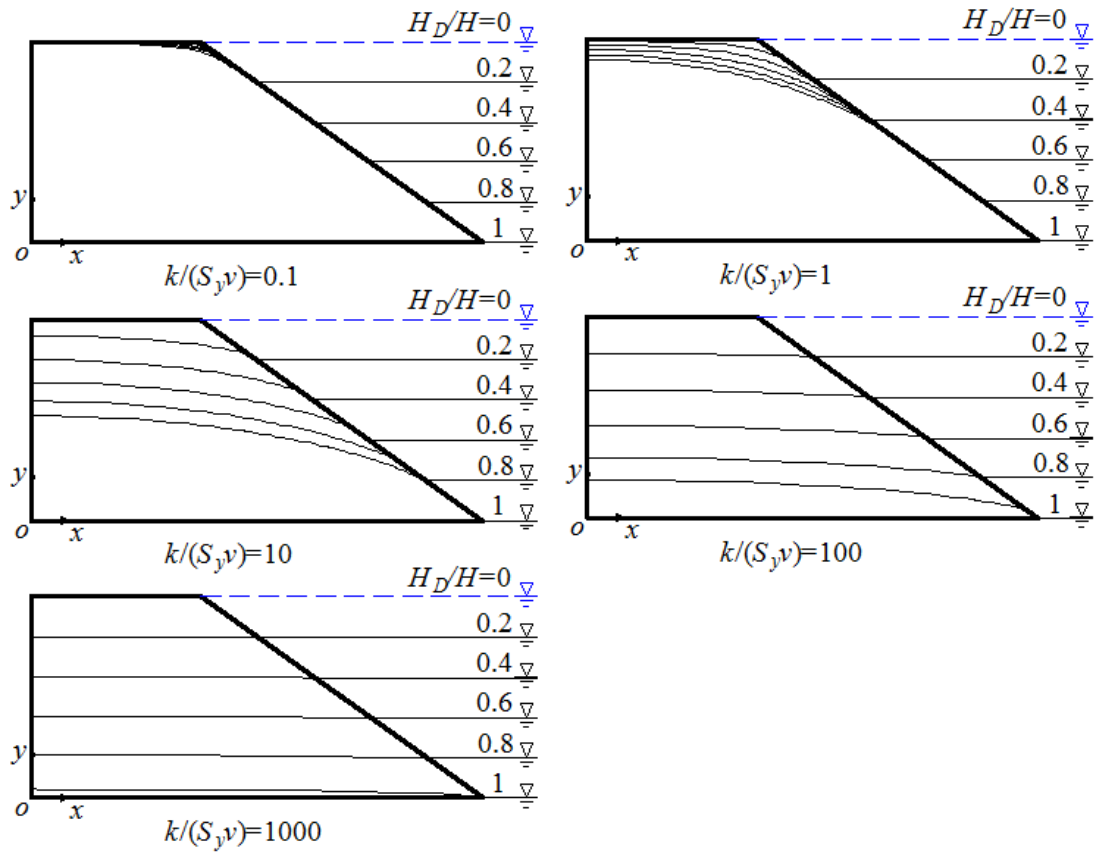


Figure 5.3 The calculated free surfaces at different drawdown levels  $H_D/H$  under conditions of  $k/(S_y v) = 0.1, 1, 10, 100$  and  $1000$

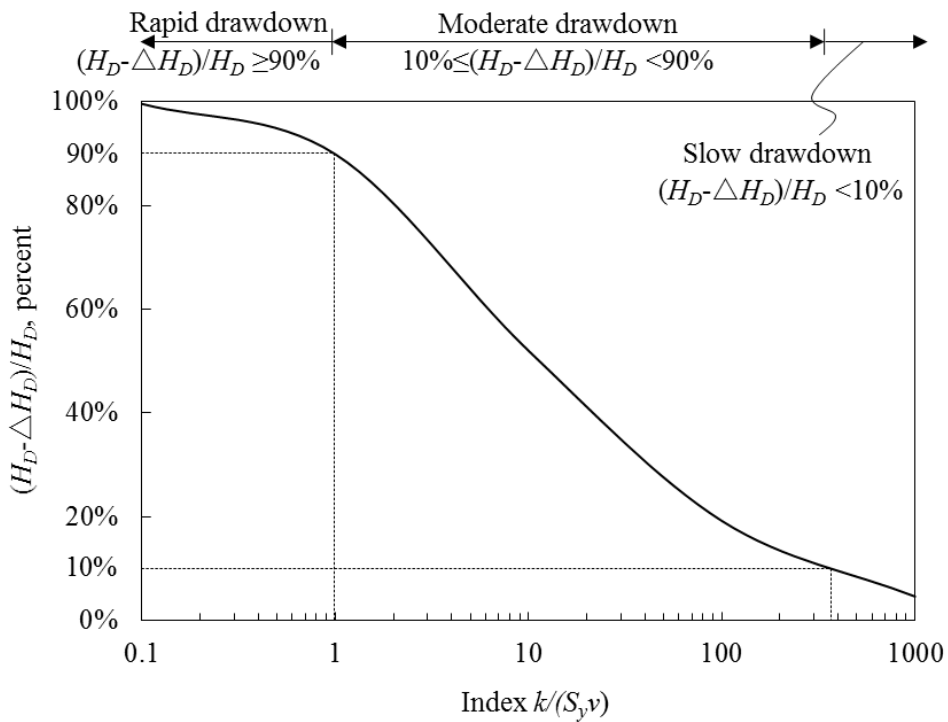


Figure 5.4 Relation between  $k/(S_y v)$  and  $(H_D - \Delta H_D)/H_D$  at end of drawdown

drawdown is judged as slow drawdown due to  $(H_D - \Delta H_D)/H_D < 10\%$ ; and (iii) when

$1 < k/(S_y v) \leq 370$ , the reservoir drawdown is judged as moderate drawdown due to  $10\% \leq (H_D - \Delta H_D)/H_D < 90\%$ . Give an example to illustrate the significance of these conclusions, as follows: for a drawdown rate  $v$  of 0.5 m/d, in clayed soils with  $k/S_y = 0.05$  m/d, the slope behaviors correspond with those under rapid drawdown in terms of  $k/(S_y v) \leq 1$ ; yet in gravel soils with  $k/S_y = 500$  m/d, the slope behaviors correspond with those under slow drawdown in terms of  $k/(S_y v) > 370$ . Thus, particular attention should be paid on the stability of clayed soil slope in this drawdown case.

### 5.3.2 The variation in SF of slopes during drawdown

The unit weight of slope soils  $\gamma$  is assumed to be 20 kN/m<sup>3</sup>. Relatively large  $c'/(\gamma H \tan \phi')$  values are typical of low slopes in soils with small internal friction angle, e.g.,  $c'/(\gamma H \tan \phi') = 0.851$  when  $c' = 30$  kPa,  $H = 10$  m and  $\phi' = 10^\circ$ ; and relatively small  $c'/(\gamma H \tan \phi')$  values describe high slopes in soils with low cohesion and large internal friction angle, e.g.,  $c'/(\gamma H \tan \phi') = 0.021$  when  $c' = 10$  kPa,  $H = 50$  m and  $\phi' = 25^\circ$ . Hence, the stability computation results should be presented for values of  $c'/(\gamma H \tan \phi')$  ranging from 0 to 1.0 (in Table 5.2).

Figure 5.5 presents the variations of the computed  $SF/\tan \phi'$  with  $H_D/H$  under conditions of  $k/(S_y v) = 0.1, 1, 10, 100$  and  $1000$ , when  $c'/(\gamma H \tan \phi') = 0.137$  ( $c'/\gamma H = 0.05$  and  $\phi' = 20^\circ$ ). For comparison, the results for fully rapid drawdown and fully slow drawdown are provided in Figure 5.5. They can be understood as the conditions of  $k/(S_y v) = 0$  and  $k/(S_y v) = \infty$ , respectively. The  $SF/\tan \phi'$  variation with  $H_D/H$  for fully slow drawdown also represents that for steady flow under reservoir level varying from the maximum to none. It can be seen from Figure 5.5 that the reservoir drawdown results in the decrease in  $SF/\tan \phi'$  as a whole. This indicates that the decreased external hydrostatic loads have a proportionately greater destabilizing effect than the increased shear strength due to the decrease in the pore-water pressures. When  $k/(S_y v) \geq 10$ ,  $SF/\tan \phi'$  increases slightly at the higher drawdown levels  $H_D/H$ , which reveals that the effect of the increased shear strength starts to prevail over that of the decreased external hydrostatic loads. The observed minimum or critical  $SF/\tan \phi'$  occurs at a relative drawdown level  $H_D/H$  between 0.7 and 0.8. Moreover, the larger  $k/(S_y v)$ , the greater  $SF/\tan \phi'$  is reached for a given  $H_D/H$  value.

The reduction in the minimum  $SF/\tan \phi'$  during drawdown relative to that during steady flow when  $c'/(\gamma H \tan \phi') = 0.137$  can be determined from Figure 5.5. Figure 5.6 presents the relation between  $k/(S_y v)$  and the relative reduction in minimum  $SF$  (that equals the relative reduction in minimum  $SF/\tan \phi'$ ) caused by drawdown. Undoubtedly, with the increase in  $k/(S_y v)$ , the relative reduction in minimum  $SF$  decreases. According to whether or not the

relative reduction in the minimum  $SF$  exceeds 4%, rapid drawdown and slow drawdown are renewedly judged by  $k/(S_y v) \leq 61$  and  $k/(S_y v) > 61$ . The same procedures can be carried out to establish the judgment criteria for different values of  $c' / (\gamma H \tan \phi')$ . It is observed from Figure 5.6 that the smaller  $c' / (\gamma H \tan \phi')$  is, the larger critical value of  $k/(S_y v)$  is, in other words, the greater value interval of  $k/(S_y v)$  corresponding to rapid drawdown. This can be explained by the fact that the variable pore-water pressures influence only the frictional strength due to  $\phi'$  but cohesive strength due to  $c'$ . Therefore, if  $c' / (\gamma H \tan \phi')$  is smaller, that is, the frictional strength occupies major portion of total shear strength compared to the cohesive strength, the stability will be more significantly influenced by the drawdown. In this case, the slope behaviors are more likely to approach those under rapid drawdown. The critical values of  $k/(S_y v)$  vary within the interval [15,74].

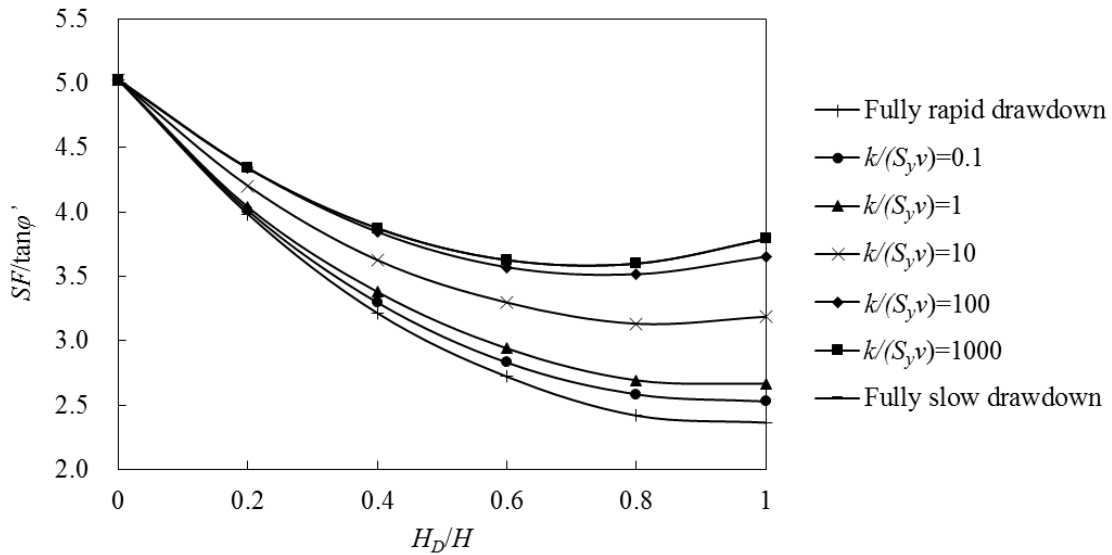


Figure 5.5 Variations of the computed  $SF/\tan \phi'$  with  $H_D/H$ , under conditions of  $k/(S_y v) = 0.1, 1, 10, 100$  and  $1000$ , when  $c' / (\gamma H \tan \phi') = 0.137$

### 5.3.3 Comparisons between old and new criteria for judging rapid drawdown

The conditions for rapid drawdown and slow drawdown in homogeneous soil slopes with  $L/H=1.2$  and  $m=2$  are charted in Figure 5.7. The different regions in the chart are defined as follows.

*In an "old" criterion,*

Region 1—rapid drawdown:  $k/(S_y v) \leq 1$ , the height of the free surface at end of drawdown is more than 90% of total drawdown level, and customarily, stability analysis of slope under fully rapid drawdown is performed.

Regions 2 and 3—moderate drawdown:  $1 < k/(S_y v) \leq 370$ , the height of the free surface

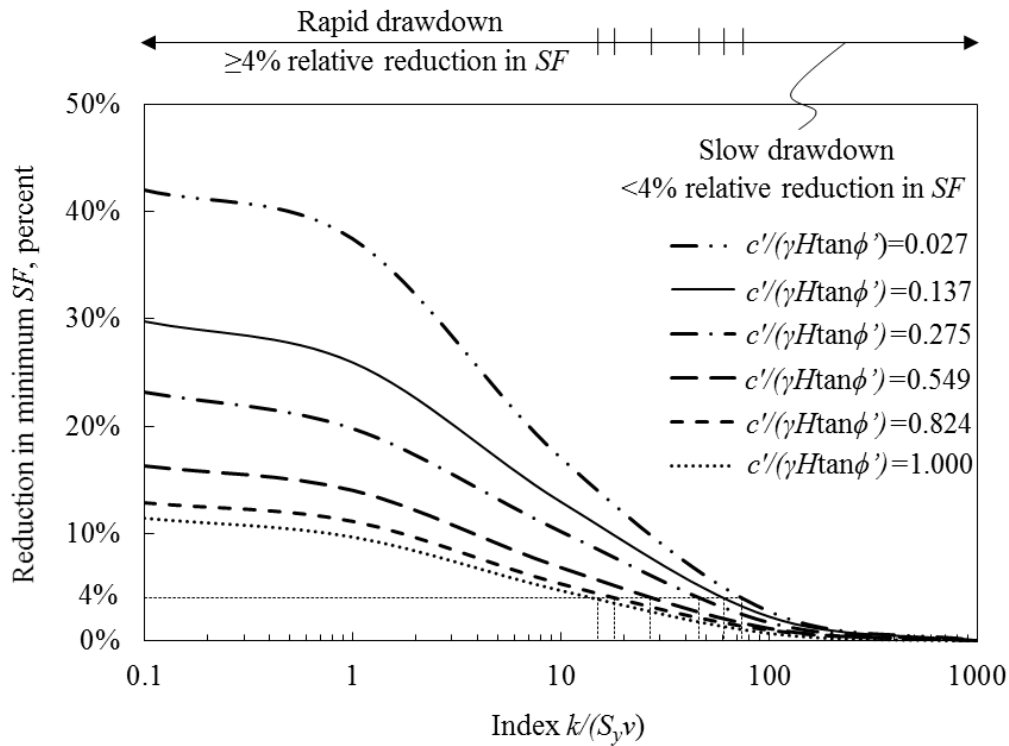


Figure 5.6 Relation between  $k/(S_y v)$  and relative reduction in minimum  $SF$  caused by drawdown

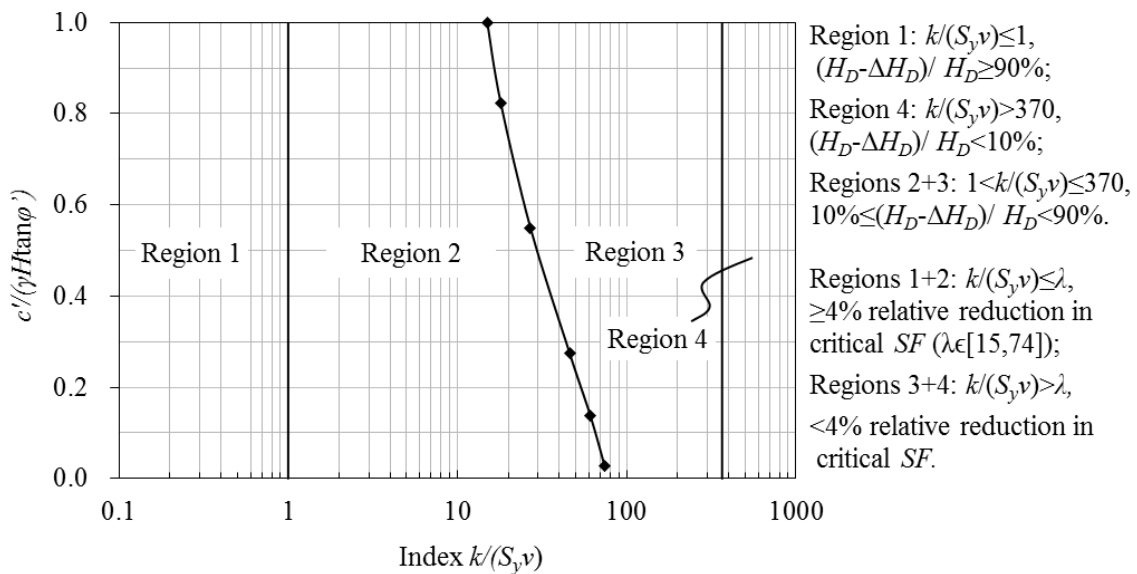


Figure 5.7 Conditions for rapid and slow drawdown in homogeneous soil slopes with  $L/H=1.2$  and  $m=2$

at end of drawdown is between 10% and 90% of total drawdown level, and analysis of slope stability subjected to transient flow is carried out as design routine.

Region 4—slow drawdown:  $k/(S_y v) > 370$ , the height of the free surface at end of drawdown is less than 10% of total drawdown level, and stability analysis of slope under

drawdown can be neglected.

*In a “new” criterion,*

Regions 1 and 2—rapid drawdown:  $k/(S_y v) \leq \lambda$ , where  $\lambda \in [15, 74]$  is dependent on  $c'/(\gamma H \tan \phi')$ , the critical safety factor of slope under drawdown is expected to reduce by more than 4% of that under steady flow, and thus stability analysis for the drawdown condition dominates the design of slope.

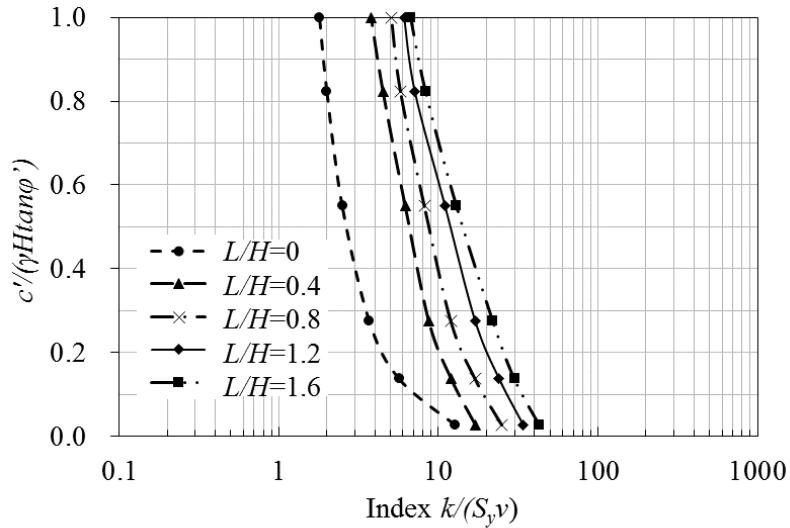
Regions 3 and 4—slow drawdown:  $k/(S_y v) > \lambda$ , the critical safety factor of slope under drawdown is expected to reduce by less than 4% of that under steady flow, and thus stability analysis for the steady flow condition dominates the design of slope.

It is interesting to note from Figure 5.7 that the region of moderate drawdown in a conventional criterion has been divided into two parts and separately merged into the regions of rapid drawdown and slow drawdown in the new criterion. If the critical safety factor of slope under drawdown condition is allowed to reduce by more than 4% (e.g., 8% for I-grade slope), the dividing line will move toward the left, which means the less drawdown cases distinguished as rapid drawdown.

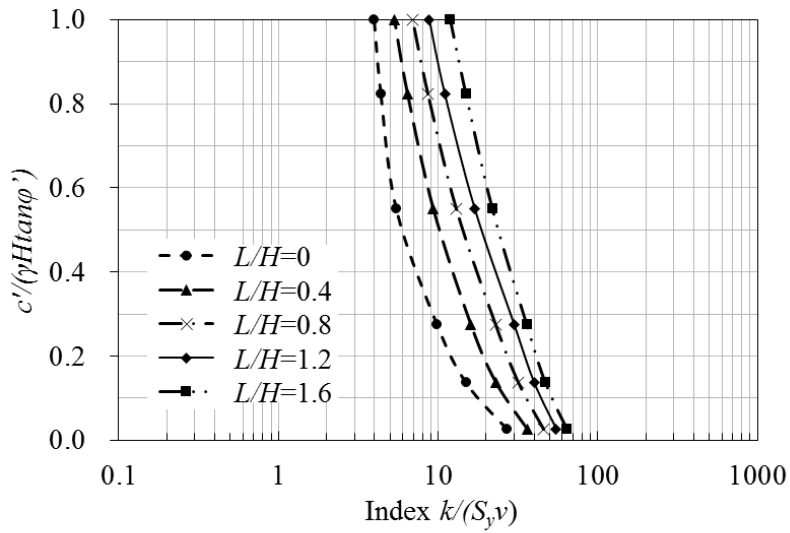
#### **5.4 Charts for quick judgment of rapid drawdown in homogeneous soil slopes**

A series of charts are produced in Figure 5.8 to facilitate the judgment of rapid and slow drawdown in homogeneous soil slopes with various relative slope crest widths and slope ratios; they are  $L/H=0, 0.4, 0.8, 1.2$  and  $1.6$ , and  $m=1, 1.5, 2, 2.5$  and  $3$ . The steep slopes (with small  $m$  values) are typical of reservoir or river bank slopes, whereas the gentle slopes (with large  $m$  values) can be the upstream slopes of earth dams (with nearly vertical central cores on the downstream sides). The information of data points in Figure 5.8 are provided in Table 5.3 for quick and easy reference.

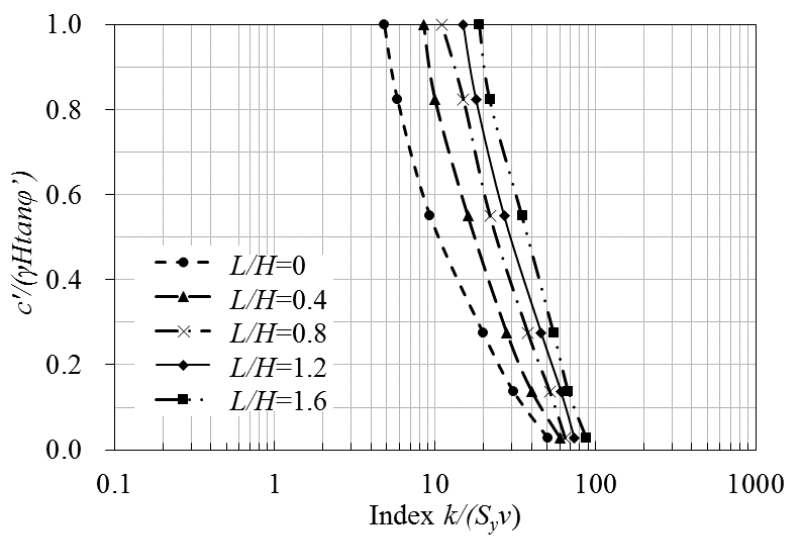
Each dividing line in Figure 5.8 divides the  $k/(S_y v) \sim c'/(\gamma H \tan \phi')$  space into two regions: left region—rapid drawdown and right region—slow drawdown. It can be found that the region of rapid drawdown (or the critical value of  $k/(S_y v)$ ) becomes larger with the growth of relative crest width  $L/H$  and slope ratio  $m$ . This finding makes sense, because the slopes with gentle slope face and wide slope crest have relatively poor drainage conditions, rendering the stability greatly impaired by reservoir drawdown. In the slope stability analysis, the rapid drawdown condition must be examined; and in the reservoir operation management, the drawdown rate shall be chosen following the principle of forming the slow drawdown condition.



(a)  $m=1$

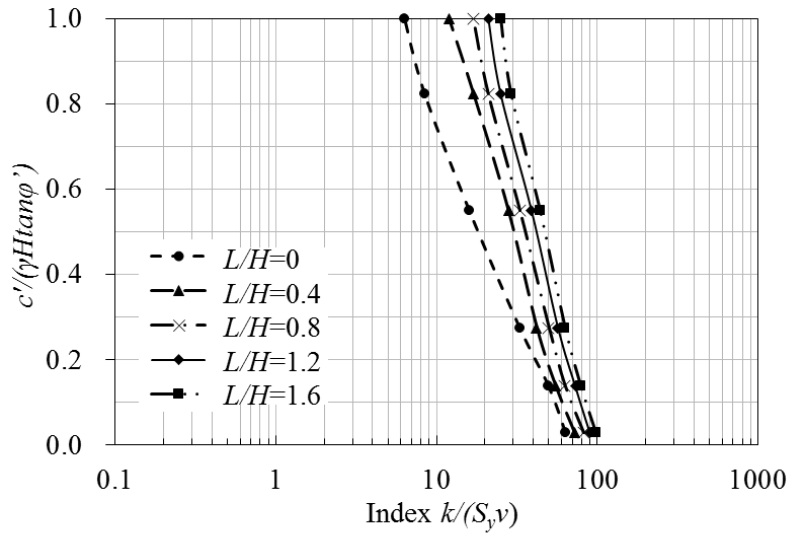


(b)  $m=1.5$

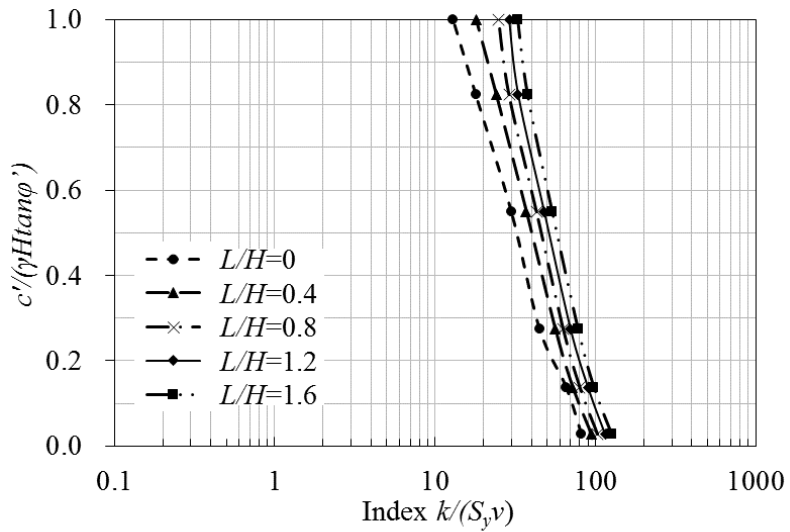


(c)  $m=2$

(To be continued)



(d)  $m=2.5$



(e)  $m=3$

Figure 5.8 Charts for quick judgment of rapid and slow drawdown in homogeneous soil slopes with different geometrical features

Table 5.3 Values of  $k/(S_yv)$  and  $c'/(γHtanφ')$  for quick judgment of rapid and slow drawdown in homogeneous soil slopes with different geometrical features

$c'/(γHtanφ')$	(a) $m=1$									
	$k/(S_yv)$									
	$L/H=0$		$L/H=0.4$		$L/H=0.8$		$L/H=1.2$		$L/H=1.6$	
	RD <sup>†</sup>	SD <sup>‡</sup>	RD	SD	RD	SD	RD	SD	RD	SD
0.027	≥12.8	<12.8	≥17	<17	≥25	<25	≥34	<34	≥43	<43
0.137	≥5.7	<5.7	≥12	<12	≥17	<17	≥24	<24	≥30	<30
0.275	≥3.7	<3.7	≥8.7	<8.7	≥12	<12	≥17	<17	≥22	<22
0.549	≥2.5	<2.5	≥6.2	<6.2	≥8.2	<8.2	≥11	<11	≥13	<13
0.824	≥2	<2	≥4.5	<4.5	≥5.8	<5.8	≥7.1	<7.1	≥8.3	<8.3



1.000	$\geq 1.8$	$< 1.8$	$\geq 3.8$	$< 3.8$	$\geq 5.1$	$< 5.1$	$\geq 6.1$	$< 6.1$	$\geq 6.7$	$< 6.7$
-------	------------	---------	------------	---------	------------	---------	------------	---------	------------	---------

(b)  $m=1.5$

$c' / (\gamma H \tan \phi')$	$k / (S_y v)$									
	$L/H=0$		$L/H=0.4$		$L/H=0.8$		$L/H=1.2$		$L/H=1.6$	
	RD	SD	RD	SD	RD	SD	RD	SD	RD	SD
0.027	$\geq 27$	$< 27$	$\geq 36$	$< 36$	$\geq 46$	$< 46$	$\geq 55$	$< 55$	$\geq 64$	$< 64$
0.137	$\geq 15$	$< 15$	$\geq 23$	$< 23$	$\geq 32$	$< 32$	$\geq 40$	$< 40$	$\geq 47$	$< 47$
0.275	$\geq 9.9$	$< 9.9$	$\geq 16$	$< 16$	$\geq 23$	$< 23$	$\geq 30$	$< 30$	$\geq 36$	$< 36$
0.549	$\geq 5.5$	$< 5.5$	$\geq 9.3$	$< 9.3$	$\geq 13$	$< 13$	$\geq 17$	$< 17$	$\geq 22$	$< 22$
0.824	$\geq 4.4$	$< 4.4$	$\geq 6.4$	$< 6.4$	$\geq 8.6$	$< 8.6$	$\geq 11$	$< 11$	$\geq 15$	$< 15$
1.000	$\geq 4$	$< 4$	$\geq 5.3$	$< 5.3$	$\geq 6.9$	$< 6.9$	$\geq 8.8$	$< 8.8$	$\geq 12$	$< 12$

(c)  $m=2$

$c' / (\gamma H \tan \phi')$	$k / (S_y v)$									
	$L/H=0$		$L/H=0.4$		$L/H=0.8$		$L/H=1.2$		$L/H=1.6$	
	RD	SD	RD	SD	RD	SD	RD	SD	RD	SD
0.027	$\leq 51$	$> 51$	$\leq 60$	$> 60$	$\leq 65$	$> 65$	$\leq 74$	$> 74$	$\leq 88$	$> 88$
0.137	$\leq 31$	$> 31$	$\leq 40$	$> 40$	$\leq 52$	$> 52$	$\leq 61$	$> 61$	$\leq 68$	$> 68$
0.275	$\leq 20$	$> 20$	$\leq 28$	$> 28$	$\leq 38$	$> 38$	$\leq 46$	$> 46$	$\leq 55$	$> 55$
0.549	$\leq 9.3$	$> 9.3$	$\leq 16$	$> 16$	$\leq 22$	$> 22$	$\leq 27$	$> 27$	$\leq 35$	$> 35$
0.824	$\leq 5.8$	$> 5.8$	$\leq 10$	$> 10$	$\leq 15$	$> 15$	$\leq 18$	$> 18$	$\leq 22$	$> 22$
1.000	$\leq 4.8$	$> 4.8$	$\leq 8.5$	$> 8.5$	$\leq 11$	$> 11$	$\leq 15$	$> 15$	$\leq 19$	$> 19$

(d)  $m=2.5$

$c' / (\gamma H \tan \phi')$	$k / (S_y v)$									
	$L/H=0$		$L/H=0.4$		$L/H=0.8$		$L/H=1.2$		$L/H=1.6$	
	RD	SD	RD	SD	RD	SD	RD	SD	RD	SD
0.027	$\geq 64$	$< 64$	$\geq 72$	$< 72$	$\geq 82$	$< 82$	$\geq 90$	$< 90$	$\geq 98$	$< 98$
0.137	$\geq 50$	$< 50$	$\geq 55$	$< 55$	$\geq 63$	$< 63$	$\geq 73$	$< 73$	$\geq 79$	$< 79$
0.275	$\geq 33$	$< 33$	$\geq 42$	$< 42$	$\geq 50$	$< 50$	$\geq 57$	$< 57$	$\geq 63$	$< 63$
0.549	$\geq 16$	$< 16$	$\geq 28$	$< 28$	$\geq 33$	$< 33$	$\geq 39$	$< 39$	$\geq 44$	$< 44$
0.824	$\geq 8.4$	$< 8.4$	$\geq 17$	$< 17$	$\geq 21$	$< 21$	$\geq 25$	$< 25$	$\geq 29$	$< 29$
1.000	$\geq 6.3$	$< 6.3$	$\geq 12$	$< 12$	$\geq 17$	$< 17$	$\geq 21$	$< 21$	$\geq 25$	$< 25$

(e)  $m=3$

$c' / (\gamma H \tan \phi')$	$k / (S_y v)$									
	$L/H=0$		$L/H=0.4$		$L/H=0.8$		$L/H=1.2$		$L/H=1.6$	
	RD	SD	RD	SD	RD	SD	RD	SD	RD	SD
0.027	$\geq 82$	$< 82$	$\geq 94$	$< 94$	$\geq 103$	$< 103$	$\geq 115$	$< 115$	$\geq 126$	$< 126$
0.137	$\geq 66$	$< 66$	$\geq 72$	$< 72$	$\geq 80$	$< 80$	$\geq 90$	$< 90$	$\geq 98$	$< 98$
0.275	$\geq 45$	$< 45$	$\geq 56$	$< 56$	$\geq 63$	$< 63$	$\geq 70$	$< 70$	$\geq 78$	$< 78$

0.549	≥30	<30	≥37	<37	≥43	<43	≥48	<48	≥54	<54
0.824	≥18	<18	≥24	<24	≥29	<29	≥33	<33	≥38	<38
1.000	≥13	<13	≥18	<18	≥25	<25	≥29	<29	≥33	<33

†RD indicates rapid drawdown; ‡SD indicates slow drawdown.

## 5.5 Conclusions

A rapid drawdown of reservoir can result in the temporary increase in hydraulic gradients which may not be withstood by adjacent soil or rock slopes and thus failures occur. In the design of reservoir bank slopes, stability analysis with regard to rapid drawdown must be performed. A conventional criterion for the judgment of rapid drawdown was set prior to stability analysis, which made use of the index  $k/(S_y v)$  and established the relation between  $k/(S_y v)$  and the relative height of free surface at end of drawdown to total drawdown level. The rapid drawdown in this criterion was defined as the one during which the height of free surface remains more than 90% of total drawdown level, and was believed to be detrimental to slope stability. Given that the ultimate concern is the effect on slope stability, it would be better to relating the index  $k/(S_y v)$  directly to the relative reduction in the safety factor caused by drawdown. As such, this chapter suggests a new criterion for judging rapid drawdown which is defined as the one causing more than 4% reduction in the critical safety factor compared to the critical safety factor under steady flow.

Consider homogeneous soil slopes against circular shear failure. The composite element modelling of transient, saturated flow with a free surface is used to estimate the transient free surfaces and pore-water pressure distributions in slopes during drawdown. Using the calculated pore-water pressure distributions as groundwater conditions, the limit equilibrium stability analyses are subsequently performed to evaluate the variations of the safety factor of slopes. The main conclusions can be summarized as follows:

(1) In the new criterion, the dividing line for distinguishing rapid drawdown from slow drawdown falls into the moderate drawdown region in the conventional criterion. This new criterion takes into account the reservoir drawdown effect on the ultimate stability of slope. It can provide a practical guide to quickly judge if there is a need for the drawdown analysis in the design of slope stabilization as well as reservoir operation.

(2) The judgment basis for rapid drawdown that causes more than 4% reduction in the critical safety factor compared to the critical safety factor under long-term steady flow, is stipulated only for II-grade slope in the Chinese design specification. If a higher safety factor has been designated to the slope under steady flow condition and hence a greater reduction

in the critical safety factor is allowed for the slope subjected to reservoir drawdown (i.e. I-grade slope), the criterion for judging rapid drawdown needs to be revised accordingly.

(3) It should be noted that the case of cohesionless slope material ( $c'=0$ ) is not involved in this analyses, since the most critical failure mechanism approaches slide along a planar surface.

(4) All the results of the drawdown analyses of homogeneous soil slopes in this study can be equally accessible to highly fractured or weak rock slopes, in which rock masses are commonly assumed to be homogeneous, isotropic and modelled as Mohr-Coulomb materials.

## References

1. Berilgen MM. Investigation of stability of slopes under drawdown conditions. *Computers and Geotechnics* 2007; **34**(2): 81–91.
2. Bishop AW, Morgenstern NR. Stability coefficients for earth slopes. *Geotechnique* 1960; **10**(4): 129–153.
3. Chen SH. Hydraulic structures. Springer Verlag: New York, 2015.
4. Chen ZY. Soil slope stability analysis: theory, method and programs. China Water and Power Press: Beijing, 2003.
5. Desai CS. Drawdown analysis of slopes by numerical method. *Journal of Geotechnical and Geoenvironmental Engineering* 1977; **103**(7): 667–676.
6. Duan XB, Xie LF. Unsteady seepage test under condition of rapid drawdown. *Chinese Journal of Yangtze River Scientific Research Institute* 2009; **26**(10): 7–12.
7. GEO-SLOPE/W International Ltd. Stability modeling with SLOPE/W 2007, an engineering methodology, 4th edition. Geo-Slope International Ltd.: Canada, 2008.
8. Gu WC. Seepage calculation principle and application. China Building Material Industry Publishing House: Beijing, 2000.
9. Liu XX, Xia YY, Lian C, Zhang KP. Research on method of landslide stability valuation during sudden drawdown of reservoir level. *Chinese Journal of Rock and Soil Mechanics* 2005; **26**(9): 1427–1431.
10. National Development and Reform Commission of P.R. China. Design specification for slope of hydropower and water conservancy project, DL/T 5353-2006. China Electric Power Press: Beijing, 2006.
11. Pinyol NM, Alonso EE, Olivella S. Rapid drawdown in slopes and embankments. *Water Resources Research* 2008; **44**(5), W00D03, doi: 10.1029/2007WR006525.
12. Shi WM, Zheng YR. Analysis on stability of landslide during reservoir drawdown. *Chinese Journal of Hydraulic Engineering* 2003; **12**: 76–81.
13. Singhal BBS, Gupta RP. Applied hydrogeology of fractured rocks. Springer Verlag: New York, 2010.
14. Zheng YR, Shi WM, Kong WX. Calculation of seepage forces and phreatic surface under drawdown conditions. *Chinese Journal of Rock Mechanics and Engineering* 2004; **23**(18): 3203–3210.

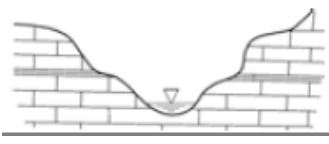
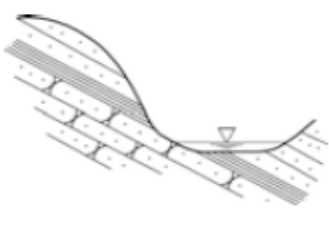
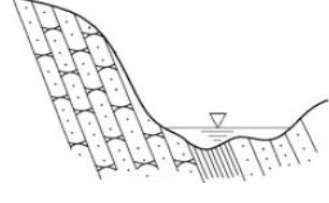
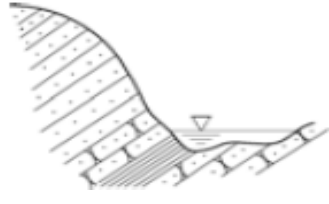

# Chapter 6 Investigation of Stability of Layered Rock Slopes Under Drawdown Conditions

## 6.1 Introduction

Layered structure is one of the most prevalent structures in rock masses. The rock structures refer to naturally occurring breaks in the rock such as bedding planes, joints and faults (which are termed here as fractures) [Hoek and Bray, 1981]. According to the relationship between slope and fracture occurrence, the layered rock masses have been divided into horizontally bedded, dipping away slightly and deeply bedded, and dipping in bedded rock masses [Sun, 1993], shown in Figure 6.1. The type of layered rock mass largely determines the failure mode. In the horizontally bedded rock slope, the possibility of shear failure is small because the dip angle of fractures or rock layers is lower than internal friction angle. Consequently, the horizontally bedded rock slope shows the higher stability. In the dipping away consequent bedded rock slope, the steeper of the dip angle of fractures, the lower the stability is. The typical failure mode of this type has been identified as planar shear failure along weak interlayers or fractures. However, if the fractures deeply dip away the slope, the failure mode may be characterized by a buckling failure [Chen et al., 2005]. The dipping in bedded rock slope generally has the higher stability than that of the dipping away consequent bedded rock slope. The failure of the dipping in bedded rock slope may manifests as a topping failure. Both bulking and toppling failure modes typically occur in rock masses with steeply dipping large-scale fractures or in highly foliated rock masses [Pritchard and Savigny, 1991; Sjoberg, 2000]. The mechanisms leading to bulking and toppling failures, particularly the formation of the failure surfaces, are not clearly defined. This is partly due to insufficient observational data and partly due to inadequate analytical treatment of these failure modes.

In the previous chapter, the stability of homogenous slopes against circular shear failure under drawdown conditions has been investigated. In these slopes, the size of individual rock blocks is very small compared to that of entire slope, and these blocks do not have reciprocal occlusal relationships in shapes. Thus, the resulting slides occur along the circular slip surfaces on the whole. This chapter continues to investigate the stability of layered rock slopes against planar shear failure under drawdown conditions. Fractures within the slopes are assumed to strike parallel to, but dip less than the slope face.

Table 6.1 Classification of layered rock mass and associated failure mode (referring to [Chen, 2015], and slightly modified)

Geologic structure		Typical profile	Failure mode
Layered structure	Horizontal		High stability
	Slightly dipping away		Planar sliding
	Deeply dipping away		Buckling
	Dipping into		Toppling
Fractured structure <sup>†</sup>			Circular sliding

<sup>†</sup>The typical profile and failure mode for fractured structure are also provided for visual comparison with those for layered structure.

## 6.2 Analysis of slope stability with respect to planar sliding

The forces acting on the sliding mass enclosed by a planar slip surface are shown in Figure 6.1. From the static equilibrium condition, the safety factor  $SF$  representing the ratio between the driving and resisting forces can be computed by the following formula:

$$SF = \frac{1}{\bar{W}' \sin \psi} \left[ c' \frac{H}{\sin \psi} + (\bar{W}' \cos \psi - \bar{U}') \tan \phi' \right] \quad (6.1)$$

where  $\bar{W}' = \bar{W} - \bar{W}_w$ ,  $\bar{W}$  is the total weight of the sliding mass,  $\bar{W}_w$  is the water weight

in the part of the sliding mass below reservoir level,  $\bar{U}' = \bar{U} - \bar{U}_s$  is the sum of the excess pore-water pressures acting on the planar slip surface, equal to the sum of the pore-water pressures  $\bar{U}$  minus the sum of the static pore-water pressures  $\bar{U}_s$  on the slip surface, and  $\psi$  is the angle between the planar slip surface and the horizontal plane. The rest of forces acting on the sliding mass include the normal force  $\bar{N}$  on the slip surface and the shear force  $\bar{T}$  along the slip surface.

Like in Section 5.2.1, the substitution of expressions of  $\bar{W} = \gamma H^2(\cot\psi - \cot\beta)/2$ ,  $\bar{W}_w = \bar{W} \cdot \gamma_w/\gamma(1-H_D/H)^2$ ,  $\bar{U} = uH/\sin\psi$  and  $\bar{U}_s = \gamma_w H^2/2\sin\psi(1-H_D/H)^2$  into Equation (6.1) concludes that  $SF/\tan\phi'$  is the function of  $c'/(\gamma H \tan\phi')$  and  $u/(\gamma H)$  if slope geometry and drawdown condition are given.

The limit equilibrium stability analysis program SLOPE/W is employed, adopting Janbu Simplified method. This method is equivalent to Equation (6.1). In SLOPE/W, the planar slip surfaces are specified with a series of data points along a given fracture surface; and the pore-water pressures on the slip surface are specified from the results of transient flow simulation using the CEM.

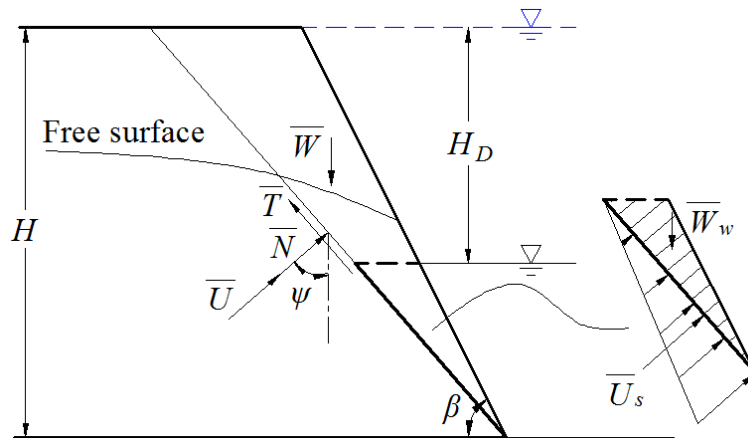


Figure 6.1 Forces acting on a sliding mass enclosed by a planar slip surface

### 6.3 Investigation of drawdown in layered rock slopes

Consider a group of evenly spaced, planar, parallel and persistent fractures in a layered rock slope, as shown in Figure 6.2. The slope has the geometries with  $L/H=0.8$ ,  $m=0.5$  and  $H=55$  m. While the reservoir level is lowered, the external stabilizing hydrostatic pressures decrease, or to say, the effective weight of the sliding mass  $\bar{W}'$  in Equation (6.1) increases. This may result in the potential sliding mass enclosed by the fracture surface intersecting

the slope face to be activated. In the following study, the variations of the pore-water pressure distribution and the safety factor of the slope during drawdown will be examined. The fracture surface passing through the slope toe (AA' in Figure 6.2) is specified as the potential slip surface.

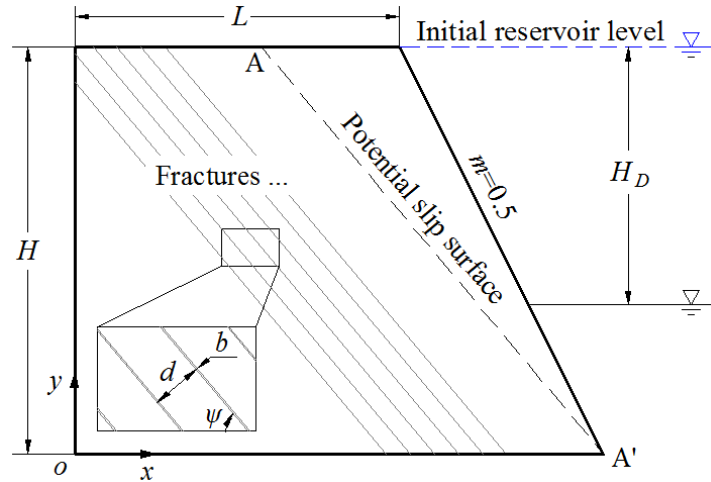


Figure 6.2 A drawdown problem in a layered rock slope containing one group of fractures dipping away the slope

### 6.3.1 Parameters influencing transient flow in layered rock slopes

For stability analysis of the layered rock slope, transient flow simulation is essential. The basic parameters defining transient flow in slope have been identified to be the hydraulic conductivity and the specific yield, as discussed in Section 5.3.1. The rock masses consist of rock matrix and fractures, so the simulation results of transient flow in the rock slope will be affected by the hydraulic parameters of both media.

In most rock types, the hydraulic conductivity for rock matrix  $k_m$  is very low. For example, the hydraulic conductivity for intact granite and basalt is about  $10^{-4}$  m/d to  $10^{-7}$  m/d. Groundwater flow in these rock masses occurs predominately along the fractures because the hydraulic conductivity for fractures  $k_f$  is usually several orders of magnitude larger than the rock matrix. The characteristics of the fractures have a major influence on the hydraulic conductivity for the rock masses. For instance, the fracture aperture  $b$  (which is actually  $b^2$ ) determines the magnitude of the hydraulic conductivity for individual fractures; the fracture spacing  $d$  represents the change in the conductivity in the direction perpendicular to the fracture surfaces; and the fracture dip angle  $\psi$  specifies the direction of the principle hydraulic conductivity.

The specific yields for rock matrix  $S_{ym}$  and for fracture  $S_{yf}$  respectively refer to the ratios of volume of water that saturated rock matrix and fracture will yield by gravity to the total



matrix and fracture volumes. In a layered rock mass, the volumetric fractions of rock matrix  $\eta_m$  and fractures  $\eta_f$  can be respectively expressed as:

$$\eta_m = \frac{\text{Matrix volume}}{\text{Total bulk volume}} \approx 1 - b/d$$

$$\eta_f = \frac{\text{Fracture volume}}{\text{Total bulk volume}} \approx b/d$$

Then, the average specific yield for the rock mass  $S_{y,aver}$  is derived by:

$$S_{y,aver} = \eta_m S_{ym} + \eta_f S_{yf} \quad (6.2)$$

Obviously, if the fracture aperture  $b$  (usually in the range of millimeters to micrometers) is much smaller than its spacing  $d$ , i.e.,  $\eta_f$  is very small,  $S_{y,aver}$  will be mainly contributed by  $\eta_m S_{ym}$  and the contribution of  $\eta_f S_{yf}$  is negligible. On the contrary, if  $\eta_f$  is not so small, both contributions of  $\eta_m S_{ym}$  and  $\eta_f S_{yf}$  should be accounted for  $S_{y,aver}$ . At this time, the rock mass is generally viewed as a continuum with anisotropy. The specific yield for limestone and dolomite is 0.001 to 0.1; and the specific yield for basalt is 0.02 to 0.1 [Singhal and Gupta, 2010].

In many of the reported work [Snow, 1969; Wyllie and Mah, 2004; Dong et al., 2006], analysis of flow in rock masses was carried out assuming the rock masses are continua. For rock masses containing one group of parallel, smooth, clean fractures, the equivalent hydraulic conductivity  $k_{equi}$  is given by [Davis, 1969]:

$$k_{equi} = k_m + \frac{k_f b}{d} = k_m + \frac{\gamma_w b^3}{12\mu d} \quad (6.3)$$

where  $k_{equi}$  is parallel to this group of fractures. As is known, the continuum approach is incapable of representing flow through individual fractures, which may yield inaccurate estimation of pore-water pressures in the vicinity of the fractures. In the following study, the CEM that follows the discrete fracture approach will be used, not only to obtain a more accurate pore-water pressure distributions in layered rock slopes, but also to show under what circumstance the discrete simulation of the fractures is essential.

### 6.3.2 Parameter setting and analysis protocols

It has been learned from the previous section that the aperture, spacing and dip angle of the fracture group and the specific yield of the rock matrix are the main parameters that influence transient groundwater flow in the layered rock slopes. Due to the small range of  $S_{ym}$  value, this study focuses on the investigation of the characteristics of the fracture group.

The hydraulic conductivity and the specific yield for rock matrix are assumed to be

constant and equal  $5.0 \times 10^{-5}$  m/d and 0.001, respectively. Different fracture apertures  $b$ , spacings  $d$  and dip angles  $\psi$  are adopted separately in three sets of parametric analyses, shown in Table 6.2. The specific yield for fractures is assumed to be 0.1. In fact, a change in the value of  $S_{yf}$  will not affect the simulation results. The drawdown rate is fixed at 0.5 m/d. After obtaining the pore-water pressures, the stability analyses are performed to estimate the variation of  $SF$  of the slopes during drawdown. The required parameters are:  $\gamma=25$  kN/m<sup>3</sup>,  $c'/\gamma H=0.1$ , and  $\phi'=20^\circ$  ( $c'/(\gamma H \tan \phi')=0.851$ ). Please note that this study does involve the discussion on judgment of rapid drawdown and slow drawdown, according to either relative height of the free surface or relative reduction of the critical  $SF$ , for the layered rock slopes, due to the complexity of the groundwater distribution pattern.

Table 6.2 Input parameters for parametric analyses of fracture characteristics shown in Figure 6.3-6.7

Parameter	Aperture $b/\mu\text{m}$	Spacing $d/\text{m}$	Dip angle $\psi/^\circ$	Equivalent hydraulic conductivity for the fracture group $k_f b/d/\text{m} \cdot \text{d}^{-1}$	Remarks
Different fracture apertures	12.1	2.5	50	$5.0 \times 10^{-5}$	1. The slope geometry is: $L/H=0.8$ , $m=0.5$ , and $H=55.0$ m; 2. The drawdown rate $v$ equals to 0.5 m/d; 3. The parameters for stability analysis are: $\gamma=25$ kN/m <sup>3</sup> , $c'/(\gamma H \tan \phi')=0.851$ when $c'/\gamma H=0.1$ , and $\phi'=20^\circ$ .
	26.1	2.5	50	$5.0 \times 10^{-4}$	
	56.1	2.5	50	$5.0 \times 10^{-3}$	
	121.0	2.5	50	$5.0 \times 10^{-2}$	
Different fracture spacings	41.4	1.0	50	$5.0 \times 10^{-3}$	
	56.1	2.5	50	$5.0 \times 10^{-3}$	
	70.7	5.0	50	$5.0 \times 10^{-3}$	
	89.1	10.0	50	$5.0 \times 10^{-3}$	
Different fracture dip angles	56.1	2.5	30	$5.0 \times 10^{-3}$	
	56.1	2.5	40	$5.0 \times 10^{-3}$	
	56.1	2.5	50	$5.0 \times 10^{-3}$	
	56.1	2.5	60	$5.0 \times 10^{-3}$	

### 6.3.3 Sensitivity analyses of fracture characteristics

#### (1) Sensitivity analysis of fracture aperture

Since the hydraulic conductivity for single fractures is proportional to the second power of the fracture aperture, a small variation in the aperture can significantly change the conductivity and hence flow in the rock slopes. For investigating the sensitivity of transient pore-water pressure distribution to the fracture aperture, four fracture apertures

corresponding to four orders of magnitude equivalent hydraulic conductivities for the fracture group (i.e.,  $k_f b/d$ ), ranging from  $5.0 \times 10^{-5}$  m/d to  $5.0 \times 10^{-2}$  m/d (in Table 6.1), are considered. Except for the fracture aperture, the fracture spacing and the fracture dip angle are specified as 2.5 m and  $50^\circ$ , respectively.

The calculated free surfaces and the hydraulic head distributions at end of drawdown in the slopes with different fracture apertures are presented in Figure 6.3. It is seen that when the fracture aperture is larger, which means the fracture hydraulic conductivity is higher, the free surface and the contours of hydraulic head are more obviously elongated in the fracture dipping direction, as shown in Figures 6.3(c) and 6.3(d). In these cases, the position of the free surface is far from the slope face and the pore-water pressures acting on the slip surface AA' are relatively low.

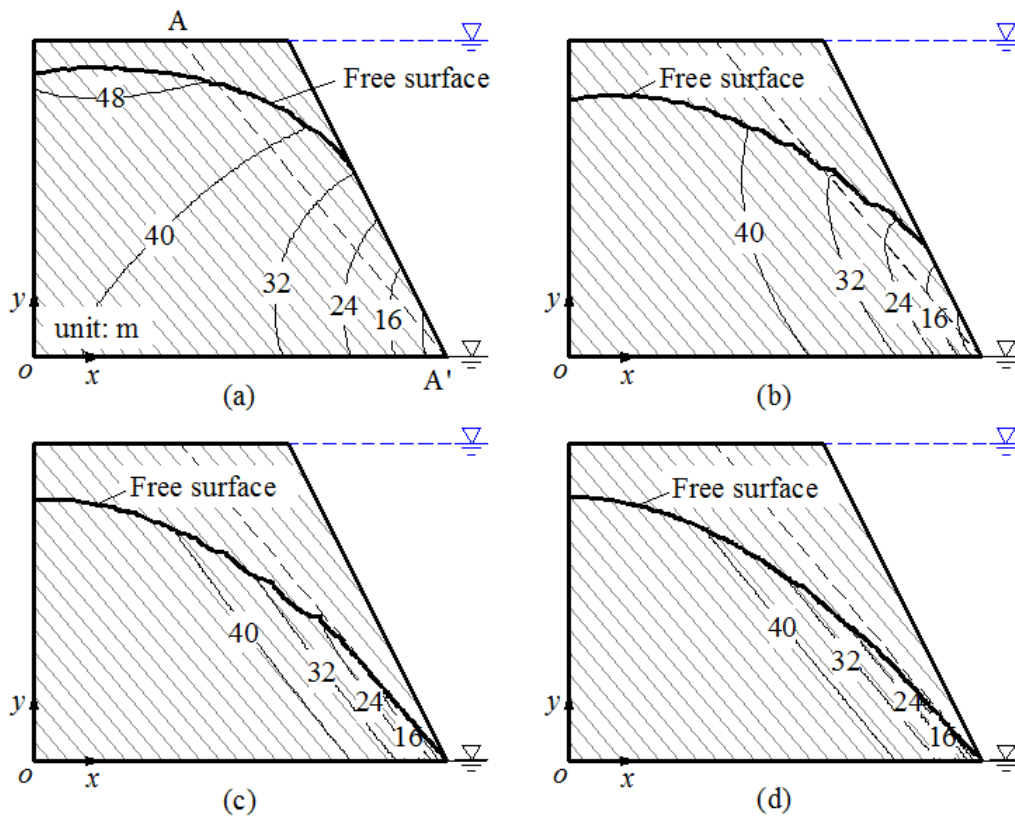


Figure 6.3 Free surfaces and contours of the hydraulic head at end of drawdown in the layered rock slopes with different fracture apertures: (a)  $b=12.1 \mu\text{m}$ ; (b)  $b=26.1 \mu\text{m}$ ; (c)  $b=56.1 \mu\text{m}$ ; and (d)  $b=121.0 \mu\text{m}$

The effects of the fracture aperture on the variation of  $SF$  of slopes during drawdown are shown in Figure 6.4. As expected, for a given relative drawdown level  $H_D/H$ , the computed  $SF/\tan\phi'$  increases as the fracture hydraulic conductivity increases. The increase of  $SF/\tan\phi'$  is attributed to the decrease in the pore-water pressures and consequent increase

in shear strength on the slip surface. These  $SF/\tan\phi'$  values of the layered rock slopes with different fracture apertures during drawdown are higher than those in the case of fully rapid drawdown, because the fractures within the slopes somehow play a role in accelerating the drainage of the slope media.

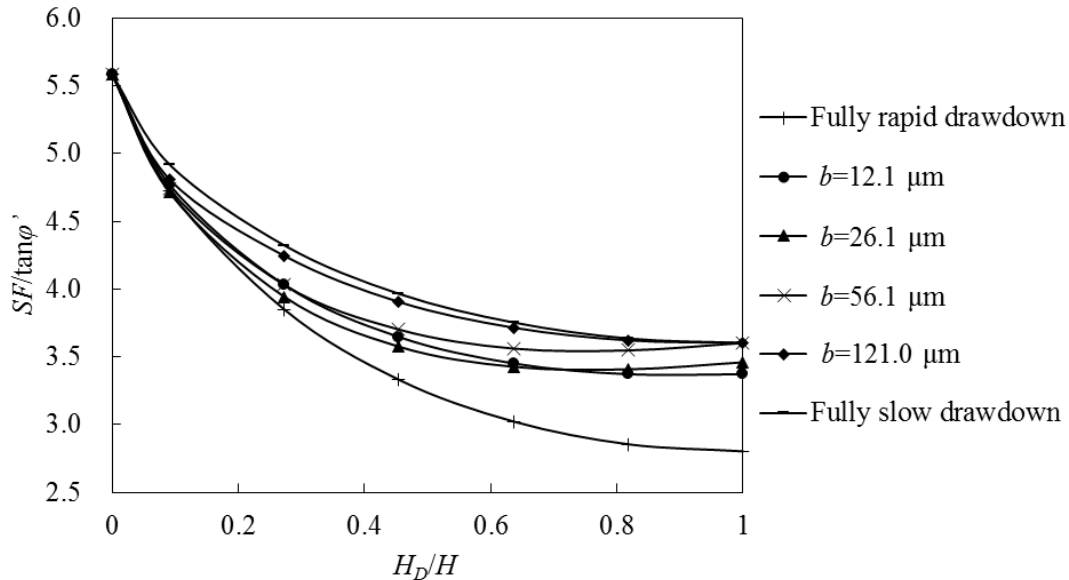


Figure 6.4 Variations of the computed  $SF/\tan\phi'$  with  $H_D/H$  for the layered rock slopes with different fracture apertures: (a)  $b=12.1 \mu\text{m}$ ; (b)  $b=26.1 \mu\text{m}$ ; (c)  $b=56.1 \mu\text{m}$ ; and (d)  $b=121.0 \mu\text{m}$

## (2) Sensitivity analysis of fracture spacing

To investigate the influence of the fracture spacing on transient flow and the stability of slopes, four fracture spacings ranging from 1.0 m to 10.0 m are adopted. The equivalent hydraulic conductivity of the fracture group is specified to be  $5.0 \times 10^{-3}$  m/d. The related fracture apertures are given in Table 6.1.

Figure 6.5 presents the free surfaces and hydraulic head contours at end of drawdown in the layered rock slopes with different fracture spacings. It can be observed that the patterns of the free surface and the hydraulic head contours are almost the same where the fracture spacing is smaller than 2.5 m. If assuming the rock masses are continua and the equivalent hydraulic parameters defined by Equations (6.3) and (6.4) are adopted, the simulation results of the hydraulic head in the slopes (not shown) are close to those shown in Figure 6.5(a). This implies that the rock masses containing densely distributed fractures act hydraulically as the homogeneous media with identical, anisotropic hydraulic conductivity. However, as the fracture spacing increases, the phenomenon that the water flow is forced to look for the preferential paths, i.e., the fractures, is gradually prominent.

Explicit representations of fracture flow using the discrete approach will be essential. As seen from Figure 6.5, the free surfaces in cases of  $d=5.0$  m and  $d=10.0$  m obviously curve at the fractures and they are lowered below the slip surface  $AA'$ .

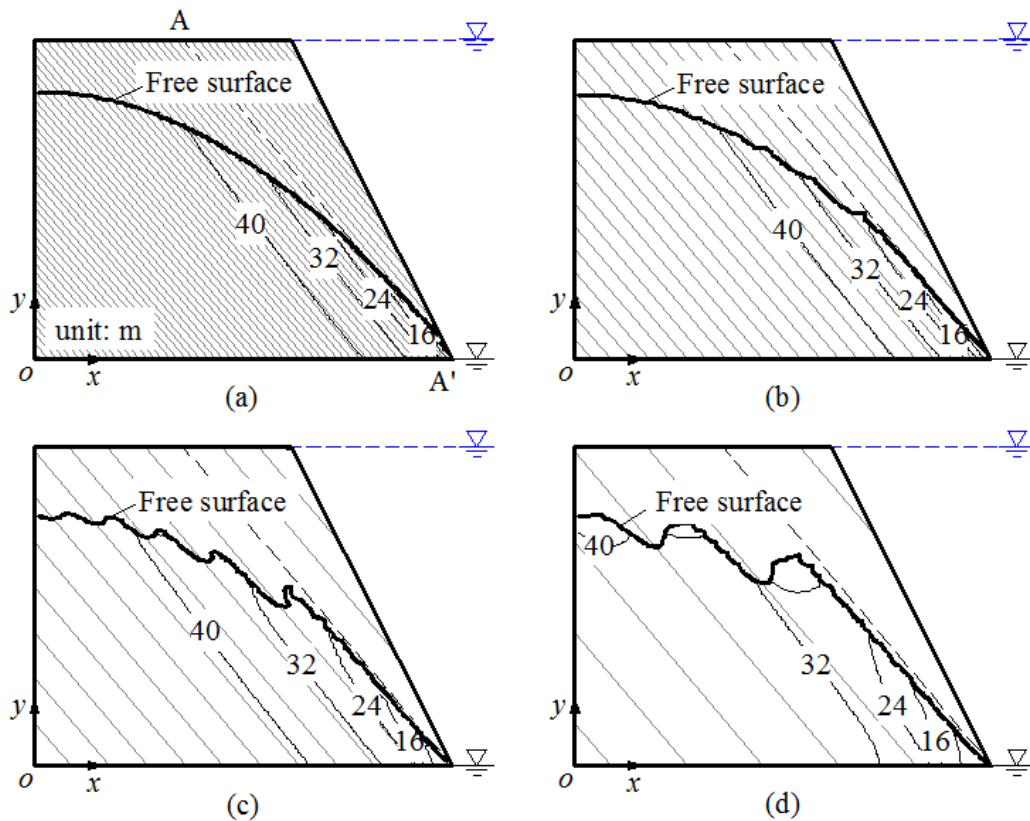


Figure 6.5 Free surfaces and contours of the hydraulic head at end of drawdown in the layered rock slopes with different fracture spacings: (a)  $d=1.0$  m; (b)  $d=2.5$  m; (c)  $d=5.0$  m; and (d)  $d=10.0$  m

Figure 6.6 shows the variations of the computed  $SF/\tan\phi'$  with  $H_D/H$ . Due to the role of drainage of the fractures, the stability of the slope during drawdown is greatly improved. The  $SF/\tan\phi'$  of slopes with  $d=5.0$  m and  $d=10.0$  m at  $H_D/H=1$  is equal to that under fully slow drawdown.

### (3) Sensitivity analysis of fracture dip angle

In addition to the conditions shown in Figure 6.3 and Figure 6.5 that respectively relate to the aperture and spacing of the fracture group, the other groundwater flow conditions that relate to various fracture dip angles may be involved. In the analyses below, four fracture dip angles ranging from  $30^\circ$  to  $60^\circ$  are considered; the fracture spacing is assumed to be 2.5 m; and the equivalent hydraulic conductivity of the fracture group equals  $5.0 \times 10^{-3}$  m/d (shown in Table 6.1).

The free surfaces and hydraulic head contours at end of drawdown corresponding to

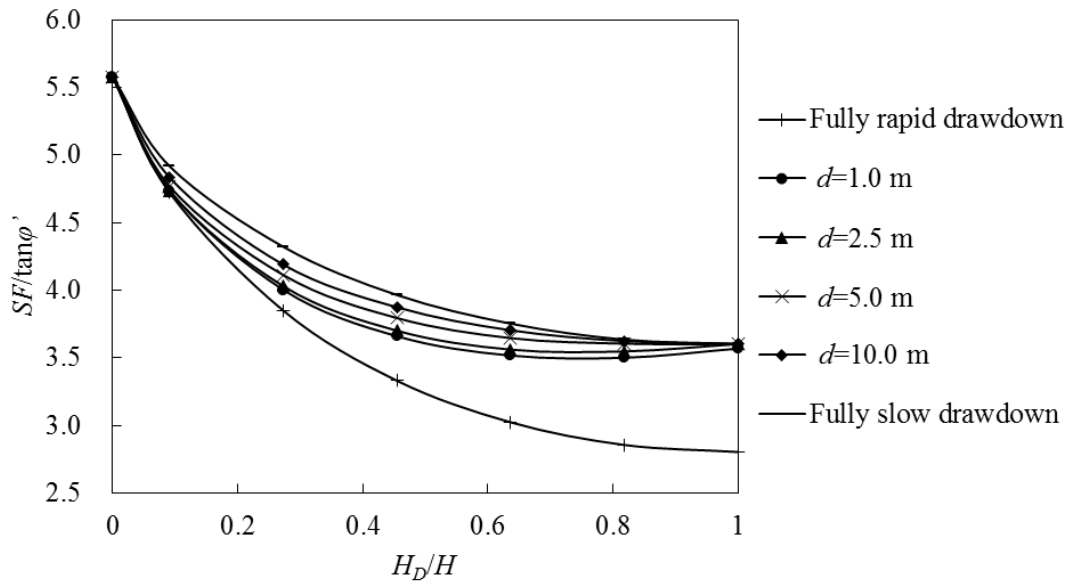


Figure 6.6 Variations of the computed  $SF/\tan\phi'$  with  $H_D/H$  for the layered rock slopes with different fracture spacings: (a)  $d=1.0$  m; (b)  $d=2.5$  m; (c)  $d=5.0$  m; and (d)  $d=10.0$  m

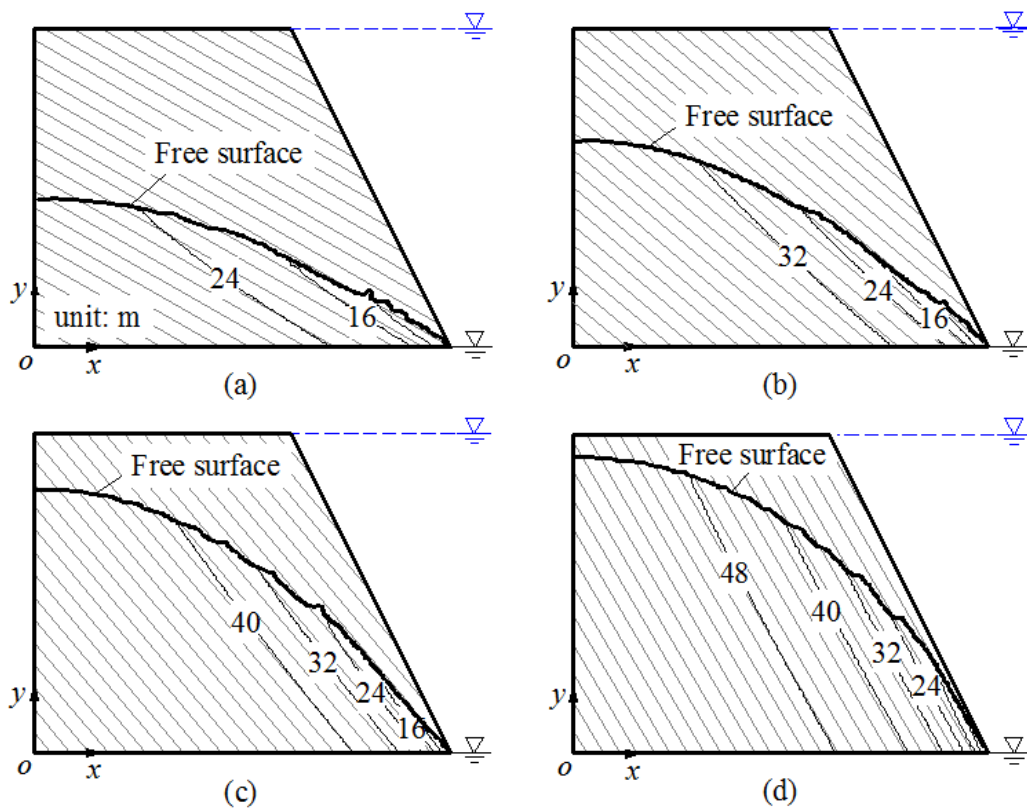


Figure 6.7 Free surfaces and contours of the hydraulic head at end of drawdown in the layered rock slopes with different fracture dip angles: (a)  $\psi=30^\circ$ ; (b)  $\psi=40^\circ$ ; (c)  $\psi=50^\circ$ ; and (d)  $\psi=60^\circ$

the fracture dip angles equal to  $30^\circ$ ,  $40^\circ$ ,  $50^\circ$  and  $60^\circ$  are shown in Figure 6.7. It can be seen from Figure 6.7 that, in the layered rock slope with fractures dipping at  $30^\circ$ , the free surface

has a flat gradient and the values of hydraulic head are relatively small, which illustrates that groundwater within the rock masses can readily drain; whereas, in the layered rock slope with fractures dipping at  $60^\circ$ , the position of the free surface and the hydraulic head values are high, which can be explained since flow to the slope face is inhibited by the fractures almost parallel to the slope face. Stability analyses for these conditions are omitted here, given the differences in the potential failure modes; they may be sliding failures along the fractures in cases of  $\psi=30^\circ$ ,  $40^\circ$ ,  $50^\circ$  and buckling failure in case of  $\psi=60^\circ$ . However, combining the above discussions with the results in Figure 6.7, the readers can easily speculate that the stability of slopes with fractures nearly parallel to the slope face during drawdown would be greatly reduced.

## 6.4 Conclusions

The stability of layered rock slopes under drawdown conditions has been investigated. Due to the presence of the fractures, the hydraulic conductivity and the specific yield for rock masses are heterogeneous, so that transient flow in the slopes during drawdown cannot be simply estimated by using the index  $k/(S_y v)$ , which is proposed in the previous chapter. In this chapter, a parametric study is conducted to investigate the influences of various characteristics of the fracture group on transient flow regimes and the stability of slopes. The main conclusions can be summarized as follows:

(1) The CEM provides accurate simulations of transient groundwater flow in the fractured rock slopes. The calculated pore-water pressures can be introduced in stability analyses to obtain the variations of the safety factor of slopes during drawdown.

(2) Different fracture characteristics lead to different pore-water pressure distributions in the slopes. In comparing cases of different fracture apertures and fracture dip angles, it can be shown that groundwater readily drain from the slopes where the fracture aperture (which is actually fracture conductivity) is large and the fracture dipping is nearly horizontal; and in contrast, high pore-water pressures will develop where the fracture conductivity is low and the fracture dipping is nearly parallel to the slope face.

(3) The necessity of discrete simulation of fracture flow to analyses of transient flow and hence slope stability is emphasized in comparing cases of different fracture spacings but identical equivalent hydraulic conductivity of the fracture group.

(4) It is worthwhile mentioning that, in the real world, rock types and details of structural geology such as distribution and persistence of fracture groups within a slope are

varied. All of these features have an influence on transient flow regime in the slope. It is only possible in this study to draw some basic law by analyzing simple slopes, such as homogeneous slopes (in Chapter 5) and layered slopes (in Chapter 6).

(5) However, when the hydraulic conductivity of one group of fractures is much higher than the other groups, the slopes can have similar behaviors to layered slopes; when the hydraulic conductivities of different fracture groups in all directions are close, the behaviors of the slopes can approach those of homogeneous slopes. For analyses of these slopes, the results in Chapter 5 and Chapter 6 provide important references. Furthermore, the methodology employed herein can be applied to these analyses.



## References

1. Chen SH. Hydraulic structures. Springer Verlag: New York, 2015.
2. Chen ZY, Wang XG, Yang J, Jia Z, Wang YJ. Rock slope stability analysis: theory, method and programs. China Water and Power Press: Beijing, 2005.
3. Davis SN. Porosity and permeability of natural materials. In *Flow through porous media*, Weist RD (ed). Academic Press: London, 1969.
4. Dong JJ, Tzeng JH, Wu PK, Lin ML. Effects of anisotropic permeability on stabilization and pore water pressure distribution of poorly cemented stratified rock slopes. *International Journal for Numerical and Analytical Methods in Geomechanics* 2006; **30**(15): 1579–1600.
5. Hoek E, Bray J. Rock slope engineering, 3th edition. Institution of Mining and Metallurgy: London, 1981.
6. Pritchard MA, Savigny KW. The Heather Hill landslide: an example of a large scale topping failure in a natural slope. *Canadian Geotechnical Journal* 1991; **28**(3): 410–422.
7. Singhal BBS, Gupta RP. Applied hydrogeology of fractured rocks. Springer Verlag: New York, 2010.
8. Sjoberg J. Failure mechanisms for high slopes in hard rock. In *Slope stability in surface mining*, Hustrulid WA, Mccarter Mk, Van-Zyl DJA (eds). Society for Mining, Metallurgy, and Exploration, Inc. (SME): Colorado, 2000; pp 71–81.
9. Snow DT. Anisotropy permeability of fractured media. *Water Resources Research* 1969; **5**(6): 1273–1289.
10. Sun GZ. Engineering geology and geological engineering. Seismological Press: Beijing, 1993.
11. Wyllie DC, Mah CW. Rock slope engineering: civil and mining, 4th edition. Spon Press/Taylor and Francis Group: London and New York, 2004.

## Chapter 7 Conclusions and Recommendations

### 7.1 Conclusions

This thesis mainly has done four aspects of research work, and the relevant conclusions and contributions are presented as follows.

#### *(1) Modelling transient, saturated flow in fractured media with a free surface*

- The composite element model for transient, saturated flow in fractured media with a free surface has been constructed. The model has the following advantages due to the use of the CEM: (i) the mesh generation is not restricted by the geometry of fractures; (ii) the model is capable of accurate descriptions of fracture flow, matrix flow and exchange of water between fractures and matrix; and (iii) if there is no fracture, the model will automatically be degenerated into the finite element model.
- Relevant solution algorithms have been proposed, including those for CEM pre-processing, numerical integral calculation, treatment of boundary conditions and solving large, sparse, symmetric system of equations. All of them have been implemented into a computer program CEM\_SATFLOW.
- The effectiveness of the model and program has been verified by comparing the example results generated by CEM\_SATFLOW with those from a commercial software COMSOL.
- The capability of the composite element model has been demonstrated by simulations of the flow problems in complicated, saturated fractured aquifers. Moreover, the simulation results provide valuable insight into the hydraulic behavior of saturated fractured media and the free surface configuration in fractured media.

#### *(2) Modelling transient, variably-saturated flow in fractured media*

- The composite element model has been further developed for transient, variably-saturated flow in fractured media. The model also has the advantages stated in the above first point.
- The concept of an effective interaction area has been incorporated in the model to account for changes in the fracture-matrix interaction area when fracture desaturates.

- An iterative procedure with under-relaxation has been applied to solve the variably-saturated flow equations. Meanwhile, the techniques of mass matrix lumping and adaptive time stepping have been introduced to improve the accuracy and efficiency of solution processes. All of them have been implemented into a computer program CEM\_UNSATFLOW.
- The effectiveness of the model and program has been verified by comparing the example results generated by CEM\_UNSATFLOW with the semi-analytical solution and those from COMSOL.
- The simulation results of flow in complicated, variably-saturated fractured aquifers have demonstrated the highly variable nature of the unsaturated fracture-matrix flow systems, and illustrated the necessity of an explicit and coupled description of the flow processes in both the fractures and matrix.

***(3) Investigation of stability of homogenous soil slopes under drawdown conditions***

- The CEM provides accurate simulations of transient flow in the slopes. The calculated pore-water pressures can be introduced into limit equilibrium analyses to obtain the variation of the safety factor of slopes during drawdown.
- It has been found that  $SF/\tan\phi'$  of slopes during drawdown depends on  $k/(S_y v)$  and  $c'/(\gamma H \tan\phi')$ .
- By relating  $k/(S_y v)$  and  $c'/(\gamma H \tan\phi')$  to the relative reduction in the safety factor, a “new” criterion for judging rapid drawdown results. The stability analysis for the rapid drawdown dominates the design of slope.
- A series of charts for quick judgment of rapid drawdown in homogeneous soil slope have produced.

***(4) Investigation of stability of layered rock slopes under drawdown conditions***

- A parametric study of the fracture characteristics has provided a quantitative description of the influence of different fracture characteristics on the pore-water pressure distributions and the safety factor of layered rock slopes under drawdown conditions.

## **7.2 Recommendations for future research**

This work has shown some need for continued research. More specifically, the following issues need to be addressed.

- The composite element models assume that the fracture has tangential and normal hydraulic conductivities. Naturally, the estimation of the conductivities has a direct effect on the modelling results. How to obtain the hydraulic parameters for the fractures and whether it is reasonable to apply these parameters to the present composite element models still need further study and demonstration.
- The main feature of the CEM is dividing the element into multiple sub-elements based on the fracture surface. However, in some special cases, such as where the fracture surface coincides with the face of element or where the fracture surface ends in the interior of the element, the CEM pre-processor requires some special handling, such as moving or stretching the fracture surface. How to coordinate the geometrical relationship between the fractures and the mesh elements to realize the division of composite elements is a difficult problem to solve in the CEM pre-processing.
- In simulating transient flow in the slopes subjected to drawdown conditions, only flow in the saturated zone is considered and flow in the unsaturated zone is neglected. In view of the influence of the matrix suction in the unsaturated soils or rock masses on the shear strength, it is necessary to demonstrate the difference in the slope stability safety factor due to neglect and consideration of the unsaturated zone.
- The limit equilibrium analysis has its own shortcomings, so how to combine the CEM with the better stability analysis method such as the FEM is worthy of further study.
- In addition, the deformation of the slope soil or rock mass may have a certain effect on transient flow and stability of slope. The use of coupled transient flow and deformation analyses together with the stability analysis to investigate the drawdown problems is the direction of future work.